NTNU – Trondheim
Norwegian University of
Science and Technology

Department of marine structures

Master thesis

Finite element analysis of marine umbilical

Author:
M.Sc.Student Adrian Risa

Supervisor:
Professor Svein Sævik

June 10, 2011

Abstract

Background

Marine umbilicals play a vital role in oil and gas production fields. The oil and gas industry is in constant change, as the resources in the reservoirs are ever decreasing. Today oil and gas exploration takes place at increasing depths, and in harsher environments. This means that components like marine umbilicals are getting more advanced. Thus accurate structural analysis is important. The focus in this thesis is an umbilical consisting of 19 copper conductors. The goal is to model it in ABAQUS, and compare the results with laboratory testing.

Results

Stress distribution and fatigue calculations were the main focus. Ultimately, it was proven that ABAQUS was able to represent the umbilical's general behavior. However, due to computational limitations and limits in the material model, the result proved inaccurate. In particular, values for axial stress and strain, exceeds the expected values.

Conclusion

The model was able to represent the general behavior from the laboratory results. Effort should be made in the future to overcome the computational problems, and the material model should be revised.

Summary

Working with this master thesis has been challenging, and rewarding. In part I effort was made towards the literature part of the thesis. General theory about marine umbilicals were treated. Loading conditions and effects were discussed, with a special focus on stress components. Special attention were given to production of electrical copper wires. This was important, for modeling the shrinking behavior of the umbilical in the analysis part.

The main focus in this master thesis, has been towards modeling the umbilical in ABAQUS. This was the continuation of the work done in the project thesis by Risa [2010]. The first step was analyses to find a converging mesh. In the end, a compromise between computational cost and accuracy had to be made. This means that in all the analyses presented in this paper, a source of inaccuracy is the mesh resolution. Theory about the final element method, and the techniques used in the analyses are presented in chapter 5.

In chapter 9, the results from the tension analyses are presented, and treated. Here it can be seen that the axial stress values obtained in ABAQUS are greater than what was expected. It also shows that the values increases from the elastic cases to the elastic-plastic cases. One of the main lessons, are that plastically shrinking the model, greatly reduce the inter layer stress difference. It is also evident that the material model used, was inadequate. This is clear when examining the axial strain, which is higher than anticipated.

Fatigue results from stress range 1 is presented in chapter 11. Obtaining good fatigue results for the elastic cases was unsuccessful, due to the large inter layer stress difference. For the elastic cases the values exceeded the SN curve used in this thesis. Uncertainty is also associated with the results from the elastic-plastic case 3. Since the conductors break away from the center conductor, during the unloading. The results from case 4, does not show this tendency, and are therefore considered more accurate.

THESIS WORK SPRING 2011

The umbilical riser is a vital part of oil and gas floating production systems providing hydraulic and electrical power and signal transmission to the wellhead machinery. The umbilical represents a complex structure where the different components are helically wound into one package, the structural response in terms of stress being governed by elastic bending and friction between layers.

This thesis work will be to continue the work conducted in the project thesis and focus on investigating stress effects in copper conductors used in umbilicals and is to be carried out as follows:

1. Literature study, including umbilical technology in general, failure modes and design criteria, relevant stress components and effects, stress models, nonlinear finite element methods with focus on the techniques applied in the ABAQUS software. In addition focus on the material properties of the copper applied in copper conductors and how the copper conductor is manufactured including details related to the diameter reduction normally applied.
2. By using ABAQUS, establish a 1 m long model for one 95 mm2 power conductor consisting of 1 + 6 + 12 circular wires installed in helix with pitch length obtained from measuring a real specimen. The model shall be based on volume and contact elements capable of handling friction between layers.
3. Apply mean tension 0-9500-0 N and compare the strain-force curve with laboratory data.
4. Apply mean tension in one end to 116.05 MPa average stress. Then vary the tension between 211 MPa and 21.1 MPa average stress. Investigate the stress variations versus the analytical mean values. Do the same exercise with 111 and 11 MPa (mean =61 MPa). Perform a simple fatigue calculation based on single tendon fatigue curve and find the number of cycles to failure
5. Apply a typical stress-strain curve for copper and apply external pressure to "shrink" the specimen into the measured diameter. Repeat the analysis carried out in items 3-4. What is the effect of shrinking with respect to fatigue? Has the correlation with the measured data changed?
6. Conclusions and recommendations for further work

The work scope may prove to be larger than initially anticipated. Subject to approval from the supervisors, topics may be deleted from the list above or reduced in extent.

In the thesis the candidate shall present his personal contribution to the resolution of problems within the scope of the thesis work

Theories and conclusions should be based on mathematical derivations and/or logic reasoning identifying the various steps in the deduction.

The candidate should utilise the existing possibilities for obtaining relevant literature.

Thesis format

The thesis should be organised in a rational manner to give a clear exposition of results, assessments, and conclusions. The text should be brief and to the point, with a clear language.

Telegraphic language should be avoided.

The thesis shall contain the following elements: A text defining the scope, preface, list of contents, summary, main body of thesis, conclusions with recommendations for further work, list of symbols and acronyms, references and (optional) appendices. All figures, tables and equations shall be numerated.

The supervisors may require that the candidate, in an early stage of the work, presents a written plan for the completion of the work.

The original contribution of the candidate and material taken from other sources shall be clearly defined. Work from other sources shall be properly referenced using an acknowledged referencing system.

The report shall be submitted in two copies:

- Signed by the candidate
- The text defining the scope included
- In bound volume(s)
- Drawings and/or computer prints which cannot be bound should be organised in a separate folder.

Ownership
NTNU has according to the present rules the ownership of the thesis. Any use of the thesis has to be approved by NTNU (or external partner when this applies). The department has the right to use the thesis as if the work was carried out by a NTNU employee, if nothing else has been agreed in advance.

Thesis supervisors
Prof. Svein Sævik, NTNU M.Sc. Frank Klæbo, Marintek

Deadline: June 14th, 2011

Trondheim, January 17th, 2011

Svein Sævik

Preface

This thesis is the continuation of the project thesis "Finite element method analysis of marine umbilical" by Risa [2010]. In the project thesis, the analysis part was limited by computational shortage. All the analyses were run on a standard desktop computer, which proved inadequate. The result was that all the analyses had to be run on a suboptimal mesh, and mass scaling had to be introduced.

One of the main objectives during this master's thesis was to eliminate the problems of computational power, by running the analyses on a supercomputer. In order to make that work, all the models had to be redone, since the supercomputer ran a different version of ABAQUS. A lot of time was also spent trying to find the optimum mesh resolution by running linear tension tests, and comparing the axial stress results.

Working with the analysis part of this thesis has been a challenging process, with a lot of trial and error. Since no similar analyses had been done at the department of Marine structures before, a lot of experimenting had to be done. Especially getting the shrinking part and the plastic material model to work, took a lot of experimenting. Countless hours of analyses which ultimately had to be scrapped, lies behind the results presented in the subsequent chapters.

Acknowledgment

This master thesis has been written by M.Sc. Student Adrian Risa during the spring semester 2011. The thesis has been written in collaboration with the department of Marine Technology at the Norwegian University of Science and Technology(NTNU). The master thesis is the continuation of the project thesis "Finite element method analysis of marine umbilical" by Risa [2010].

Included in this thesis are results from full scale tests of the actual umbilical, carried out by PhD. Student Fachri Nasution. I would like to thank Fachri Nasution for providing me with results, and guidance.

I would also like to thank professor Svein Sævik , for support and guidance throughout the process of writing this master's thesis.

I will also give my thanks to M.Sc Frank Kæbo at Marintek, for help and consulting regarding ABAQUS FEA, and the support department for NOTUR, for help with running analyses on the supercomputer Njord

Contents

List of Figures

List of Tables

Abbreviation

FEA: Finite element analysis
FEM: Finite element method
FE: Finite element
DOF: Degree of freedom
ROV: Remote operated vehicle
DNV: Det norske veritas
NTNU: Norwegian university of science and technology
NTH: Norges tekniske høgskole
ALE: Arbitrary Lagrangian Eulerian
VIV: Vortex induced vibrations

Nomenclature

σ_h/σ_H: Hoop stress
D: Outer diameter
t: Wall thickness
p_i: Internal pressure
p_o,p_{ext}: External hydrostatic pressure
σ_a: Axial stress
r_i: Inner radius
r_o: Outer radius
N: Normal force
A: Cross section area
η_σ: Utilization factor
σ_{SMYS}: Minimum specified yield stress
σ_e: Maximum equivalent stress
L_p: Pitch length. Distance for a helical component to make a complete revolution.
R_h: Helical radius.
α_h: Lay angle
p_{init}: Initiation pressure, buckling
p_{pr}: Propagation pressure, buckling
p_c: Collapse pressure, buckling
R: R-ratio, fatigue
σ_m: Middle stress
$\Delta\sigma$: Equivalent stress
σ_{UTS}: Ultimate tensile strength
E: Young's modulus
σ_y: Yield stress
N: Number of cycles to failure

Part I

Theory

Chapter 1

Marine umbilical

1.1 general

A marine umbilical is defined as an assembly of fluid conduits, electrical and fiber optic cables, either on their own or with combinations of each other, cabled together for flexibility. The umbilical plays an important part in any offshore oil and gas field. It provides electricity, hydraulic power, and control signals to the subsea components, like wellhead machinery and ROVs.

Connecting a subsea structure with a surface structure, the umbilical is subjected to dynamic loading from the sea environment. The current trend is that oil and gas extraction takes place at increasing water depths, and in harsher environments. Which implies that structural analyses, and design are getting more challenging.

1.1.1 Components

Oil and gas production fields are found throughout the world, in different environments, and often demands tailored equipment. Marine umbilicals are therefore highly specialized products, tailored for a specific task. Figure 1.1, shows a typical umbilical. The key components are described below.

Fluid conductors: There are 2 main types of fluid conductors on the marked according to de Almeida et al [2009]; Steel tubes and thermoplastic hoses.

Fibre optic cable: Transmitting data signals to and from the subsea system.

Electric conductor: Can be divided into 2 groups; high and low voltage conductors. Can have its own armor members for strength.

Armor: Umbilicals usually have a combination of different types of armor for coping with tension and bending: Flexible steel armor, steel members for tension, polymer sheaths and so forth.

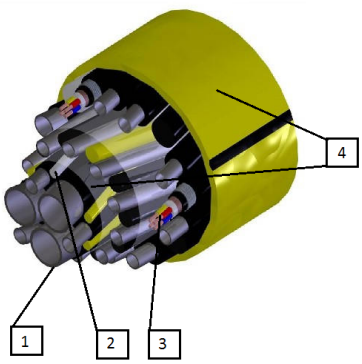

Figure 1.1: Detail overview of a marine umbilical: 1: Steel tube 2: Fibre optic 3: Electric conductor 4: Armor

1.1.2 Assembly

The components are typically cabled together helically, to reduce the operational loads on the components, and increase the structural flexibility. In multi layered umbilicals the layers are usually contra rotated, which can be observed in figure 1.1.

1.1.3 Umbilical system

There are several different designs for installation of umbilical systems on the market today. The deciding factors when choosing a system is economy, operational depth, movement of surface vessel and environmental loads. A few of the most common designs are shown in figure 1.2.

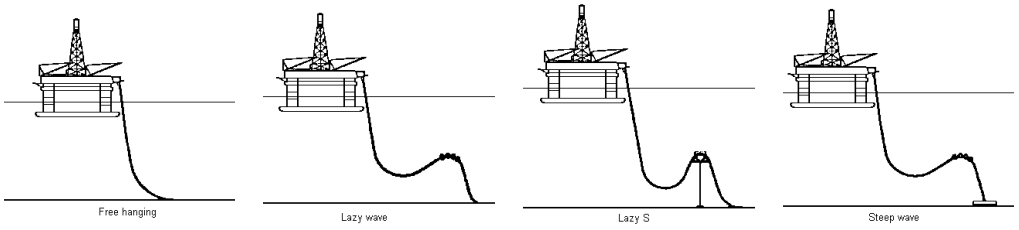

(a) Free hanging catenary (b) Lazy wave (c) Lazy s (d) Steep wave

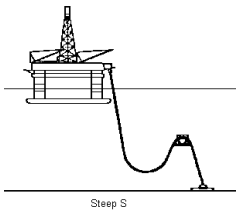

(e) Steep s

Figure 1.2: Umbilical installation layouts

The typical components other than the umbilical cable itself in the system is the bending stiffener, the buoyancy module and the hang-off assembly. According to Stanton et al. [2009]:

Hang-off assembly The top end of the dynamic umbilical is terminated with a hang-off assembly to secure the umbilical to the vessel. The hang-off assembly is designed to withstand all installation and operational loads

Bending stiffener Bending stiffeners are utilized to provide the umbilical with a continuous transition between the umbilical, with its inherent low bending stiffness, and a rigid end fitting, which is very stiff. Bending stiffeners are made of a polyurethane molded material, and are bolted to the end fitting. Each umbilical top connection is usually equipped with a bending stiffener.

Buoyancy module A lazy-wave configuration is obtained with a buoyant section which is provided by using buoyancy modules distributed over an appropriate length of umbilical. The buoyancy modules are typically composed of an internal clamp and a syntactic foam buoyancy element.

Mid-water arch A lazy-S configuration is obtained with a buoyant mid water arch supporting the umbilical at the mid length. Each mid-water arch accommodates 2 or 3 umbilicals or flexible risers. A pair of tethers made of chain is used to connect the mid-water arch to a gravity base, acting as an anchoring point.

1.1.4 Environmental loads

The umbilical system is installed and operated in a sea environment. The system will then be subjected to current loads, wave loads, wind loads and hydrostatic pressure. The system can also be subjected to dynamic motions from the surface vessel. All of these loads and motions are dynamic and varies with time, as weather conditions change. The load response in the umbilical system will be discussed in chapter 2.

Chapter 2

Load response

2.1 General

In section 1.1.4 it was stated that the umbilical system is subjected to various types of dynamic loading. From chapter 1 it is known that umbilicals consists of several different components. These components are in most cases free to move relative to each other. This gives the umbilical its flexible nature, but also makes structural analysis complex. In particular dealing with the sliding behavior between components are challenging, and important with respect to fatigue assessment.

2.2 Stress components

2.2.1 Axial stress

The umbilical system consist mainly of tubes (pressure vessels) and solid components like electrical conductors. There are 3 main load conditions that will give axial stress: Tensile loading, bending motion and pressure loading.

Pressure vessels

Difference in external and internal pressure, will give an axial stress component. This component is expressed in equation 2.1

$$\sigma_a = \frac{p_i r_i^2 - p_o r_o^2}{r_o^2 - r_i^2} \tag{2.1}$$

Solid homogeneous components

Axial stress due to tensile loading can be expressed with Navier's formula according to equation 2.2

$$\sigma_a = \frac{N}{A} \tag{2.2}$$

2.2.2 Bending motion

Response in bending is complicated, since relative motion between components occurs. According to ISO-13628-5 [2009] the physical behavior can be divided into 2 regimes:

Stick regime: Where plane surfaces remain plane. This behavior governs until the shear stress between components at the neutral axis of the umbilical exceeds the frictional resistance governed by the friction coefficient, and the internal reaction forces from tension and torsion.

Slip regime: Friction resistance is exceeded and relative displacements occur. For a curved shape case, the helical components move from the compressive side towards the tensile side of the umbilical.

2.2.3 Frictional stress

Relative motions between components as explained under slip regime will give stress due to friction. Being able to predict frictional stress accurately is important for fatigue analyses. According to Sævik [2010], attention on the problem of corrosion fatigue in risers have been important the last years. Corrosion fatigue is associated with intrusion of seawater as a result of damage to the external sheath, or from corrosive gases from the well. The consequence of this is that even small bending motions contributes to the fatigue process.

In Sævik [2010] two slip regimes are identified: For a circular helix on a straight cylinder which thereafter is bent into a constant curve radius, there exist two limit curves: The loxodromic curve having no transverse slip, and the geodesic curve with associated transverse slip. The 2 slip curves are shown in figure 2.1

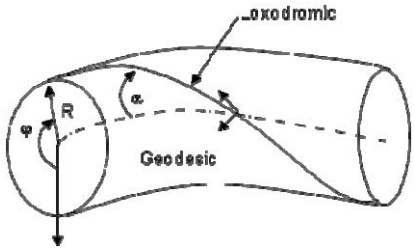

Figure 2.1: Slip regime paths

In evaluation of cycle to cycle dynamic bending stress, transverse slip can be neglected according to Sævik [2010]. Further it is assumed that the slip will take place in the longitudinal direction, thus following the loxodromic curve. This leads to the following assumptions according to Sævik [2010]:

- The friction stress due to relative displacements between layers is only a result of longitudinal slip.
- The elastic torsion and bending stresses can be found by differential geometry

In the same paper 2 alternative FEM formulations for dealing with frictional stress are presented and evaluated:

Sandwich beam model for friction: Considers the potential energy of the tendon sliding on the supporting core. The model includes each tendon, so that the boundary condition of each tendon affects the results.

Moment based model for friction: The equilibrium state is assumed described on stress resultant level, which means that the boundary condition of each individual tendon cannot be taken into account. The friction moment over the cross section is considered.

In ISO-13628-5 [2009] analytical methods for calculating the frictional stress is mentioned. In these methods the curvature is assumed to be constant. Elastic bending and relative displacements are based on differential geometry. The friction stress is estimated based on considering the friction force on a quarter pitch length of the helical components, and the friction stress is treated as a harmonic function with maximum tensile and compressive stresses at the tensile and compressive sides of the umbilical.

2.2.4 Hoop stress

When a cylindrical vessel is subjected to a pressure load, the vessel will develop stresses in all directions according to Kashani and Young [2007]. The stress component acting in the circumferential direction is labeled hoop stress, see figure 2.2. This applies to the umbilical both as a global structure, and to internal components like steel tubes.

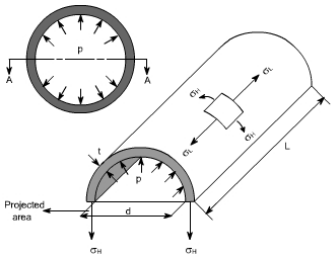

Figure 2.2: Hoop stress σ_H

There are 2 analytical models for calculating the hoop stress. The Barlow thin wall method and by using Lame equations. The Barlow method is only valid for pressure vessels with a diameter-to-wall thickness ratio greater than 20, whereas the Lame equations are valid for any cross section. In offshore codes hoop stress is defined as equation 2.3 according to DNV [2010]

$$\sigma_h = \frac{D-t}{2t}(p_i - p_o) \tag{2.3}$$

2.2.5 Radial stress

In section 2.2.4 it was stated that a pressure load develops stress in all directions. The longitudinal stress component is termed radial stress. It is analytically expressed in equation 2.4, note that it varies quadratically over the wall thickness.

$$\sigma_r = \frac{p_i r_i^2 - p_o r_o^2}{r_o^2 - r_i^2} + \frac{r_i^2 r_o^2 (p_o - p_i)}{r(x)^2 (r_o^2 - r_i^2)}, x \in [0, t] \tag{2.4}$$

2.2.6 Contact stress

Contact stress between 2 general bodies submitted to a total load P, is treated in Young and Budynas [2002]. Equation 2.5 takes the geometry of the 2 bodies into account. At the point of contact, R_1 and R_1' represent the minimum and maximum radii of body 1, and R_2 and R_2' for body 2. This is illustrated in figure 2.3.

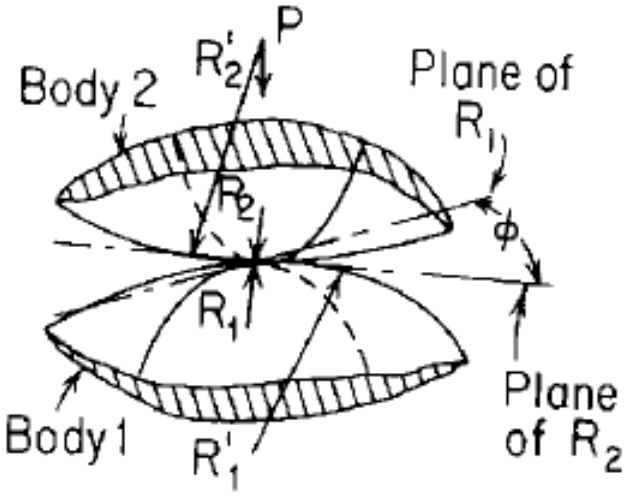

Figure 2.3: Contact between 2 elastic bodies

$$K_D = \frac{1.5}{\frac{1}{R_1} + \frac{1}{R_2} + \frac{1}{R_1'} + \frac{1}{R_2'}} \tag{2.5}$$

$$C_E = \frac{1-\nu_1^2}{E_1} + \frac{1-\nu_2^2}{E_2} \tag{2.6}$$

In equation 2.6, ν_1 and ν_2 is the Poisson's ratio for the 2 bodies. E_1 and E_2 are the Young's modulus. The parameters α, β and λ are given in tables.

$$y = \lambda \sqrt[3]{\frac{P^2 C_E^2}{K_D}} \tag{2.7}$$

The parameter y is the relative motion of approach along the axis of loading of 2 points, one in each of the contact bodies.

$$d = \beta \sqrt[3]{P K_D C_E} \tag{2.8}$$

$$c = \alpha \sqrt[3]{P K_D C_E} \tag{2.9}$$

$$(\sigma_c)_{max} = \frac{1.5P}{\pi c d} \tag{2.10}$$

Equation 2.10 expresses the maximum contact stress between the 2 bodies. It is important to note that the expressions presented in this section are only valid for elastic theory.

2.2.7 Von mises

The Von Mises stress resultant from equation 2.12 is often used to define the point of material yielding.

$$\sigma_y = \sigma_{mises} \tag{2.11}$$

$$\sigma_{mises} = \sqrt{\frac{1}{2}((\sigma_x - \sigma_y)^2 + (\sigma_y - \sigma_z)^2 + (\sigma_z - \sigma_x)^2) + 3(\tau_{xy}^2 + \tau_{yz}^2 + \tau_{zx}^2)} \tag{2.12}$$

2.3 Fatigue assessment

The frictional stress components discussed in section 2.2.3 are important for fatigue calculations. Critical areas are normally at the floater interface where bend limiting devices, (e.g. bend stiffener or bellmouth) are applied to avoid over-bending in extreme load situations, and reduce long-term fatigue loading, according to Sødahl et al. [2010].

In this paper the focus will be on stress 'hot spots' caused by conductor to conductor interaction, as a result of tensile loading. ABAQUS FEA will be used to analyze the structural behavior during tensile loading. Fatigue assessment will then be carried out with the methods described in section 2.3.1.

2.3.1 Fatigue calculations

According to Sævik [1999] equivalent stress for a multi axial stress state is defined as in equation 2.13.

$$\Delta\sigma = \sqrt{\Delta\sigma_x^2 + \Delta\sigma_y^2 + \Delta\sigma_z^2 - \Delta\sigma_x\Delta\sigma_y - \Delta\sigma_x\Delta\sigma_z - \Delta\sigma_z\Delta\sigma_y + 3\Delta\tau_{xy}^2 + 3\Delta\tau_{xz}^2 + 3\Delta\tau_{zy}^2} \tag{2.13}$$

The middle stress component is then defined as in equation 2.14.

$$\sigma_m = \sqrt{\sigma_x^2 + \sigma_y^2 + \sigma_z^2} \tag{2.14}$$

In equation 2.14, $\sigma_{x,y,z}$ is understood as $\frac{(\sigma_{max}+\sigma_{min})}{2}$.

The R-ratio is defined in equation 2.15

$$R = \frac{\sigma_{min}}{\sigma_{max}} \tag{2.15}$$

For a S-N diagram defined by a given R-ratio the corresponding value is defined by Gerber as equation 2.16

$$\Delta\sigma = \Delta\sigma_0(1 - (\frac{\sigma_m}{\sigma_{UTS}})^2) \tag{2.16}$$

Chapter 3

Failure modes and design criteria

3.1 Introduction

In chapter 1 it was stated that the umbilical cable plays a vital part in offshore oil and gas production, and that it is subjected to dynamic loading from the sea environment. In chapter 2 the stress components due to various load states were described. It is critical that the umbilical system is properly designed, so that it maintains its structural integrity in operational conditions. Therefore it exists rules and regulations with respect to design criterion, and what load states to be considered. These rules and regulations vary with the different oil and gas fields. In this master thesis the focus will be on "DNV, FS-OS-F101, Submarine pipeline systems" and "Norsk standard, ISO 13628-5".

3.2 Load classifications

According to ISO-13628-5 [2009], the loads are classified into the following terms:

- **Functional loads:** Are all loads acting on the umbilical during manufacture, installation and operation, including those loads that can act on the umbilical in still water, with the exception of wind, wave or current loads.
- **Environmental loads:** Are loads induced by external forces caused directly or indirectly by all environmental parameters acting on the umbilical, including those induced by waves, currents and vessel motion.
- **Accidental loads:** Are loads caused directly or indirectly by unplanned activities. Accidental loads shall be understood as loads to which the umbilical can be subjected to in case of abnormal conditions, incorrect operation or technical failure as defined by the purchaser.

3.3 Design criteria

When designing an umbilical system the probabilistic occurrence of the environmental loads, and combinations of loads must be considered. Both structural integrity and fatigue must be considered, according to rules and regulations.

3.3.1 Extreme load combinations

The extreme load combinations shall reflect the most probable extreme combined load effect over a specified design time period. Extreme load combinations shall be defined for permanent, as well as temporary design conditions according to ISO-13628-5 [2009].

- **Normal operation:** This applies to the permanent operational state of the umbilical, considering functional and environmental loads. Design conditions with a 10^{-2} annual exceedence probability shall be applied.[1]
- **Abnormal operation:** This applies to the permanent operational state of the umbilical considering functional, environmental and accidental loads. Combined design conditions with an annual exceedence probability between 10^{-2} and 10^{-4} shall be considered.
- **Temporary conditions:** This applies to temporary conditions, such as installation, retrieval, pressure testing and other intermediate conditions prior to permanent operation. The applicable return period for the design condition depends on the seasonal timing and duration of the temporary period.

3.3.2 Fatigue load conditions

Fatigue damage shall be calculated considering all relevant cyclic loading imposed on the umbilical over its design life covering fabrication, temporary conditions including installation, as well as in-place operation. Consideration shall be given to the long-term probabilistic nature of the fatigue loading. The following sources of fatigue damage shall be evaluated according to ISO-13628-5 [2009]:

- Wave-frequency response of the umbilical due to direct wave loading as well as wave induced host motion.
- Slow drift host motions including variation of mean position
- VIV response of the umbilical under steady current conditions
- Cyclic loading during fabrication and installation.
- Cyclic loading due to operation of the umbilical.

3.3.3 Structural strength

Stress criterion

Formal demands regarding maximum allowable stress for a pressure vessel is presented in ISO-13628-5 [2009]. The maximum allowable stress is defined from the ultimate strength of the material σ_{SMYS} and a utilization factor η_σ, given in equation 3.1. The maximum equivalent stress σ_e is defined in equation 3.2, where the stress components σ_h, σ_a and σ_r are as defined in section 2.2.

$$\sigma_e \leq \eta_\sigma \sigma_{SMYS} \tag{3.1}$$

$$\sigma_e = \sqrt{\frac{(\sigma_h - \sigma_a)^2 + (\sigma_a - \sigma_r)^2 + (\sigma_r - \sigma_h)^2}{2}} \tag{3.2}$$

[1] 100 year return period

3.4 Failure modes

In this section design and acceptance criteria for possible modes of structural failure for the umbilical system will be discussed. This is known as limit state criteria according to DNV [2010]. The criterion stated in DNV [2010] regards submarine pipeline systems, but they will also apply to internal components in an umbilical like steel tubes, and the umbilical as a global structure.

3.4.1 Bursting

If the difference between the external and internal pressure reaches a critical value bursting may occur. Bursting means a mechanical breach of the pressure vessel, and a permanent loss of pressure containment.

3.4.2 Local buckling

Tube buckling

Buckling of the pressure vessel as a result of excessive external pressure forces. This state occurs when the external pressure p_{ext} is larger than the collapse pressure p_c.

Propagation buckling

Propagation buckling cannot be initiated unless local buckling has occurred. In order to get buckling of the pressure vessel, the external pressure needs to be larger than the collapse poressure p_c. Initiation pressure p_{init} is the pressure required to start a propagating buckle, this pressure depends on the size of the initial buckle. Propagating pressure p_{pr} is the pressure required to continue a propagating buckle according to DNV [2010]. The pressures has the the following relationship: $p_c > p_{init} > p_{pr}$

Combined loading

Distinction is made between 2 conditions: *Load-Controlled condition*, the structural response is primarily governed by the imposed loads. *Displacement-controlled condition*, the structural response is primarily governed by imposed geometric displacements. Buckling due to combined loading implies that the buckling is a result of a combined load state, with both geometric displacements and imposed loads.

3.4.3 Global buckling

Global buckling implies buckling of the pressure vessel as a bar in compression. The effect of external and internal pressure should be taken into account. Distinction shall be made between load-controlled and displacement controlled buckling according to DNV [2010].

3.4.4 Material failure

When a structural component is subjected to stress that exceeds the material yield stress, plastic deformation will occur. This can lead to both local and global failure. Several environmental factors are important for material failure, the most important being temperature. High temperature can be critical to metals like copper, which has a low creeping temperature. When metals are exposed to low temperature, the risk of brittle fracture increases.

Chapter 4

Material properties and manufacturing

4.1 Copper

The conductors of the umbilical modeled in this thesis are made of copper. There are several reasons for why copper is the preferred material for conductors:

- High conductivity
- Ductility
- Corrosion resistance
- Fatigue resistance
- Production cost

Pure copper (99.99% Cu) is a noble metal, with high conductivity. Copper exhibit high conductivity because of its conduction electrons show relatively little resistance to movement under an electric field. Copper in particular is an excellent conductor because outermost electrons have a large mean free path (about 100 atomic spacings) between collisions. The electrical resistivity is inversely related to this mean free path. According to Pops [1999].

In the electrical cable industry two forms of copper is used for making copper conductors: electrolytic tough pitch (ETP) copper and oxygen-free electronic (OFE) copper. For the ETP conductors the highest conductivity is achieved for 200 parts per million (ppm) of oxygen. The disadvantage of ETP copper is that it is not recommended for use in hydrogen environments, due to its susceptibility to hydrogen embrittlement.

In hydrogen environments, it is recommended to use OFE copper to avoid problems with hydrogen embrittlement.

4.1.1 Production of copper wire

Production of electrical copper cables consists of several stages. The stages varies with the desired mechanical and conductivity properties of the finished product. Generally it can be divided into 4 stages, according to Pops [1999]:

Stage 1: Production of copper rods
Copper rods are made from solid pure copper by a continuous casting and rolling process. Benefits of continuous casting include less microsegregation of impurities, reduction of copper oxide particles on the surface, fewer steel inclusions resulting from contact with mill rolls, almost total elimination of welds, and lower overall processing costs.

Stage 2: Drawing copper wire
The copper rods are drawn through die casts, to make copper wire. The die casts initial diameter is the same as the rod, but it is gradually reduced. This causes the diameter of the copper rods to shrink, as well as increasing the length. The process is usually done with no added heat, thus being a cold work process. Multiple die casts are used until the wire has its desired diameter. Since it is a cold work process, stress and strains are introduced to the wires, thus making them more brittle. The finished wires are spooled onto reels.

Stage 3: Annealing
The wire made in stage to is put into an electrical furnace, heating it to above the recrystallization temperature and then cooled down again. Annealing occurs by the diffusion of atoms within a solid material, so that the material progresses towards its equilibrium state. Heat is needed to increase the rate of diffusion by providing the energy needed to break bonds. The movement of atoms has the effect of redistributing and destroying the dislocations in metals. The effect of annealing is that the dislocations imposed by the drawing process are removed, and the copper becomes ductile again. The process must take place in a protected environment, to avoid oxidation.

With different production processes, annealing could be applied to the finished wire, or sometimes in between drawing dies.

Stage 4: Creating cables
The finished copper wire can either be used as is, or they can be cabled together. The umbilical of interest in this thesis consists of several stranded copper wires, cabled together. The wires are put into a stranding machine, bunching them together to the desired configuration. The finished stranded cable are then drawn through a nossle for compacting and ensuring a circular shape. In figure 4.1 a concentric cable consisting of 19 stranded wires with insulation are shown.

Figure 4.1: Concentric copper cable

Chapter 5

The finite element method

5.1 Introduction

The theory and concept behind the finite element method is complex and extensive. Several books about the theory behind it and its application exists. It is assumed that the reader is familiar with the finite element method, and only applications and concepts that are essential for the analysis part of this thesis will be treated.

5.2 Foundation

The finite element method is based on 3 principles according to Sævik et al. [2010]:

1.Equilibrium
Known from structural mechanics to be equilibrium of forces and moments.

2.Kinematic compatibility
Compatibility in the structure means that all adjacent cross sections will have the same displacement and deformation and that the material itself will be continuous as it deforms. No cracks will occur and the strain will be finite. According to Sævik et al. [2010]

3.Material law
Stress-strain relationship. Exemplified by Hooke's law as $\sigma = E\epsilon$.

5.2.1 Governing equations

The 3 principles is then combined into differential equations. These equations are then organized into matrix equations. For static problems the global matrix equation including all the degrees of freedom in the system can generally be written as in equation 5.1. $\mathbf{R}$ is termed the load vector, and includes all external loads. $\mathbf{K}$ is termed the stiffness matrix, and can generally include both linear and nonlinear terms. $\mathbf{r}$ is the displacement vector.

$$\mathbf{R} = \mathbf{K}(\mathbf{r})\mathbf{r} \tag{5.1}$$

Equation 5.2 is the general equation of motion. $\mathbf{Q}(\mathbf{t})$ is the global dynamic load vector. $\mathbf{M}$ is generally the mass matrix. $\mathbf{C}$ is the damping matrix, and $\mathbf{K}$ and $\mathbf{r}$ are the same as the static case.

$$\mathbf{M}\ddot{\mathbf{r}} + \mathbf{C}\dot{\mathbf{r}} + \mathbf{K}\mathbf{r} = \mathbf{Q}(\mathbf{t}) \tag{5.2}$$

5.3 Nonlinear FEM

In mathematics nonlinear systems represent systems whose behavior are not expressible as a sum of the behaviors of its predictors. In particular, the behavior of nonlinear systems are not subject to the principle of superposition.

As mentioned in section 5.2.1 the differential equations governing the system can be both linear and nonlinear. The umbilical studied in this thesis will contain several nonlinear features. Nonlinearities withing the finite element method can according to Sævik et al. [2010] be classified into 3 effects:

1. Geometry
Nonlinear behavior occurs when the stiffness matrix **K** and/or the load vector **R** from equation 5.1 becomes functions of the displacement vector **r**. A typical example is so called "snap-through" buckling.

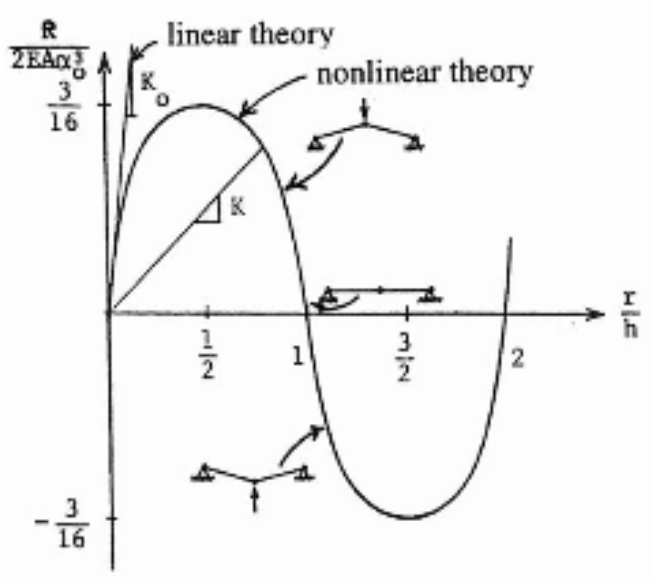

Figure 5.1: Snap-Through buckling

2. Material
Figure 5.2 shows a typical measured stress versus strain curve for a metal. By examining the curve, it is clear that real metals behavior cannot be modeled with linear theory alone. Linear theory is typically applied up to the point of yielding. There are several different material models associated with the finite element method on the marked. The 2 most relevant material models for this thesis is treated in section 5.3.1.

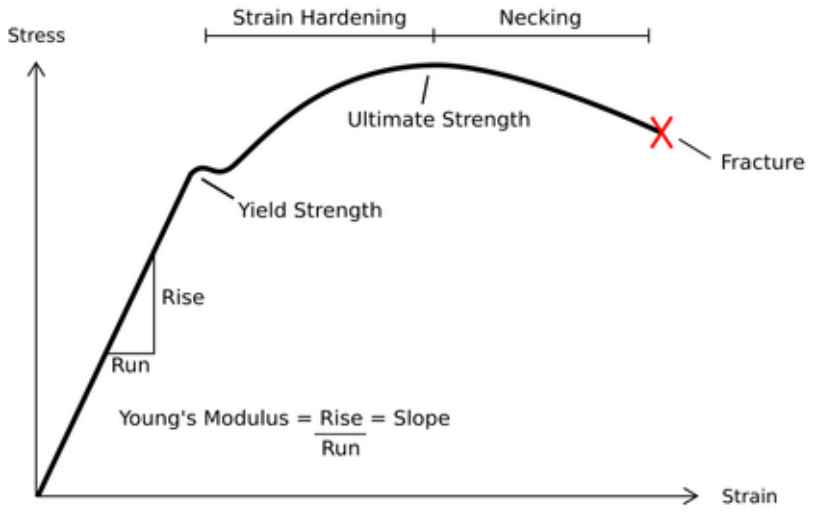

Figure 5.2: Typical stress-strain curve for a metal

5.3.1 Metal plasticity

According to Sævik et al. [2010], the metal plasticity theory is based on the following principles:

1. The total strain can be divided into a plastic and an elastic component:

$$\epsilon = \epsilon^e + \epsilon^p \tag{5.3}$$

2. The elastic component ϵ^e can always be calculated by the elastic material law:

$$\epsilon^e = (C^e)^{-1} : \sigma \tag{5.4}$$

3. The plastic strain ϵ^p is calculated based on:

(a) Yield criterion, generally expressed in term of a yield function f:

$$f(\sigma, \bar{\epsilon}^p) = 0 \tag{5.5}$$

where σ is the stress tensor and $\bar{\epsilon}^p$ is the equivalent plastic strain used to describe hardening. Equation 5.5 can be interpreted as a yield surface in the 6 dimensional stress space. for $f < 0$ the stress is in the elastic range, and the total strain ϵ is governed by the elastic component ϵ^e. Plastic strain occurs for $f = 0$ which is at the yield surface. $f > 0$ has no meaning, as it is outside of the yield surface. The stress must remain on the yield surface during plastic deformation. This is ensured by the *consistency condition* given in equation 5.6.

$$df = \bigtriangledown_\sigma f : d\sigma + \frac{\partial f}{\partial \bar{\epsilon}^p} d\bar{\epsilon}^p = 0 \tag{5.6}$$

(b) Flow rule:
The flow rule is normally based on Drucker's postulate for a stable material, where the following must be satisfied:
1. The yield surface is convex.
2. The plastic strain increment is parallel to the yield surface normal.
3. The plastic strain increment is a linear function of the stress increment.

(c) Hardening rule:
The hardening rule describes the hardening of the material after the yield limit is exceeded, and plastic deformation occurs. The 2 most common hardening models associated with the finite element method are *kinematic hardening*, and *isotropic hardening*.

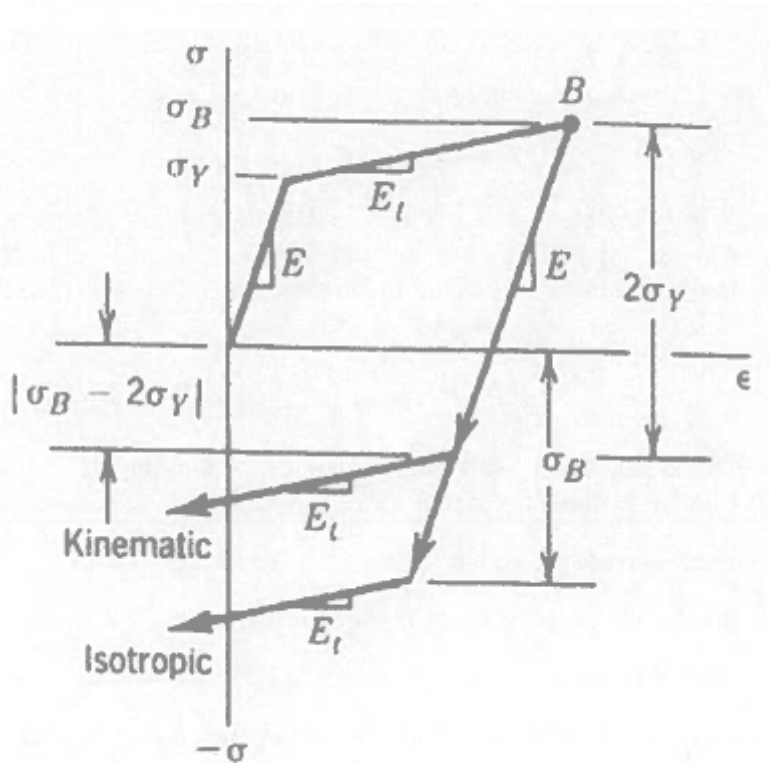

Figure 5.3: Isotropic and kinematic hardening

The principle of the 2 hardening models is shown in figure 5.3. The figure shows the stress-strain curve for a specimen undergoing uniaxial loading. Tensile loading is applied until the stress reaches a point σ_B in the plastic range, before it is unloaded, and finally compression loading is applied. The difference between kinematic and isotropic hardening are shown as the yield limit for the reverse loading. This occurs at $2\sigma_y$ for the kinematic model and at $-\sigma_B$ for the isotropic model. Most metals behave somewhere in between those models.

5.4 Methods used in Abaqus

5.4.1 Annealing

The anneal procedure is intended to simulate the relaxation of stresses and plastic strains that occurs as metals are heated to high temperatures. Physically, annealing is the process of heating a metal to a high temperature, to allow the micro structure to recrystallize, removing dislocations caused by cold working of the material. Then the metal is cooled down again, in a controlled manner. According to systemes [2007].

During the anneal procedure, ABAQUS/Explicit sets all appropriate state variables to zero. These variables include stresses, backstresses, strains, and velocities. According to systemes [2007].

5.4.2 Constraints

Kinematic coupling constraint is a constraint, which constrains a group of nodes to a reference node. It limits the motion of the group of nodes to the motion of the reference node. It requires that the user specifies a reference node, which acts as a master node for the constrained group of nodes which, becomes slave nodes. All translational and rotational degrees of freedom of the slave nodes can be constrained to the master node. This is mathematically formulated as $N = X^s - X^m$, where N is the reference configuration position of the slave node, X^m is the position of the reference node, and X^s is the position of the slave node. According to systemes [2007].

A variant of kinematic coupling constraint is the "Tie rigid body" constraint, which is applied to constrain an analytical rigid body.

5.4.3 Interaction

Contact definition

The overclosure distance h is used to determine if a master surface and a slave surface are in contact. The criteria is formulated as:

$h < 0$: No Contact

$h \geq 0$: Contact

In two dimensions the overclosure h along the unit contact normal $\vec{n}$ between a slave point X_{N+1} and a master line $P(\xi)$, where ξ parametrizes the line, is determined by finding the vector $(P(\xi) - \vec{X}_{N+1})$ from the slave node to the line that is perpendicular to the tangent vector $\vec{v}$ at P. This can be expressed mathematically as in equation 5.7 according to systemes [2007]

$$h\vec{n} = P(\xi) - X_{N+1} \tag{5.7}$$

when:

$$\vec{v}(P(\xi) - X_{N+1}) = 0$$

Hard contact

Hard contact is the general contact algorithm offered in Abaqus. The contact constraint is enforced with a Lagrange multiplier representing the contact pressure in a mixed formulation. Let the contact pressure be denoted p and the overclosure distance h, then the contact formulation can be expressed as equation 5.8 according to systemes [2007]:

$p = 0$ for $h < 0$: No Contact
$h = 0$ for $p > 0$: Contact

$$d\partial\Pi = \partial p dh + dp\partial h \tag{5.8}$$

5.4.4 Element technology

In the thesis outline in section it was stated that the umbilical should be modeled with volume and contact elements. After consultations with M.Sc. Frank Klæbo and Professor Svein Sævik it was decided to use the general 3D brick element, C3D8R.

C3D8R
The name C3D8R is an abbreviation for the key features of the element. C means that it is continuous, 3D that it is 3 dimensional, 8 is the number of nodes and R means that it has reduced integration capabilities.

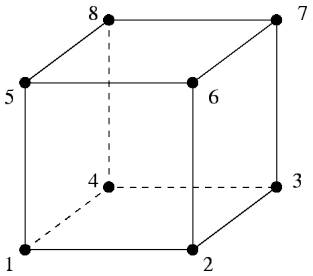

Figure 5.4: C3D8R

C3D8R is a first order isoparametric element. The isoparametric interpolation is s defined in terms of the isoparametric element coordinates g, h, r. They each span from $[-1, +1]$ with the origo at the center of the element. The interpolation function for the element is given in equation 5.9 according to systemes [2007].

$$\begin{aligned} u = &\frac{1}{8}(1-g)(1-h)(1-r)u_1 + \frac{1}{8}(1+g)(1-h)(1-r)u_2 + \frac{1}{8}(1+g)(1+h)(1-r)u_3 \\ &+\frac{1}{8}(1-g)(1+h)(1-r)u_4 + \frac{1}{8}(1-g)(1-h)(1+r)u_5 + \frac{1}{8}(1+g)(1-h)(1+r)u_6 \\ &+\frac{1}{8}(1+g)(1+h)(1+r)u_7 + \frac{1}{8}(1-g)(1+h)(1+r)u_8 \end{aligned} \tag{5.9}$$

5.4.5 Explicit dynamic analysis

The explicit dynamics analysis procedure in Abaqus/Explicit is based upon the implementation of an explicit integration rule together with the use of diagonal element mass matrices. The equations of motion for the body are integrated using the explicit central difference integration rule.

The key to the computational efficiency of the explicit procedure is the use of diagonal element mass matrices. Because the inversion of the mass matrix that is used in the computation for the accelerations at the beginning of the increment is triaxial as in equation 5.10. Here i is the increment, $\mathbf{M}$ is the diagonal mass matrix, $\mathbf{F}$ is the applied force vector and $\mathbf{I}$ is the internal force vector.

$$\dot{\mathbf{r}}^{(\mathbf{i})} = \mathbf{M}^{-1}(\mathbf{F}^{(\mathbf{i})} - \mathbf{I}^{(\mathbf{i})}) \tag{5.10}$$

The explicit procedure needs no iterations and no tangent stiffness matrix. According to systemes [2007]

Stability

The explicit procedure integrates through time by using many small time increments. The central difference operator is conditionally stable, and the time increment can be expressed as in equation 5.11, according to Sævik et al. [2010].

$$\Delta t < \frac{\lambda_e}{c} \tag{5.11}$$

In equation 5.11 λ_e is the characteristic element length, and c is the acoustic wave speed of the material. c is for metals generally expressed as:

$$c = \sqrt{\frac{\rho}{E}}$$

Where ρ is the density of the metal and E is the Young's modulus.

From equation 5.11 it is clear that the size of the stable increment time is solely dependent on the mesh properties, once material properties are defined. This proved to be a crucial factor for the analysis part in this thesis, and will be discussed later on.

5.4.6 Stress and strain

Stress components

Abaqus reports stress components as S_{ij} where $i, j \in [1, 3]$. S_{ii} is direct stress in the i direction, and S_{ij} is shear stress in the i-j plane. The stress components are Cauchy or "true" stress as defined in equation 5.12. Here A_c is the current area, F is the force and σ the stress.

$$\sigma = \frac{F}{A_c} \tag{5.12}$$

Von mises stress is defined in ABAQUS as in equation 5.13

$$\sigma_{mises} = \sqrt{\frac{3}{2}\mathbf{S} : \mathbf{S}} \tag{5.13}$$

Where $\mathbf{S}$ is the deviatoric stress defined as:

$$\mathbf{S} = \sigma + p\mathbf{I}$$

Here p is the equivalent contact stress defined as:

$$p = -\frac{1}{3}trace(\sigma)$$

Strain

The default strain components in ABAQUS/Explicit is logarithmic strain as defined in equation 5.14. The strain components follow the same orientation principle as the stress components.

$$\epsilon^L = \sum_{i=1}^{3} \ln \lambda_i \mathbf{n}_i \mathbf{n}_i^T \tag{5.14}$$

Where λ_i is the principal stretches and $\mathbf{n}_i$ are the principal stretch directions.

Chapter 6

Computer resources

6.1 Software

6.1.1 ABAQUS FEA

Abaqus FEA is a software package developed by Dassualt systems. The software package contains different modules for finite element method work:

ABAQUS/CAE: Post and preprocessor software.

ABAQUS/Standard: Implicit integration scheme solver.

ABAQUS/explicit: Explicit integration scheme solver.

ABAQUS/CFD: Computational fluid dynamic package.

The typical work flow for an operator working with ABAQUS FEA is shown in figure 6.1.

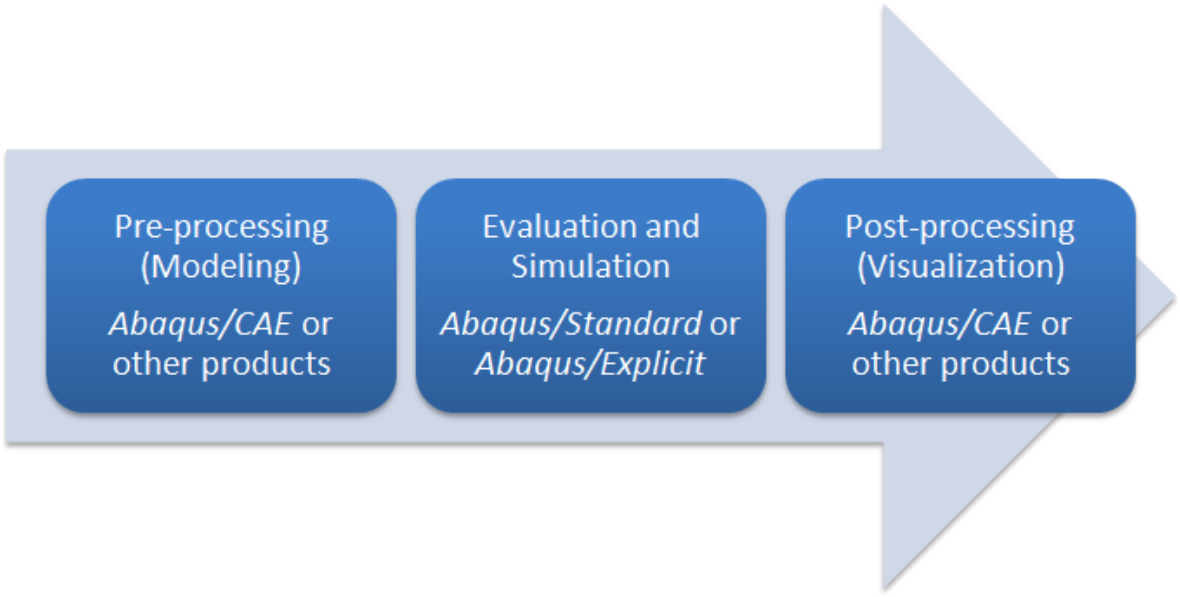

Figure 6.1: FEA process with Abaqus

ABAQUS/CAE v6.7 will be used for all pre-processing purposes in this master thesis. Post-processing of the result files will be done in ABAQUS/CAE v6.7 and MatLab R2010a.

6.1.2 MatLab

MatLab is a technical computing language developed by Mathworks. It is a computer programming language which has much in common with C and Fortran. However it has numerous built in function designed to make technical computing faster and more efficient. MatLab is a general programming tool capable of handling a wide array of tasks and visualize the results from these.

MatLab is chosen to visualize the results obtained from Abaqus FEA, because of the powerful built in plotting features.

6.2 Hardware

In Risa [2010] all the Abaqus analyses were run on a standard desktop computer. The lack of computational power proved to be a limiting factor for the results. A course mesh had to be used together with mass scaling, just to be able to run the analyses.

To eliminate the problem of computational power, it was decided that the analyses in this thesis should be run on a supercomputer. The advantage of running an explicit FEA on a supercomputer, is that the problem can be discretized into several domains. This means that all the DOF's are divided on the number of domains. Which again means that each domain only contains a small part of the total number of equations. The effect of this is that the run time for a given analysis is reduced significantly. As a rule of thumb, it is normal to use a 1 to 1 ratio between number of domains and number of processors.

6.2.1 Njord

Njord is the name of the supercomputer used in this master thesis. It is part of Notur -the Norwegian meta center for computational science. Table 6.1 contains key specifications about Njord found in Nagel [2010]. The operating system of Njord is IBM AIX, which is a Linux

Peak performance	23 [Tera flops/s]
Nodes	180
Processors	1536
Total memory	6.5 [TiB]
Centralized storage	100 [TiB]
Operating system	IBM AIX(Linux affinity)
Weight	30 [tonnes]

Table 6.1: Njord, technical specifications

affinity type operating system. This means that Njord is operated through a terminal without a graphical user interface. So software like ABAQUS has to be launched via a shell script. The script contains all the information Njord needs to run an analysis, for more information please see Nagel [2010], and the example script provided in appendix A. The result files are then exported from Njord onto a desired computer for post-processing of the results. In this master thesis ABAQUS/CAE was used to view and generate data files, and MatLab to create graphical plots.

Chapter 7

The finite element model

7.1 Introduction

The focus of this section is to explain how the finite element model of the umbilical was constructed. Point 2 under section gives a description of the fundamental properties of the umbilical:

By using ABAQUS, establish a 1 m long model for one 95 mm2 power conductor consisting of 1 + 6 + 12 circular wires installed in helix with pitch length obtained from measuring a real specimen. The model shall be based on volume and contact elements capable of handling friction between layers.

7.2 Units

ABAQUS FEA does not have an inherent system of units, and it is therefore up to the operator to choose an appropriate set of units. The system of units used in this thesis is presented in table 7.1.

System of units	
Length	$m \times 10^{-3}$
Mass	$kg \times 10^{3}$
Time	s
Force	N
Stress	MPa

Table 7.1: System of units

7.3 Axis system

The default global coordinate system in ABAQUS/CAE is the "right handed" Cartesian, shown in figure 7.1. Letters and numbers are used interchangeably to label the axes:

$$[x, y, z] = [1, 2, 3]$$

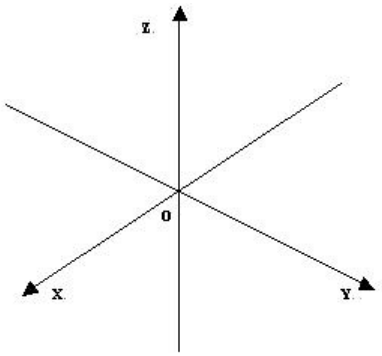

Figure 7.1: Global coordinate system

7.4 Geometry

It was decided that the model should consist of 19 copper conductors each with a circular cross-section with a radius $r = 1.25mm^2$. The pitch length for the helically twisted conductors was $L_p = 250mm$. In order to create a model of the umbilical, 3 parts were constructed:

Center conductor
It was created using the feature *solid revolve*. The top of the conductor was placed at the origin of the global coordinate system and a solid cylinder with radius $r = 1.25$ and height $h = 1000$ was created. The part was then partitioned into several sections. This was done to be able to give each partition its own mesh and material properties.

Layer 1 and 2 conductors
They were constructed in a similar fashion as the center conductor. The only difference being that a pitch length and a helical radius needed to be defined.

The parts were then assembled together to model the umbilical. The feature *radial pattern* was used to copy and place the helically twisted conductors around the center conductor.

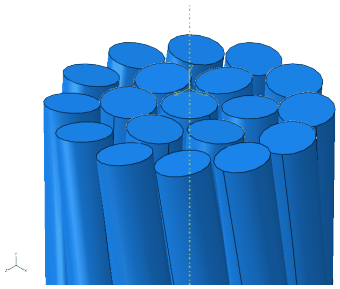

(a) Assembled

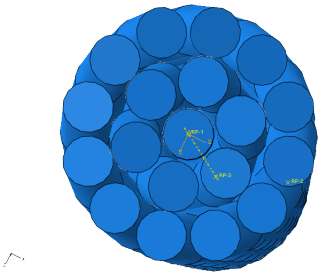

(b) Cross-section

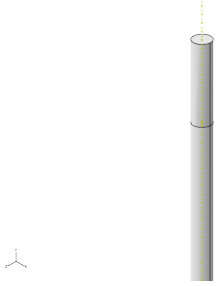

(c) Center conductor

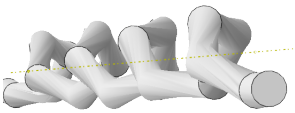

(d) Layer 1 conductor

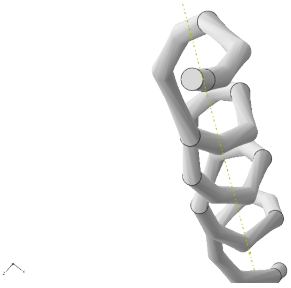

(e) Layer 2 conductor

Figure 7.2: Umbilical FE model

7.5 Interactions

7.5.1 Loads and boundary conditions

To be able to change boundary and loading conditions fast and efficiently, 2 reference points were created. The first located at the bottom of the umbilical at $[0, -1010, 0]$, and the second at the top at $[0, 10, 0]$. Kinematic coupling restraints were then made from the reference points to their respective end cross-sections, making the reference points masters and the coupling nodes slaves. This allowed applying boundary conditions and loads directly to the reference points, rather than to each node at the cross-section surfaces. This method was also used in Corre and Probyn [2009]. Figure 7.3 shows the kinematic coupling constraint at the top end.

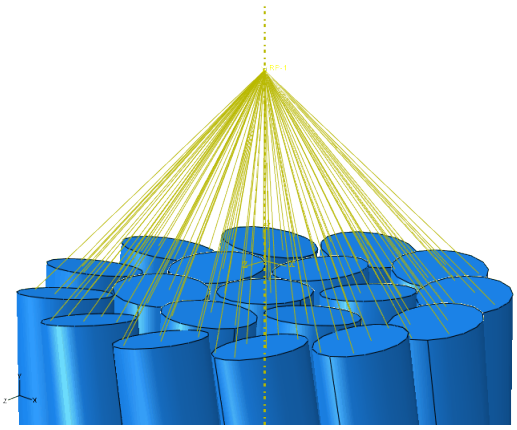

Figure 7.3: Kinematic coupling

7.5.2 Contact

In order to represent the real-life umbilicals physical behavior, modeling contact properties between the conductors are essential. The *general contact, "all with itself"* algorithm where ABAQUS automatically identifies all possible contact pairs in the model was used. *"Hard contact"* was selected as contact property. The techniques are described in section 5.4.3.

7.6 Contact surface

To achieve shrinking of the umbilical, two strategies were tested. The first attempt was made with a uniform pressure distribution attacking normal to the circumferential direction. This method failed, and it was abandoned after intensive testing. The second strategy employed was creating an analytical rigid part, shaped like a funnel. The umbilical was then translated through this part, causing it to plastically deform into the desired diameter.

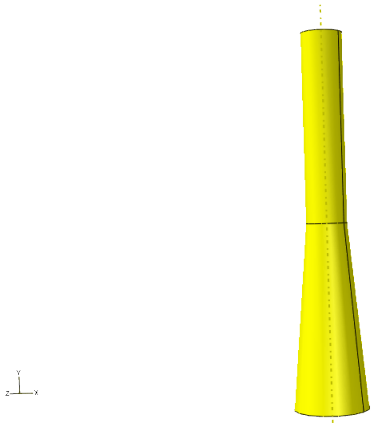

Figure 7.4: Funnel

The funnel was modeled as a 3 dimensional analytical rigid shell. Its initial radius is $r_i = 10mm$ and its final radius is $r_f = 5.5mm$, to shrink the umbilical to the target cross-section area of $95mm^2$. The constant area end-part is added for numerical stability. The *tie-rigid body* constraint was used together with a reference point to fix all translations and rotations.

Part II

Analysis set-up and results

Chapter 8

Hand calculations

8.1 Introduction

To get an estimate of stress and strain values, a few analytical calculations were performed. Simple formulas known from structural engineering was utilized, along with linear elastic theory. The main idea was to get an idea of how much the lay angle of layer 1 and 2 would affect the axial stress.

8.2 Stress and strain

8.2.1 Axial stress

The axial stress component was discussed in section 2.2.1 and it was stated that Navier's formula according to equation 2.2 is suited for solid bodies. However when applied to the umbilical, it is important to take the lay angle of the helical components into consideration. The relationship between pitch length, helical radius and lay angle is shown in equation 8.1.

$$L_p = \frac{2\pi R_h}{\tan(\alpha_h)} \tag{8.1}$$

Using equation 8.1 the lay angle for the umbilical was calculated:
Layer 1: $\alpha_h \simeq 1.79$[deg]
Layer 2: $\alpha_h \simeq 5.38$[deg]
Center: $\alpha_h = 0.0$[deg]
To simplify further calculations, the average lay angle for the umbilical was calculated:
Average lay angle: $\alpha_h \simeq 3.97$[deg]

The average normal force on the umbilical was then calculated based on the average lay angle:
$N_{avg} = \frac{N}{\cos(\alpha_h)} \simeq 9522.85$[N]

Finally the axial tension was calculated and found to be:
$\sigma_a = \frac{N_{avg}}{A} \simeq 102.10$[MPa]

8.2.2 Axial strain

Hooke's law was then utilized to get an estimate of the axial strain:

$$\epsilon_a = \frac{\sigma}{E} = \frac{102.10 \times 10^6}{115 \times 10^9} = 8.88 \times 10^{-4}$$

8.2.3 Key results

The key results from this chapter is summarized in table 8.1.

Axial stress σ_a[MPa]	Axial strain ϵ_a[-]
102.10	8.88×10^{-4}

Table 8.1: Hand calculations: Key results

Chapter 9

Tension

9.1 Introduction

Under point 3 and 5 in section it is stated:
Apply mean tension 0-9500-0 N and compare the strain-force curve with laboratory data.

Apply a typical stress-strain curve for copper and apply external pressure to "shrink" the specimen into the measured diameter. Repeat the analysis carried out in items 3-4. What is the effect of shrinking with respect to fatigue? Has the correlation with the measured data changed?

The model described in chapter 7 was used as a base for these calculations. In addition to the points mentioned above, it was also decided to run 2 different sets of boundary conditions, for the umbilical's top and bottom end surfaces.

9.2 Load condition

During the laboratory tests of the umbilical conducted at Marintek's laboratories a $10Hz$ load frequency was used. The results for this frequency was good. It was therefore decided to implement this load frequency to the ABAQUS model. To minimize transient effects, the load was applied as a *cosine* function. MatLab was used to create an input file for the force vector, and figure 9.1 shows a plot of it. The load was applied to the top reference point in the positive y-direction, resulting in tensile loading.

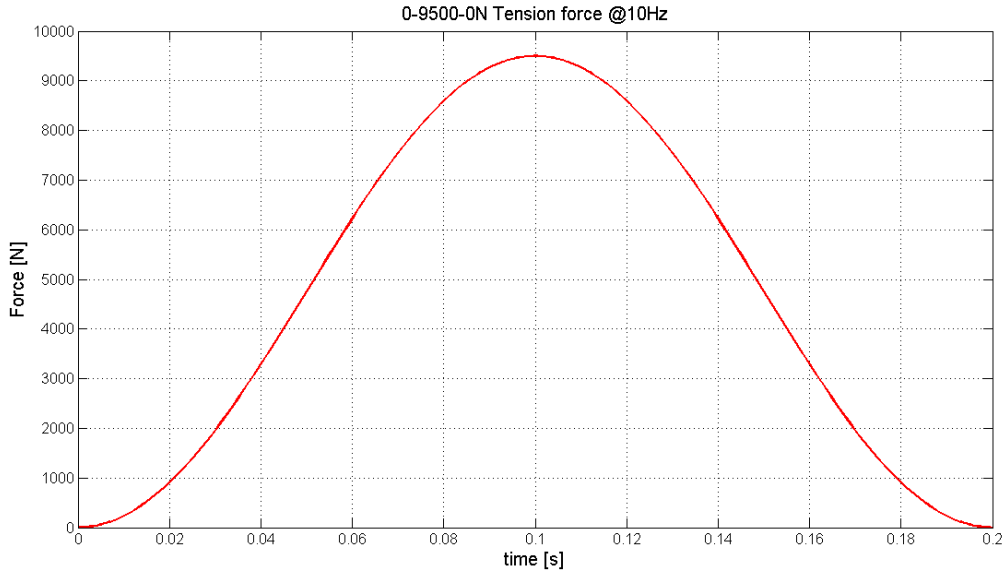

Figure 9.1: Tensile load vector

9.3 Mesh

In section 5.4.5 it was stated that the size of the stable increment for the explicit solution procedure, is governed by geometric features of the element. The finite element method is an approximate method, and convergence towards the correct solution is depended on the number of elements, among other parameters. This represents a challenge, and the line between cost and results have to be drawn. In the preface of this thesis, several tests with different mesh resolutions were tested with the elastic material model. The trend was that the axial stress was reduced with higher resolution as expected.

Unfortunately, computational problems with Njord, meant that the mesh resolution had to be restricted. For the elastic case, it was possible to run on 320 processors, but only 128 processors with the elastic-plastic model. Having more elements along the circumferential direction was prioritized over the length direction after consulting with professor Svein Sævik. Ultimately running a coarser mesh than initially desired means sacrificing some accuracy. The global height of the elements are $h = 1mm$, the other specifications are listed in table 9.1.

	Element type	Number of elements circumferential	$\frac{elements}{conductor}$
Center	C3D8R	13	13000
Layer 1	C3D8R	13	13091
Layer 2	C3D8R	14	14112
Umbilical	C3D8R	259	260890

Table 9.1: Mesh properties

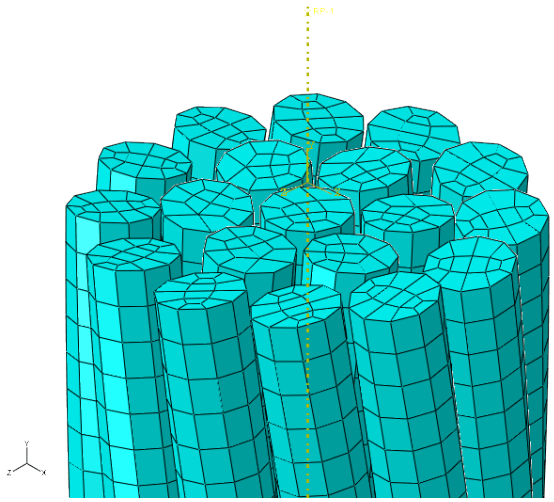

Figure 9.2: Mesh

9.4 Material model

Two material models were created to model linear-elastic and elastic-plastic material behavior. Input parameters for the material models were based on tensile testing of a single conductor at Marintek's laboratory. The test was conducted on a conductor taken from the outer most layer of the umbilical. The results of the tensile test are presented in figure 9.3. Consequently the stress and strain values are lower than for the inner layer and the core conductor. Tests performed at a later stage, revealed that for the center conductor $\sigma_y = 120\text{MPa}$ and $\sigma_{UTS} \simeq 250\text{MPa}$.

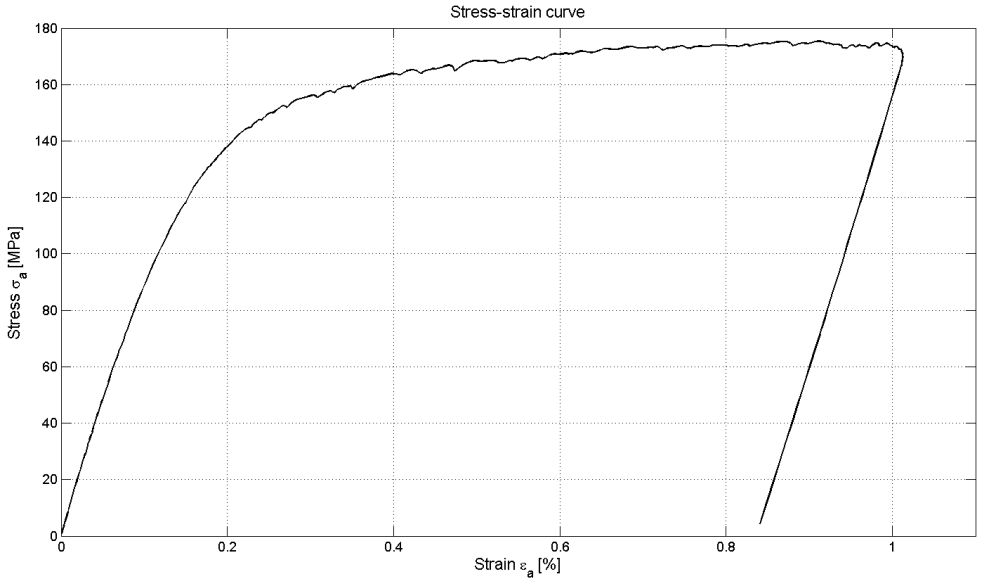

Figure 9.3: Stress-strain curve for outer most layer

By examining the data from figure 9.3 a stress-strain curve was created as input for ABAQUS. This curve is presented in figure 9.4. In this curve σ_y and σ_{UTS} is estimated as 80MPa and 175MPa accordingly.

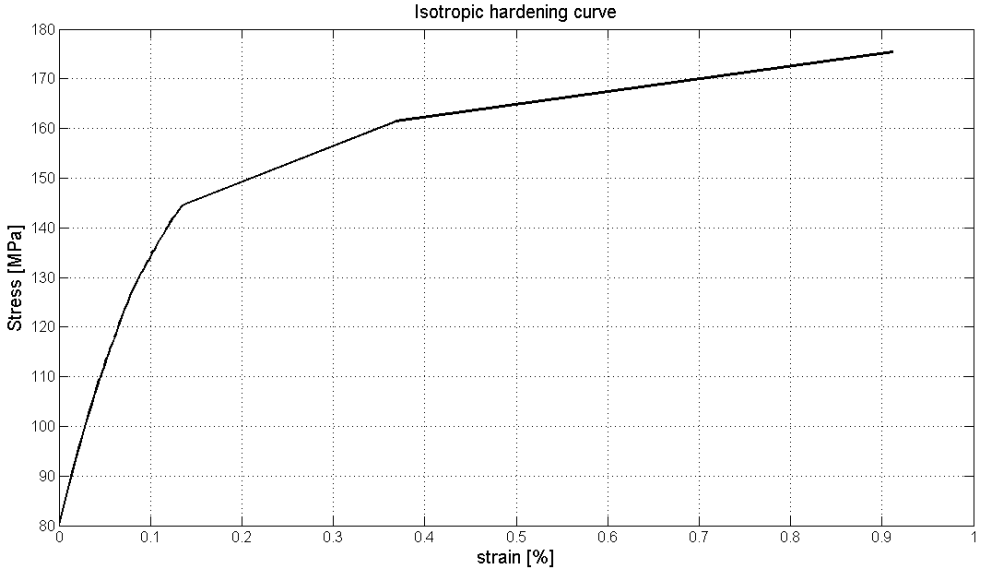

Figure 9.4: Isotropic hardening input

Originally it was decided to use a *kinematic hardening model*, but after a lot of testing, this proved unsuccessful. One factor may have been that ABAQUS only allows two sets of input data for this model: σ_y and σ_{UTS} and the corresponding strains. It was therefore decided to use a *isotropic hardening model*, where ABAQUS allows the user to define multiple stress-strain pairs, in between σ_y and σ_{UTS}. The data from figure 9.3, were then used to create the input for the isotropic hardening model, shown in figure 9.4.

The elastic material behavior was modeled without fail stress/strain. Table 9.2 shows the input parameters and their values.

	Copper
ρ	9000 $\frac{kg}{m^3}$
E	115000 MPa
ν	0.343

Table 9.2: Elastic material properties

9.5 Cases

The load case presented in section 9.2 was run in 4 different cases. In these cases material model and boundary conditions were varied. The key input parameters which differs from case to case is presented in table 9.3.

	DOF	Case 1	Case 2	Case 3	Case 4
Top reference point	x	free	free	free	free
	y	free	free	free	free
	z	free	free	free	free
	x-rot	free	free	free	free
	y-rot	free	fixed	free	fixed
	z-rot	free	free	free	free
Bottom reference point	x	fixed	fixed	free	fixed
	y	fixed	fixed	fixed	fixed
	z	fixed	fixed	free	fixed
	x-rot	fixed	fixed	free	fixed
	y-rot	fixed	fixed	free	fixed
	z-rot	fixed	fixed	free	fixed
Material model		Elastic	Elastic	Elastic-plastic	Elastic-plastic

Table 9.3: Input data for case 1 - 4

9.6 Analysis procedure

In ABAQUS analyses are divided into steps. In these steps load and boundary conditions are applied to the model. In this section the steps used to model the tension analyses will be explained.

9.6.1 Case 1 and 2

Step 1: Initial
Initial step where the boundary conditions are applied.

Step 2: Tension
The boundary conditions applied in *Initial* are propagated. The tension load is applied according to section 9.2.

9.6.2 Case 3 and 4

Step 1: Displacement
The umbilical is translated through the *funnel*, described in section 7.6. This causes the umbilical to plastically deform as the diameter is shrunk.

Step 2: Stop
In order to stop the motion created in the previous step, all degrees of freedom for all nodes in the umbilical are set to fixed. This causes the umbilical's motion to stop.

Step 3: Annealing
The built in procedure *annealing* is applied, as described in section 5.4.1. Effectively setting all the state variables to zero.

Step 4: Tension
All previous boundary conditions are removed. Boundary conditions according to table 9.3 are applied. The tension force is applied as described in section 9.2.

9.7 Results

9.7.1 Analysis data

All the cases were run at the supercomputer Njord. Some key data from the analyses are given in table 9.4.

	Case 1	Case 2	Case 3	Case 4
Integration scheme	Explicit	Explicit	Explicit	Explicit
Precision	Double	Double	Double	Double
Steps	2	2	4	4
Increment size	8.78×10^{-8}	8.76×10^{-8}	7.06×10^{-8}	7.26×10^{-8}
Total increments	1.97×10^{6}	2.27×10^{6}	10.28×10^{6}	10.18×10^{6}
Processors	320	320	128	128
CPU-time	04:27:08	05:21:51	132:50:38	129:24:27

Table 9.4: Analysis statistics

Note that there is a major difference between the elastic, and the elastic-plastic cases in CPU-time. This is mainly due to that these analyses had to be run on 128 processors. The reason for this was never determined. When the number of processors were set higher than 128 for the elastic-plastic cases, the analyses failed every time. After consulting the support department for Njord, effort was made to fix the issue, but ultimately it proved unsuccessful.

The data also shows that the maximum stable increment decreases from the elastic to the elastic-plastic cases. This can be explained by the shrinking process where the umbilical is plastically deformed, thus deforming the elements.

9.7.2 Stress and strain

The results from the analyses were post-processed in ABAQUS/CAE and MatLab. Particularly stress and strain components on an element level throughout the load history was of interest. By examining the model it was clear that that the stress levels near the top and the bottom were highly influenced by the boundary conditions. The stress levels at the top end are shown in figure 9.5

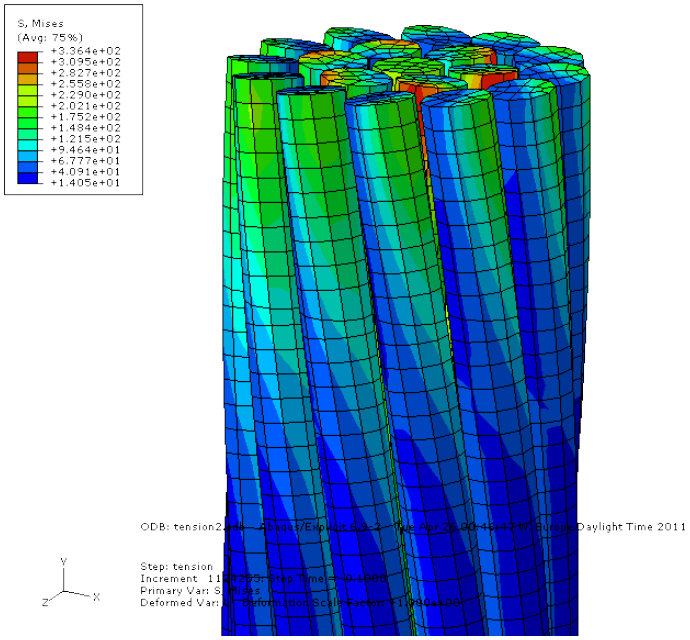

Figure 9.5: Von Mises stress state at the top end

According to the contour plot, the Von Mises stress reach values in excess of 336MPa. Therefore it was decided to measure stress and strain values at the center of the umbilical, $y = -500$, to minimize the effect of the boundary conditions.

The fact that the stress levels are so high near the top and the bottom of the umbilical, proved to be a challenge for the elastic-plastic cases. Clearly 336MPa of stress is outside of the defined isotropic hardening model, discussed in section 9.4. The result was large local plastic deformations that ultimately caused the analyses to 'blow up'. To overcome this problem the top and bottom 10mm of the umbilical were given a different material model.

After a lot of experimenting, a kinematic hardening model with the following parameters were chosen:
$\sigma_y = 400\text{MPa}$, $\epsilon = 0$
$\sigma_{UTS} = 800\text{MPa}$, $\epsilon = 0.09$
This allowed the umbilical to be plastically deformed in the shrinking step, while avoiding local plastic deformation in the tension step.

Figures 9.6 and 9.7 shows the axial stress for the cross-sections at $y = -500$. Note the big difference between the elastic and the elastic-plastic cases. In the elastic cases the difference between each layer is significantly larger than for the elastic-plastic cases. This will be elaborated in more detail later on in this section.

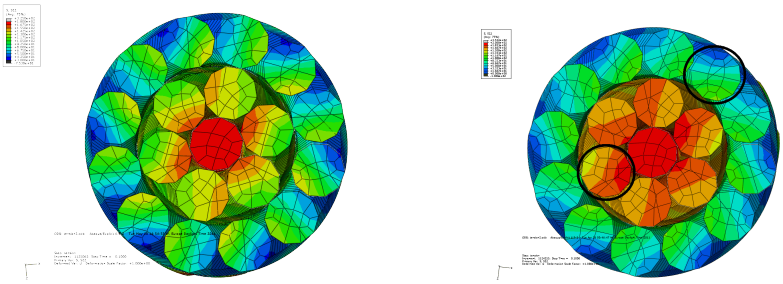

(a) Case 1 (b) Case 2

Figure 9.6: Stress state at the center elastic cases

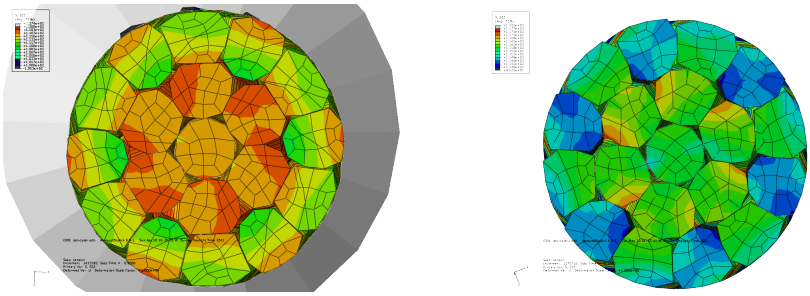

(a) Case 3 (b) Case 4

Figure 9.7: Stress state at the center elastic-plastic cases

One essential goal with the analyses, was to get a picture on how the different stress components varies with applied load. To do this all the elements over the cross-section at the center of the umbilical were chosen. The stress values taken at the integration points of the elements, were then recorded for the tension step. The average values were then calculated using ABAQUS/CAE. This was done for the complete umbilical, as well as for each individual layer. For the different layers, all the elements sorting to the layer was averaged.The stress values were then exported to a MatLab script for visualization and further post processing. Key values for stress and strain are presented in table 9.5.

Table 9.5: Stress and strain components

Axial stress σ_{22}[MPa]				
	Case 1	**Case 2**	**Case 3**	**Case 4**
Center	196.82	173.10	116.15	115.59
Layer 1	168.06	135.13	116.63	116.55
Layer 2	71.51	90.01	113.39	115.01
Average	106.87	107.77	114.51	115.51
Von Mises σ_{mises}[MPa]				
Center	201.87	176.31	116.84	116.69
Layer 1	175.35	139.03	117.71	117.16
Layer 2	83.83	93.43	113.72	116.65
Average	117.31	111.32	115.09	116.81
Axial strain ϵ_{22}[-]				
Center	1.7×10^{-3}	1.5×10^{-3}	5.91×10^{-2}	6.09×10^{-2}
Layer 1	1.5×10^{-3}	1.2×10^{-3}	6.05×10^{-2}	6.15×10^{-2}
Layer 2	6.4×10^{-4}	7.99×10^{-4}	5.09×10^{-2}	5.93×10^{-2}
Average	9.4×10^{-4}	9.55×10^{-4}	5.42×10^{-2}	6.00×10^{-2}

The results in table 9.5 are taken at the point of maximum load. Examining the results reveals several trends. The difference between stress values for the different layers decrease significantly from case 1 and 2, to case 3 and 4. This was expected as the shrinking process shrinks the layers together, giving larger contact areas. Secondly, in both the elastic and elastic-plastic cases, the average axial stress increases with more constraints at the ends. At the same time, it also gives the least difference in axial stress from layer to layer.

The average axial stress value increases with roughly 7.5% from the elastic cases to the elastic-plastic cases. This is due to ABAQUS reporting stress values as Cauchy stress, as described in section 5.4.6.The umbilical undergoes a shrinking process, and plastical deformation during the load step, which reduces the current area, thus larger stress.

The axial strain values are also much larger for the elastic-plastic cases. In fact, they are about 60 times larger than the linear-elastic cases. This is a direct cause of the material curve used, and coincides perfectly with the data in figure 9.3. The axial strain was estimated to 8.88×10^{-4}[-] in chapter 8, which is about 7.5% less than case 2.

To verify the strain data, the umbilical was measured in ABAQUS. It was done by selecting a node in the center of the center conductor at both ends. This was done both at the end of the shrinking step, and at peak load. After the shrinking process, no elongation of the umbilical had occurred. Suggesting that the only effect of the shrinking was packing density of the conductors. The elongation at peak load corresponded with the values in the table above.

9.7.3 Stress variation

By examining the contour plots in figure 9.6 and 9.7, it is clear that the axial stress varies over the cross section of the conductors. The stress patterns illustrated in the contour plots shows a symmetric behavior along the axial length of the umbilical. The maximum and minimum axial stress were measured over the cross sections of the conductors, to get an idea of how much it changes. The results are given in table 9.6. As expected the difference is greater for the elastic cases. The greatest difference is seen for layer 2, where the difference is over

Table 9.6: Stress variation over the conductors

	Case 1	Case 2	Case 3	Case 4	Unit
Center	14.76	7.94	1.85	1.61	MPa
Layer 1	76.00	51.83	4.79	3.04	MPa
Layer 2	107.64	100.33	6.94	1.85	MPa

100MPA, for both case 1 and 2. The trend in all the cases are that the difference is increasing from the center conductor to layer 2 conductor. However, this does not apply for case 4, which shows a decrease from layer 1 to layer 2.

9.7.4 Distance between hot spots

The axial stress shows a symmetrical pattern along the axial direction of the umbilical. This is illustrated in figure 9.8, where the hot spots are clearly visible. The hot spots are thought to be located at contact points between layer 2 and layer 1. The distance between the hot spots were measured in ABAQUS. For case 3 the distance was measured to 9.01mm, and 10.55mm for case 4. Although showing similar symmetry, this was not possible to measure for case 1 and 2. Contour plots showing the stress pattern for all the cases are given in the appendix.

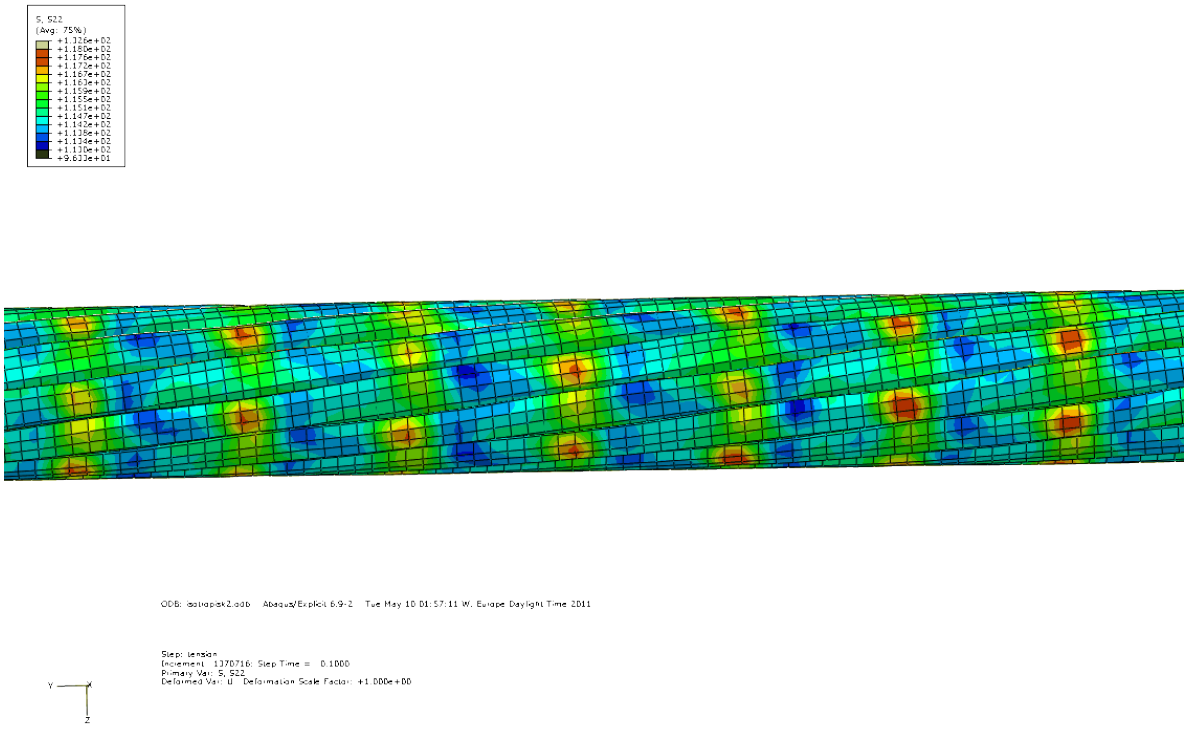

Figure 9.8: Axial stress pattern case 4

9.7.5 Case 1

In figure 9.9 axial stress is plotted against the load history. The stress history follows the shape from the load history, shown in figure 9.1. The difference in axial stress between the layers are big throughout the load history. Especially the difference between layer 2 and

the center conductor is significant. This is because of the small contact areas between the conductors.

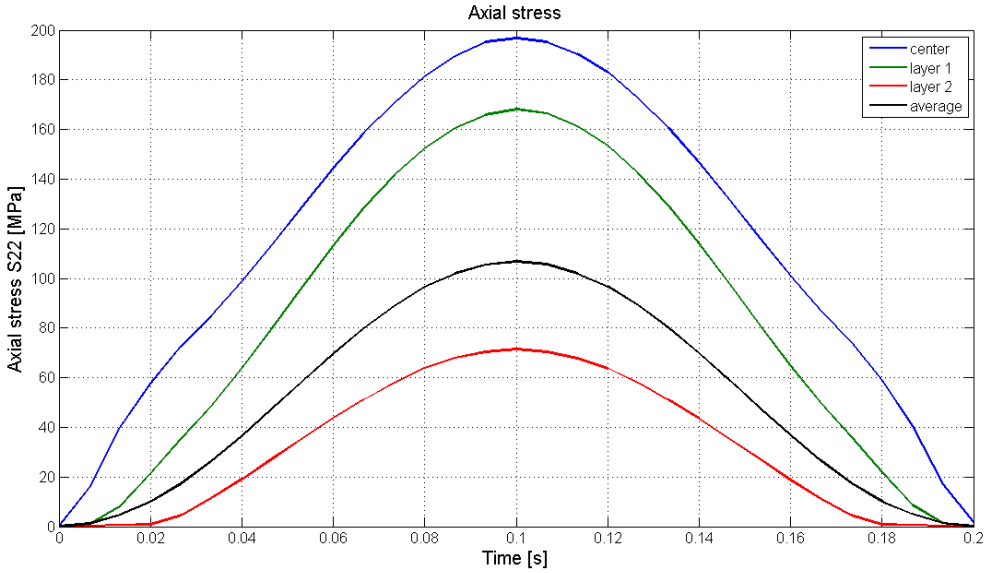

Figure 9.9: Axial stress, Case 1

In figure 9.10, average axial stress is plotted versus average logarithmic strain. It is clear that the results follows linear elastic theory. Both the loading and the unloading follows the same linear line segment. The slope confirms that the Young's modulus is 115GPa, the same as the input.

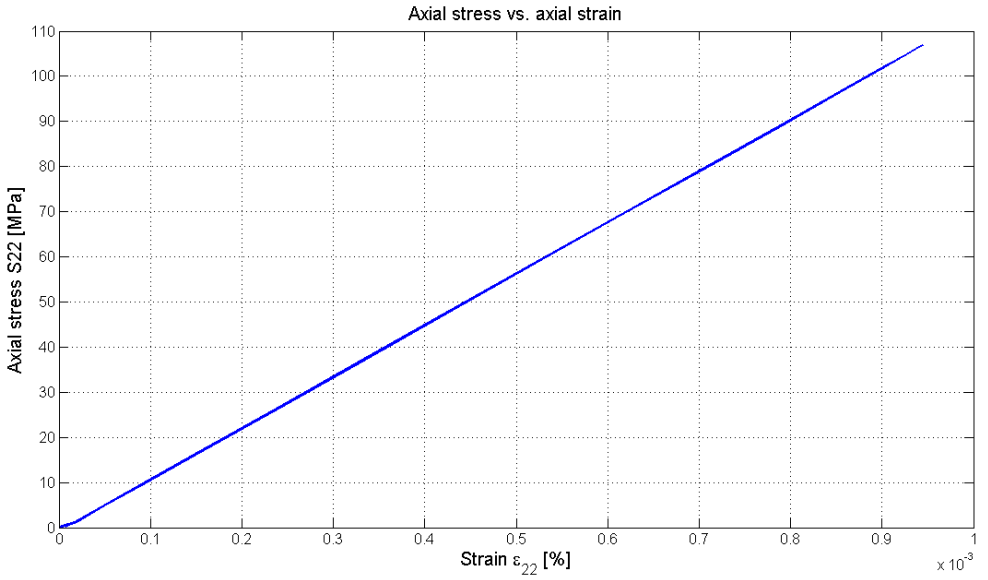

Figure 9.10: Axial stress versus strain, Case 1

9.7.6 Case 2

Axial stress for the load step is plotted in figure 9.11. Again it shows a significant difference in stress values for the different layers. By comparing the plot in case 1 and case 2, it is seen that the difference is reduced. This is probably because of the difference in boundary conditions. The logic behind that assumption is that it forces the conductors to come into contact with each other. This will then give greater contact stress, thus deforming them more. Which in turn will give higher stress levels, because the cross-section area is reduced.

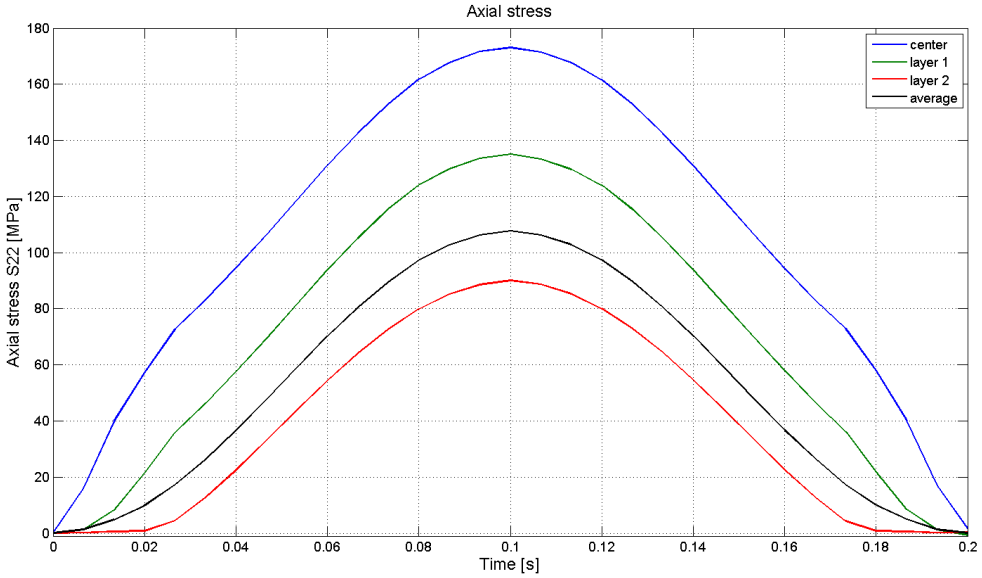

Figure 9.11: Axial stress, Case 2

9.7.7 Case 3

Axial stress is plotted for the load step in figure 9.12. The plot illustrates the effect of the shrinking process, as it is clear that the difference between the layers are reduced compared to case 1 and 2. The difference is larger before the point of yielding, which can be explained by the shrinking process and the boundary conditions. After the umbilical passes through the funnel, it becomes less compact, because of the spring back. This is a weakness with the model, as the real life umbilical is restrained from this movement. The fact that the boundary conditions allows rotation, is clear when examining the deformed shape. In figure C.16 a conductor from layer 2 is shown in its deformed shape at the point of maximum load.

The boundary conditions are also believed to be the cause of the irregularity at the point of zero load. At which point the center conductor is subjected to compressive stress of -40MPa.

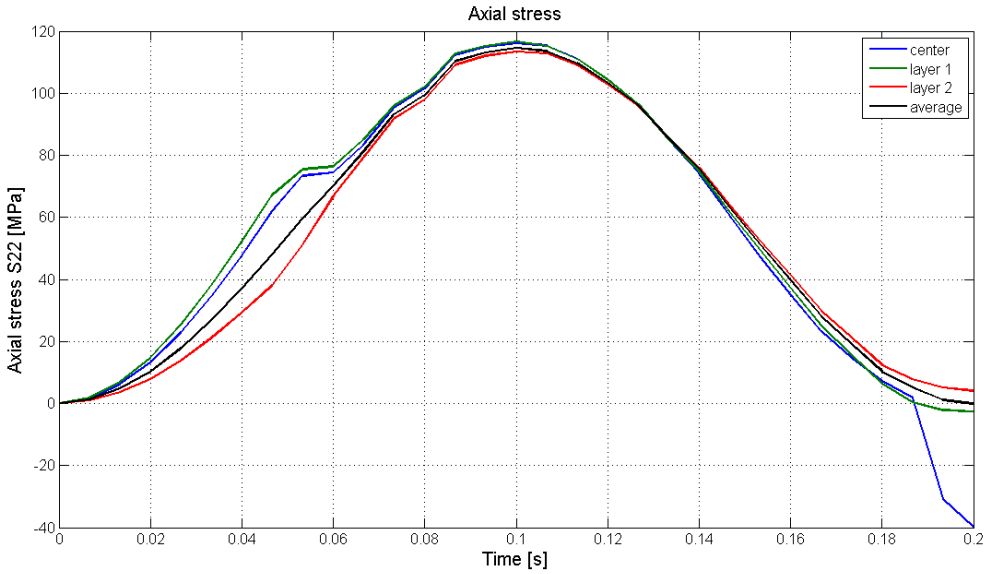

Figure 9.12: Axial stress, Case 3

The stress versus strain plot in figure 9.13, illustrates that the plastic strain is the dominant part of the total strain. It also proves that the umbilical's stress versus strain course, coincides well with the one from the laboratory test, from figure 9.3.

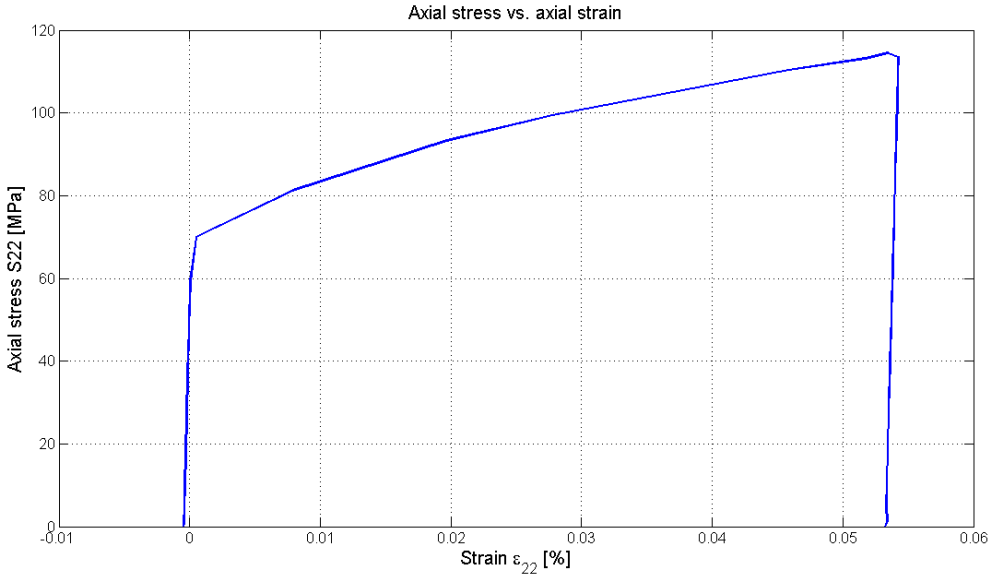

Figure 9.13: Axial stress Vs. Axial strain, Case 3

9.7.8 Case 4

The axial stress course for case 4 is similar to the one observed for case 3. However it is noted that the increased constraints in the boundary conditions leads to less variation in the stress. In fact, after the point of yielding, it is hard to separate the curves.

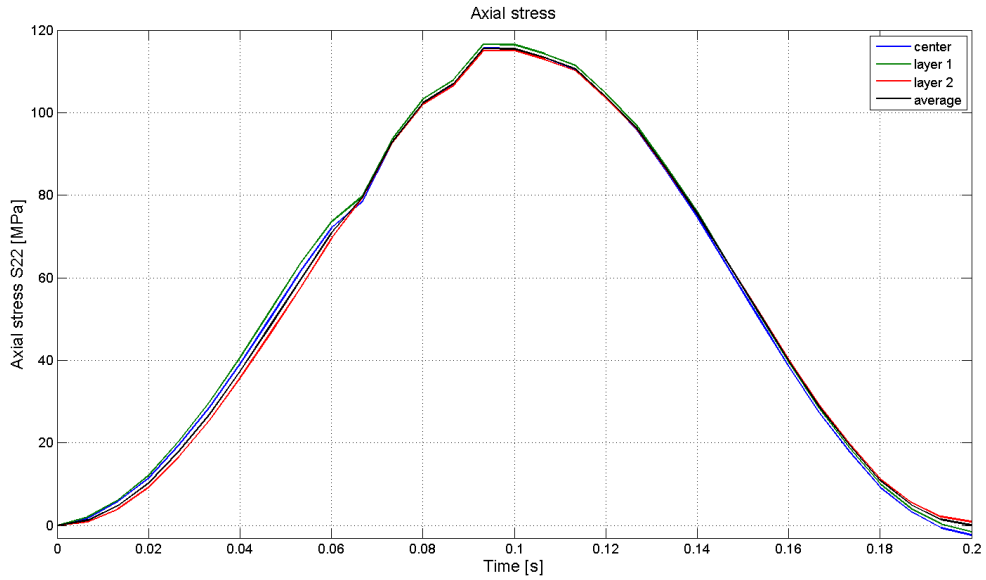

Figure 9.14: Axial stress, Case 4

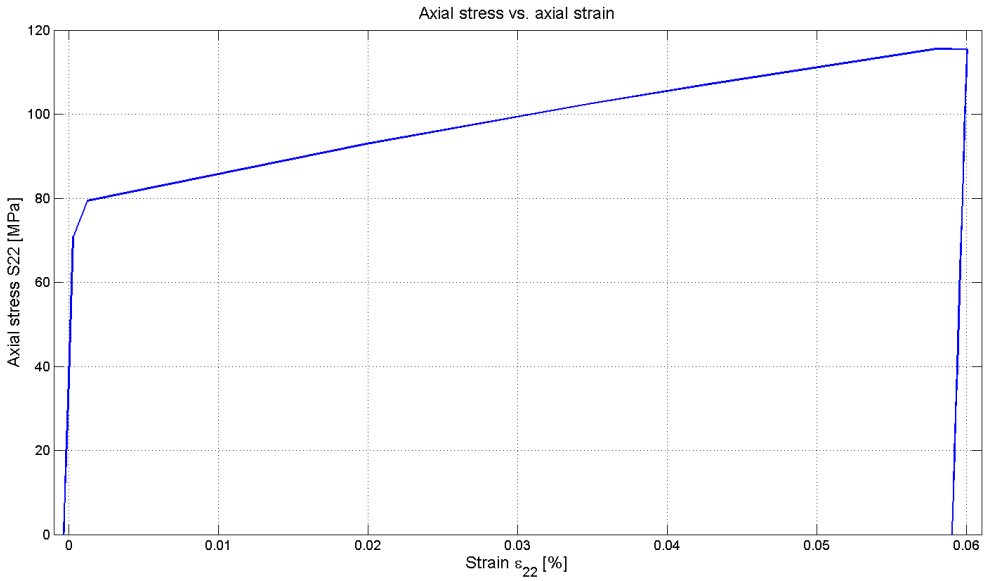

Figure 9.15: Axial stress Vs. Axial strain, Case 4

The stress versus strain curve of figure 9.15, follows the same trend as the one for case 3. The area of plastic strain does however look more linear. In both cases the unloading follows an approximately linear course, which is expected.

9.8 Laboratoy results

PhD. student Fachri Nasution conducted several tests of a full scale umbilical. The tests included dynamic tensile loading of both the complete umbilical, as well as tests on single

conductors. The graph in figure 9.16 shows tensile loading plotted against axial strain, for the complete umbilical. The test was performed at a frequency of 10Hz. Notice that the umbilical was subjected to several load cycles with a maximum tensile load of 16600N. In comparison, the ABAQUS analysis was done for 1 cycle with a maximum tensile load of 9500N.

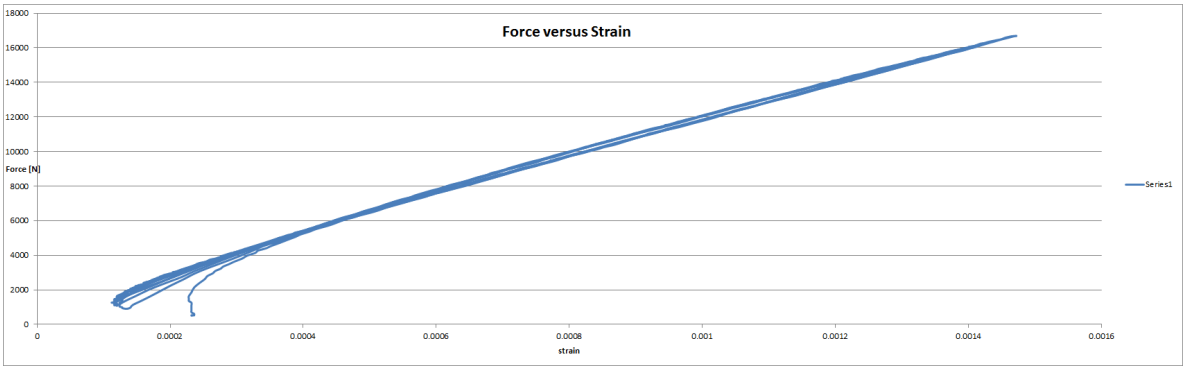

Figure 9.16: Force versus Strain

The difference between the material behavior of the laboratory results and those used in ABAQUS are significant. This is apparent when comparing figure 9.16 with the stress-strain curve of figure 9.15 for case 4.In figure 9.16 there is an approximately linear relationship between force and strain throughout the load range. Whereas in Case 4 the relationship becomes nonlinear after the yield limit at 80MPa.

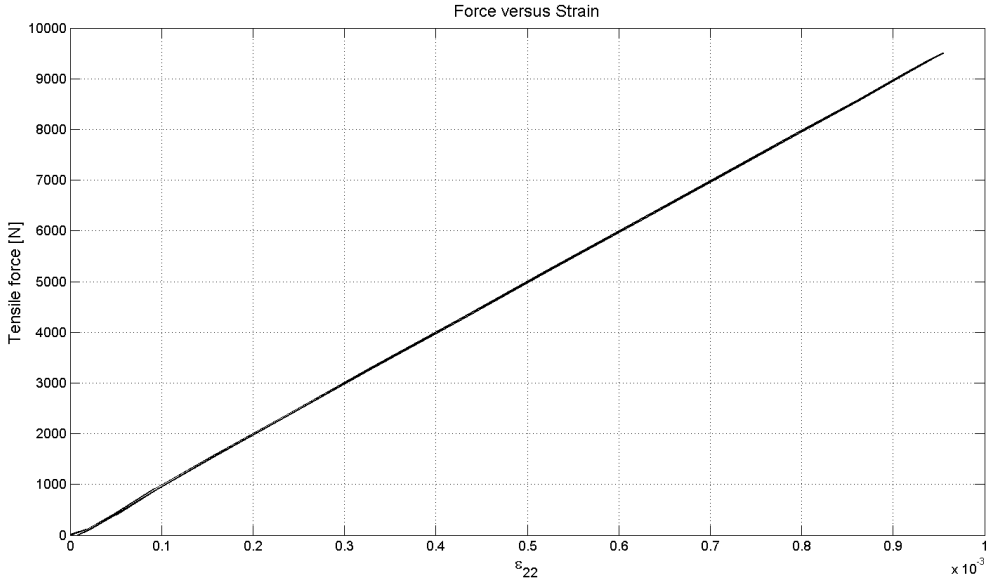

Figure 9.17: Force versus Strain, Case 2

The slope from the graphs in figure 9.17 and 9.16 are given in table 9.7, as well as the strain at 9500N. Note that the slope from the laboratory data gives a Young's modulus of 115.6GPa. This coincides with the value used in ABAQUS. When the force versus strain curves are compared, the slope of the 2 curves are different. This is because the ABAQUS analyses gives higher values for strain than the laboratory test. By using Hooke's law, the difference becomes

clear:

$\sigma_{ABAQUS} = 109.83\text{MPa}$
$\sigma_{Laboratory} = 89.24\text{MPa}$

This indicates that the axial stress from ABAQUS is higher than what was expected. At the same time the stress from the laboratory test is lower than expected. However it is important to note that the strain data from the laboratory test is very sensitive to the measuring instruments used. Particularly calibrating the strain to be 0 for 0 force is difficult.

	Case 2	Laboratory
slope, $\frac{dy}{dx}$	10.04×10^6	11.56×10^6
ϵ_{22} @ 9500N	9.55×10^{-4}	7.76×10^{-4}

Table 9.7: Comparison laboratory versus Case 2

Chapter 10

Dynamic tension

10.1 Introduction

In the thesis outline given in section , it was stated:

Apply mean tension in one end to 116.05 MPa average stress. Then vary the tension between 211 MPa and 21.1 MPa average stress. Investigate the stress variations versus the analytical mean values. Do the same exercise with 111 and 11 MPa (mean =61 MPa). Perform a simple fatigue calculation based on single tendon fatigue curve and find the number of cycles to failure.

Apply a typical stress-strain curve for copper and apply external pressure to "shrink" the specimen into the measured diameter. Repeat the analysis carried out in items 3-4. What is the effect of shrinking with respect to fatigue? Has the correlation with the measured data changed?

The analyses in this section is based on the experience from chapter 9. That means that all relevant properties for the cases in this section, are identical to those in section 9, unless otherwise is stated. This is done for simplicity, and to be able to compare results across load cases.

10.2 Load condition

The same principals as in section 9.2 were used. The tension force F_{mean} corresponding to the mean stress σ_{mean}, was calculated based on a cross-section area of $95mm^2$. The results are given in table 10.1.

	Range 1
σ_{max}[MPa]	111
σ_{mean}[MPa]	61
σ_{min}[MPa]	11
$F_{mean}[N]$	5795

Table 10.1: Input data for tensile loading

A script was written in MatLab, to create an input vector for the ABAQUS analyses. This is plotted in figure 10.1. Again a *cosine* curve was applied to reduce transient effects. The load frequency was 10Hz.

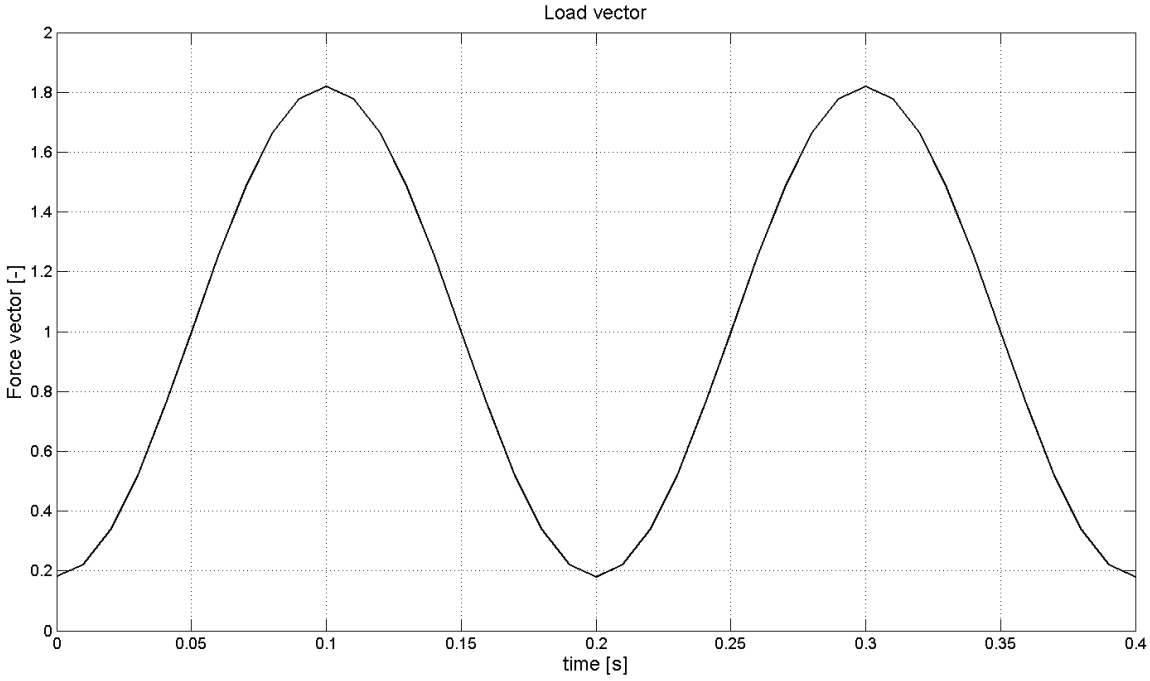

Figure 10.1: Load vector

It was chosen to do 2 load cycles at 10Hz as seen in the graph. Ideally more cycles are desired. However each cycle is "computationally expensive". In fact the "price" of one cycle is roughly: $\frac{time}{\frac{time}{increment}} = \frac{0.2}{7.5\times10^{-8}} = 2.67 \times 10^6$[increments].

10.3 Cases

For the load case presented in section 10.2, 4 individual cases were analyzed. These cases were set up in the same way as for the ones discussed in section 9.5. In fact the only difference between them are the load step.

10.4 Fatigue calculations

In section 2.3.1 the basic equations based on the paper "Lifetime theory" by Sævik [1999] was presented. The fatigue calculations in this thesis will be based on the SN curve from Karlsen [2010]. The SN curve is given in figure 10.2.

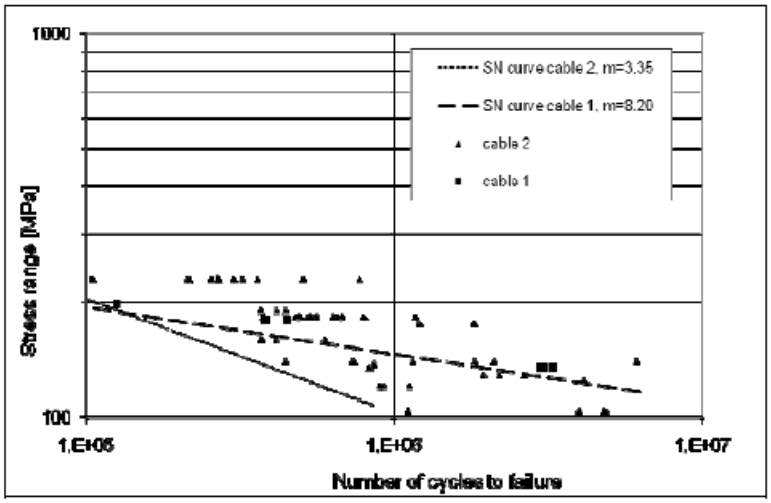

Figure 3 : SN curves for wires from Nexans conductors

Figure 10.2: SN Curve

According to Karlsen [2010]:
Axial fatigues testing of copper wires from all parts of the cross section from two different Nexans cables have been performed. By linear regression the slope of the curves were found to be 8.20 and 3.35 for the 3.5 and 2.5 mm wires respectively. The 2.5 mm wires were taken from the 95 mm2 conductor made as basis for this study. All tests were performed in stress control at R=0.1 at between 10 and 20 Hz.

10.4.1 Equations

The modeled umbilical has conductors with a diameter of 2.5mm. Therefore the slope corresponding to 3.35 was used. To be able to use the SN curve, the following steps were made:

Step 1:
$\Delta\sigma_0^c$ was calculated based on the results. The superscript "c" indicates calculated values based on the results.

$$\Delta\sigma_0^c = \frac{\Delta\sigma^c}{1 - (\frac{\sigma_m^c}{\sigma_{UTS}})^2}$$

Step 2:
Next expressing σ_m^t and $\Delta\sigma^t$ by the R-ratio $R = \frac{\sigma_{min}}{\sigma_{max}}$. Here the superscript "t" refers to the SN curve.

$$\Delta\sigma^t = (1 - R)\sigma_{max}$$

$$\sigma_m^t = \frac{1}{2}(1 + R)\sigma_{max}$$

Step 3:
Using the expressions from step 2, σ_m^t can be expressed as:

$$\sigma_m^t = \frac{(1 + R)\Delta\sigma^t}{2(1 - R)}$$

Further the following relationship between the SN curve and the results can be established:

$$\Delta\sigma_0^c = \frac{\Delta\sigma^t}{1 - (\frac{(1+R)\Delta\sigma^t}{2\sigma_{UTS}(1-R)})^2}$$

Which finally gives a quadratic equation with respect to $\Delta\sigma^t$:

$$(\Delta\sigma^t)^2\Delta\sigma_0^c(\frac{1 + R}{2\sigma_{UTS}(1 - R)})^2 + \Delta\sigma^t - \Delta\sigma_0^c = 0 \tag{10.1}$$

10.4.2 Calculation procedure

Step 1:
Locate the element with the highest stress concentration. This was done by using ABAQUS to locate the element with the highest axial stress, excluding the zones affected by the boundary conditions. Axial stress was chosen as the deciding parameter, since the loading condition is purely tensile.

Step 2:
Extract values for all the stress components, and export them to MatLab.

Step 3:
MatLab was then used to locate the maximum and minimum values for the axial stress. Based on their location in the time history, the corresponding values were selected for the other stress components. This is illustrated in figure 10.3, where the maximum and minimum values are encircled. The stress component $\Delta\sigma_0$ was then calculated.

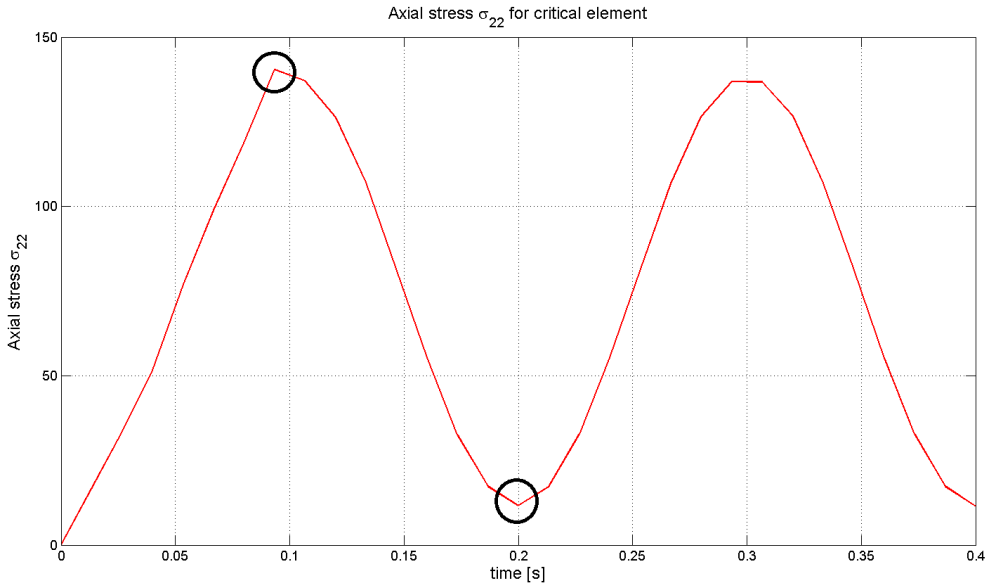

Figure 10.3: Axial stress for critical element case 4

Step 4:
MatLab was used to solve equation 10.1, and to determine the number of cycles to failure, from the SN curve in figure B.1

Chapter 11

Results Range 1

11.1 General

The analyses in this section has a lot in common with those done in chapter 9. It is therefore no surprise that the results show similar behavior. Conclusions made about the stress and strain distribution made previously, are valid also for these analyses. The stress and strain part of the results, will not be treated in as great detail as in chapter 9. Instead greater focus will be made towards the fatigue results.

11.2 Stress and strain

In table 11.1, peak stress values taken from the fatigue calculations are presented. The values are the maximum, and minimum axial stress values for the critical elements. Just like it was observed in chapter 9, the values exceed those calculated based on a cross section area of $95mm^2$. Particularly, the values from the elastic cases are much larger than the target values. This is explained by the large difference between the layers, where the center conductor is carrying most of the stress.

Axial stress, σ_{22}					
	Case 1	Case 2	Case 3	Case 4	Target
σ_{max} [MPA]	230.47	211.52	140.74	143.37	111
σ_{mean} [MPA]	147.72	137.55	80.82	76.65	61
σ_{min} [MPA]	64.95	63.58	20.89	9.93	11

Table 11.1: Range 1, axial stress

Axial stress is plotted against time in figure 11.1. Just like for case 3 in chapter 9, it is observed that severe springback occurs during unloading. This is seen in the figure as the difference in stress magnitude increases during the unloading phase. Figure 11.2 shows the umbilical in its deformed state at the end of the load cycle. It is also clearly visible when looking at figure 11.2, where severe deformation have taken place around the bottom. This is because the boundary conditions allow the conductors to rotate.

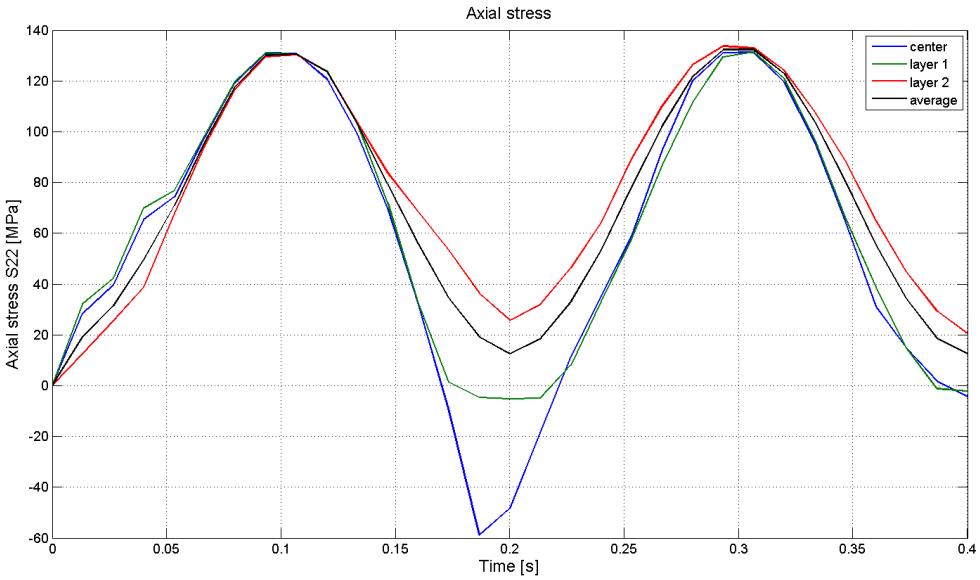

(a) Case 3

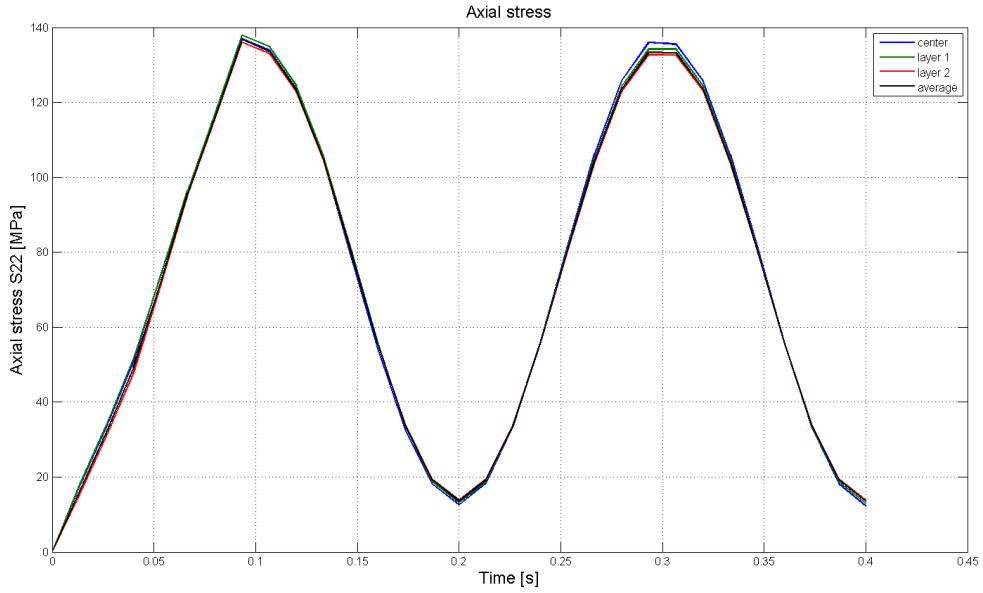

(b) Case 4

Figure 11.1: Axial stress

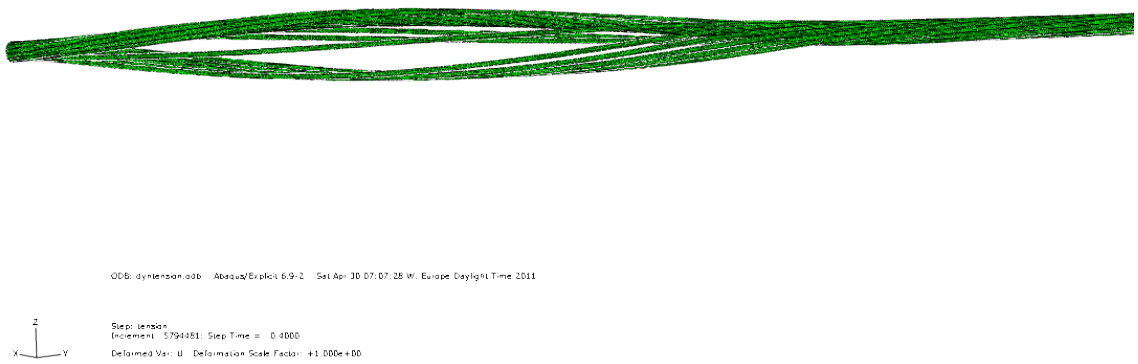

Figure 11.2: Deformation case 3

The axial stress plot for case 4 illustrates that after the yield limit is reached, there are very little difference between the layers. Again it follows the same trends which were observed in chapter 9. The axial stress plots for the elastic cases are given in the appendix. They show linear behavior, with large differences in stress levels between the layers.

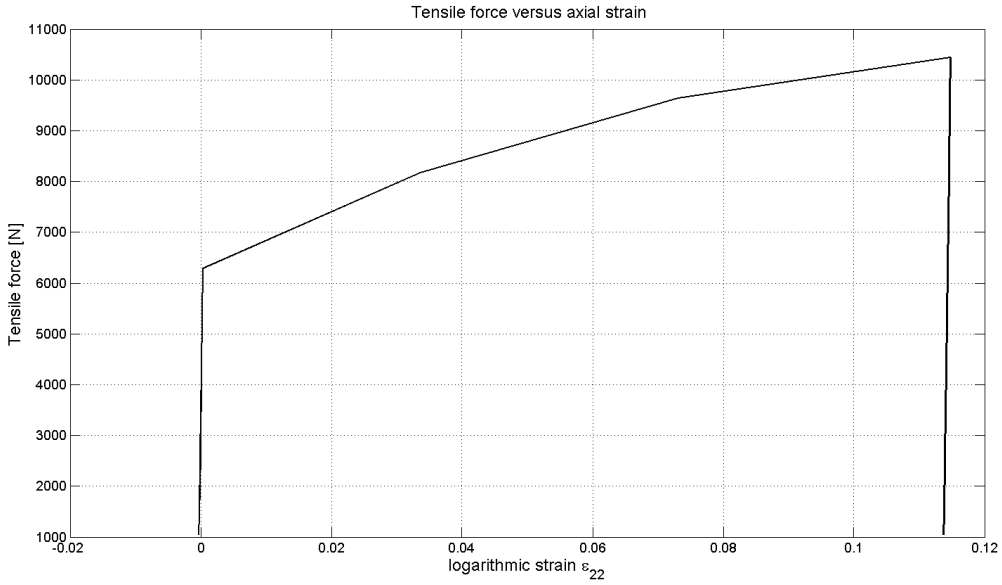

Figure 11.3: Force versus strain Case 4

Applied force is plotted against axial strain in figure 11.3, for case 4. By examining the figure

it is clear that the plastic strain is the dominating strain component, which was expected. It also shows that after the first load cycle, it follows a linear path on the next load cycle. Which confirms that the hardening model is working as intended.

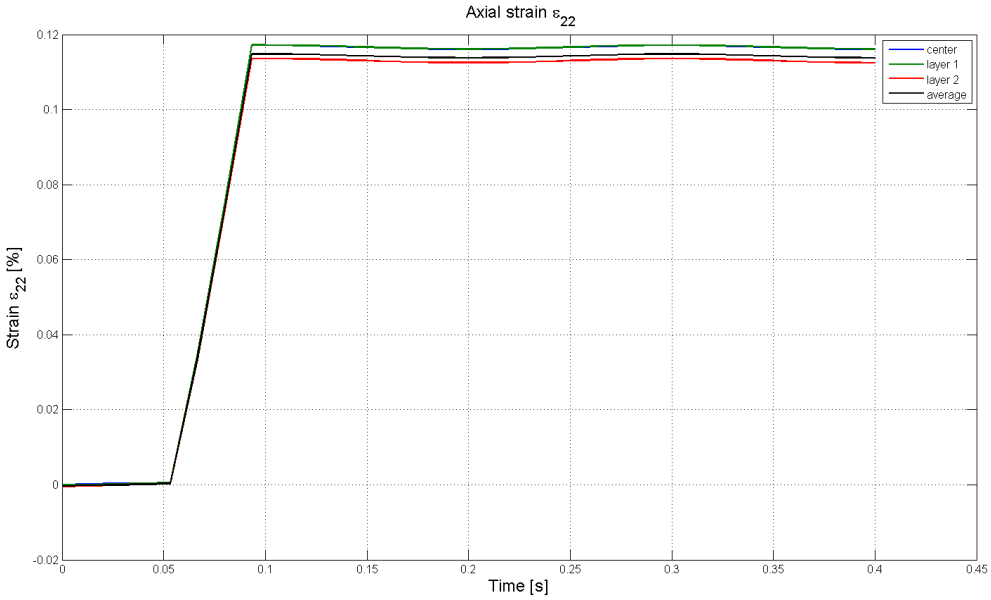

Figure 11.4: Axial strain case 4

Axial strain for case 4 is plotted against the load history in figure 11.4. Again it shows that the total strain is dominated by the plastic strain component, for the first load cycle. After that it is dominated by the elastic strain component, and it is seen that it follows the same shape as for the elastic cases.

11.3 Fatigue

The fatigue calculations were carried out as explained in section 10.4.1. For the elastic-plastic cases, the critical elements were located at contact points between layer 1 and 2. The highest values of axial stress, were located on the hot spots of layer 2 conductor. The critical elements are shown for all the conductors in the appendix. This was however not the situation for the elastic cases. Here it was deemed necessary to do fatigue calculations for all the layers. The reasoning behind that, is the significant difference between the layers.

One source of inaccuracies for the fatigue calculations, are the mesh resolution used. It is previously stated that the mesh is a compromise, and that a finer mesh gave more accurate values for axial stress. This is magnified for the fatigue calculations, because of the relatively small size of the hot spots. Normally, a local model with an extra fine mesh is used for fatigue calculations. This however is difficult to do in practice for the umbilical, since the location of the hot spots are not easily determined.

Another source of inaccuracies are the material model, which as previously stated is too soft, compared to the real life umbilical. Finally the SN curve used, does not necessarily represent the behavior of a conductor taken from the outer most layer. This because it is based on conductors from all parts of 2 different umbilical cables from Nexans. Whereas the laboratory

tests conducted by Fachri Nasution, shows that the stress-strain behavior of the different layers are different.

Fatigue life				
	Case 1	Case 2	Case 3	Case 4
R [-]	0.1			
σ_{UTS} [-]	170			
$\Delta\sigma^c$ [MPa]	178.22	146.90	119.48	135.06
σ_m^c [MPa]	147.74	137.59	80.87	76.89
$\Delta\sigma_0^c$ [MPa]	728.18	425.88	154.43	169.80
$\Delta\sigma^t$ [MPa]	230.08	201.79	123.83	131.73
N [-]	-170676	83899	785546	714455

Table 11.2: Fatigue results

Results from the fatigue calculations are given in table 11.2. Note the significant difference between the elastic, and the elastic-plastic cases. For the elastic cases it is observed that the values for $\Delta\sigma^t$ are outside of the SN curve's range, which has a maximum $\Delta\sigma = 200$MPa. The results in the table for the elastic cases are from the center conductor which proved to be the critical part. Fatigue calculations for the other layers are given in the appendix. This demonstrate the effect of the shrinking process, decreasing the inter layer stress difference.

The mesh resolution is also more critical in the elastic cases, because the inter layer contact points have a much smaller surface, than for the elastic-plastic cases. Thus capturing accurate stress results from the hot spots impossible.

From the stress and strain plots, it is evident that case 4, has higher levels for stress and strain. This correlates with the results obtained in chapter 9. It is also seen that case 4 has fewer cycles to failure, than case 3. However, this result is uncertain. In figure 11.2, it is illustrated that layer 1 and 2, separates from the core. It is thought that this behavior will cause structural failure well before the estimated cycles to failure. In fact the critical element for the fatigue calculations for case 3, is selected outside this region.

11.4 Stress range 2

The analyses for stress range 2 were not completed. The material model used in this analysis proved inadequate for this load condition. This because the maximum axial stress was in excess of 211MPa, and the material model used has a maximum value of 175MPa. Several attempts were made to overcome this problem. One attempt was to extrapolate the material curve to include stress up to 300MPa. Due to large values of strain, the elements were severely deformed, giving a increment size of the order of 10^{-10}. Another attempt was made with a new material model, based on another stress versus strain curve with higher values for stress. Unfortunately that proved unsuccessful too.

Chapter 12

Conclusions and future work

12.1 Conclusion

The finite element method is a numerical method. The accuracy of results is affected by how accurately the model represents the physical model. It is stated that the mesh used in the analyses, are not optimal. Likewise the material model used to represent the nonlinear material behavior was too soft, compared to the full scale umbilical. Therefore it must be expected that all the results have some degree of inaccuracy. As an indicator of that, values for axial strain and stress, were higher than anticipated.

The results indicates that boundary conditions are important. In all the analyses, the tendency is that more constraints give less difference between the layers. For the elastic-plastic cases, the effect of the shrinking step is clearly visible. After this step, it is seen that the conductors obtain the same shape as the physical umbilical. The stress and strain behavior changes dramatically, compared to the elastic cases. The inter layer stress and strain difference are greatly reduced.

It is difficult to draw precise conclusions from the fatigue calculations. For the elastic cases, the large difference in stress between the layers are a problem. The results show that $\Delta\sigma$ is outside of the defined SN curve. Problems are also evident for case 3, where the boundary conditions allow the conductors to separate from the core. The results from case 4, are the only results that are deemed good, as far as fatigue goes. This makes it hard to make definite conclusions regarding the difference between the elastic, and the elastic-plastic cases. However it is stated that without the shrinking step, the center conductor experience much higher values of axial stress than the other layers. Thus making it vulnerable for material failure.

Examining the load versus stress history for all the stress components, show that the axial stress component is dominating. This is true for all the analyses.

As a closing remark, it is stated that all the analyses shows "good" behavior. The elastic-plastic cases with prevented rotation, represents the general behavior of the full scale umbilical. However it must be stated that values from the analyses are plagued with inaccuracy.

12.2 Future work

One of the main challenges with conducting the analyses presented in this thesis, are computational cost. In the future, effort should be made towards getting the analyses to run on more processors. If this problem is overcome, a finer mesh can be used. Thus reducing the inaccuracy caused by the mesh. A beam element model should be made for the elastic cases. This was proven successful in the paper by Corre and Probyn [2009]. With beam elements, the computational cost are reduced to a state where the analyses can be run on an ordinary desktop computer.

One of the key issues in this thesis was the material model. Effort should be made to create a new model, incorporating the latest stress versus strain data from the laboratory tests.

With a revised material model, analyses for stress range 2, should also be carried out.

In the future the model used for the analyses should be subjected to scrutiny. Particularly, finding boundary conditions that represents the full scale umbilical, should be done. Perhaps using springs instead of fixing nodes, could lead to less problems at the ends.

Bibliography

Vincent Le Corre and Ian Probyn. Validation of a 3-dimensional finite element analysis model of a deep water steel tube umbilical in combined tension and cyclic bending. In *OMAE2009-79168*, 2009.

Fernando Buscacio de Almeida et al. Characterization and technical comparison between steel tube umbilicals and thermoplastic hoses umbilicals. In *OMAE2009-79701*, 2009.

DNV. *Submarine pipeline systems, FS-OS-F101.* Det norske veritas, 2010.

ISO-13628-5. *Petroleum and natural gas industries desing and operation of subsea production systems. Part 5: Subsea umbilicals.* Standard Norge, 2009.

Stian Karlsen. Fatigue of copper conductors for dynamic subsea power cables. In *OMAE2010-21017*, 2010.

M. Kashani and R. Young. Hoop stress approximation in offshore design codes. *Science direct*, 2007.

Henrik R. Nagel. *Njord documentation.* Notur, 2010.

Dr. Horace Pops. The metallurgy of copper wire. 1999.

Adrian Risa. Finite element method analysis of marine umbilical. *NTNU*, 2010.

Svein Sævik. Lifetime theory. Technical report, Marintek, 1999.

Svein Sævik. Comparison between theoretical and experimental flexible pipe bending stresses. In *OMAE2010-20352*, 2010.

Svein Sævik, Torgeir Moan, and Carl M. Larsen. Advanced structural analysis. In *Lecture notes TMR4305.* NTNU, 2010.

Nils Sødahl, Geir Skeie, Oddrun Steinkjer, and Arve Johan Kalleklev. Efficient fatigue analysis of helix elements in umbilicals and flexible risers. In *OMAE2010-21012*, 2010.

Paul Stanton, Weiyong Qiu, Qiang Cao, Filippo Librino, and Guillermo Hahn. Global design and analysis of umbilical in offshore applications. In *OMAE2009-79841*, 2009.

Dassault systemes. *Abaqus v6.7 documentation.* SIMULIA, 2007.

Warren C. Young and Richard G. Budynas. *Roark's formulas for Stress and Strain.* McGraw-Hill, 7 edition, 2002.

Appendix A

Shell script

```
#!/bin/ksh
# @ job_name           = range2
# @ account_no         = ntnu907
# @ class              = large
# @ job_type           = parallel
# @ node               = 20
# @ tasks_per_node     = 16
# @ node_usage         = not_shared
# @ checkpoint         = no
# @ resources          = ConsumableCpus(1) ConsumableMemory(832 mb)
# @ network.MPI        = sn_all,,us
# @ error              = $(job_name).$(jobid).err
# @ output             = $(job_name).$(jobid).out
# @ environment        = COPY_ALL
# @ env_copy           = all
#
# @ queue
#
module load abaqus/6.9-2

case=$LOADL_JOB_NAME

w=$WORKDIR/$USER/abaqus/$case
if [ ! -d $w ]; then mkdir -p $w; fi

cp abaqus_v6.env $w
cp $case.inp $w

cd $w

cpuspernode=16
procs=`cat $LOADL_HOSTFILE |wc -w`

mp_host_list="["
nodes=`cat $LOADL_HOSTFILE | sort -u|paste -s -d' ' '`
for n in `echo $nodes`
```

```
do
mp_host_list="${mp_host_list}['$n',${cpuspernode}],"
done
export mp_host_list=`echo ${mp_host_list} | sed -e "s/,$/]/"`
echo "mp_host_list=${mp_host_list}" >> abaqus_v6.env

abaqus job=$case cpus=$procs mp_mode=mpi double=both interactive scratch=$w

llq -w $LOADL_STEP_ID
```

Appendix B

SN-curve

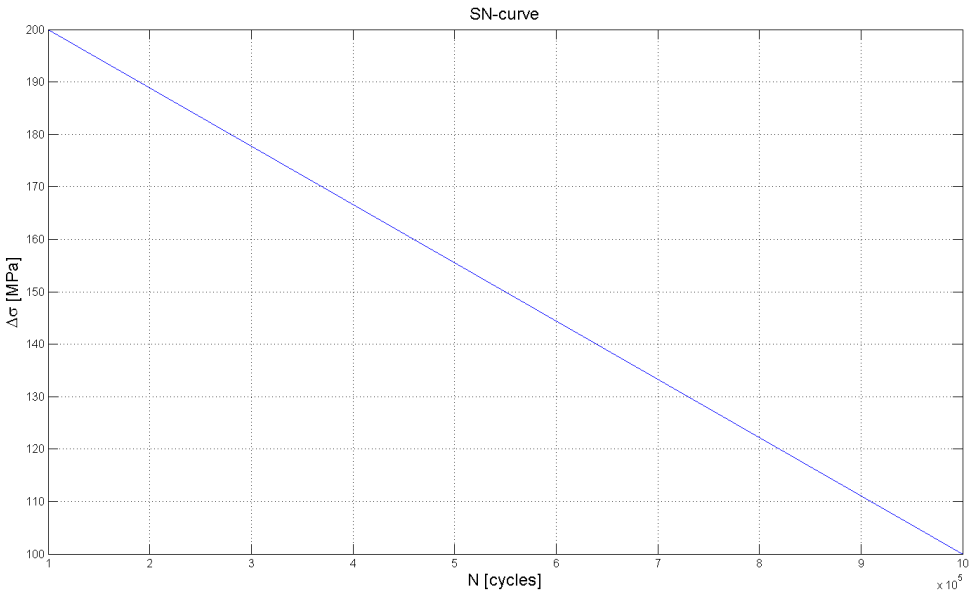

Figure B.1: SN curve

The SN curve that was used for fatigue calculations. Based on figure 10.2, taken from Karlsen [2010].

Appendix C

Tension

C.1 case1

C.1.1 Stress

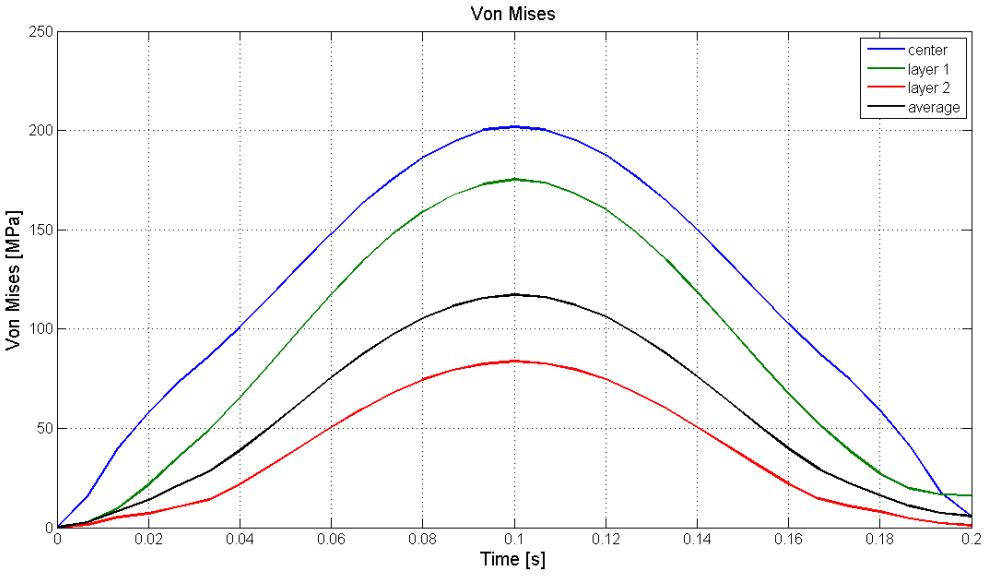

Figure C.1: Von Mises Stress σ_{mises}

C.1.2 Strain

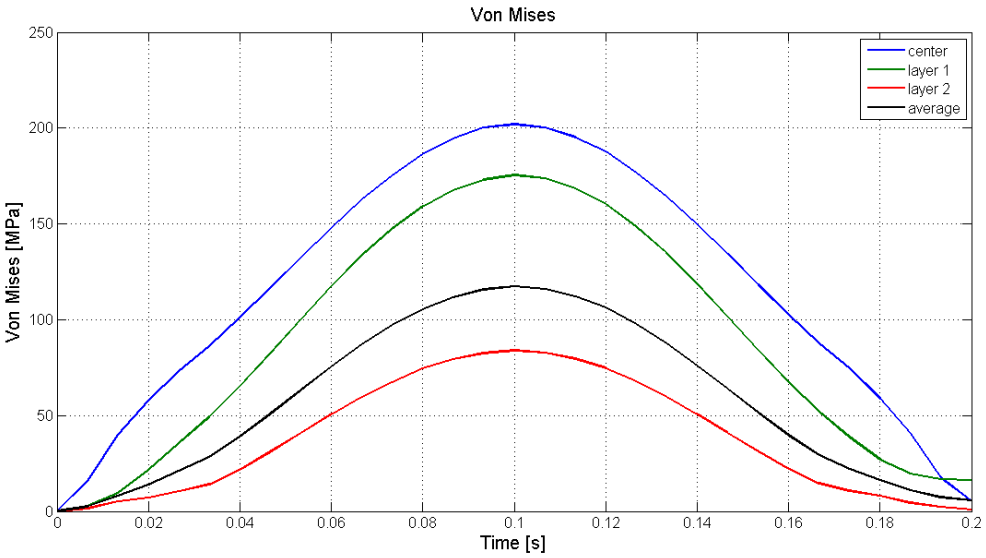

Figure C.2: Logarithmic axial strain ϵ_{22}

C.1.3 Axial stress pattern

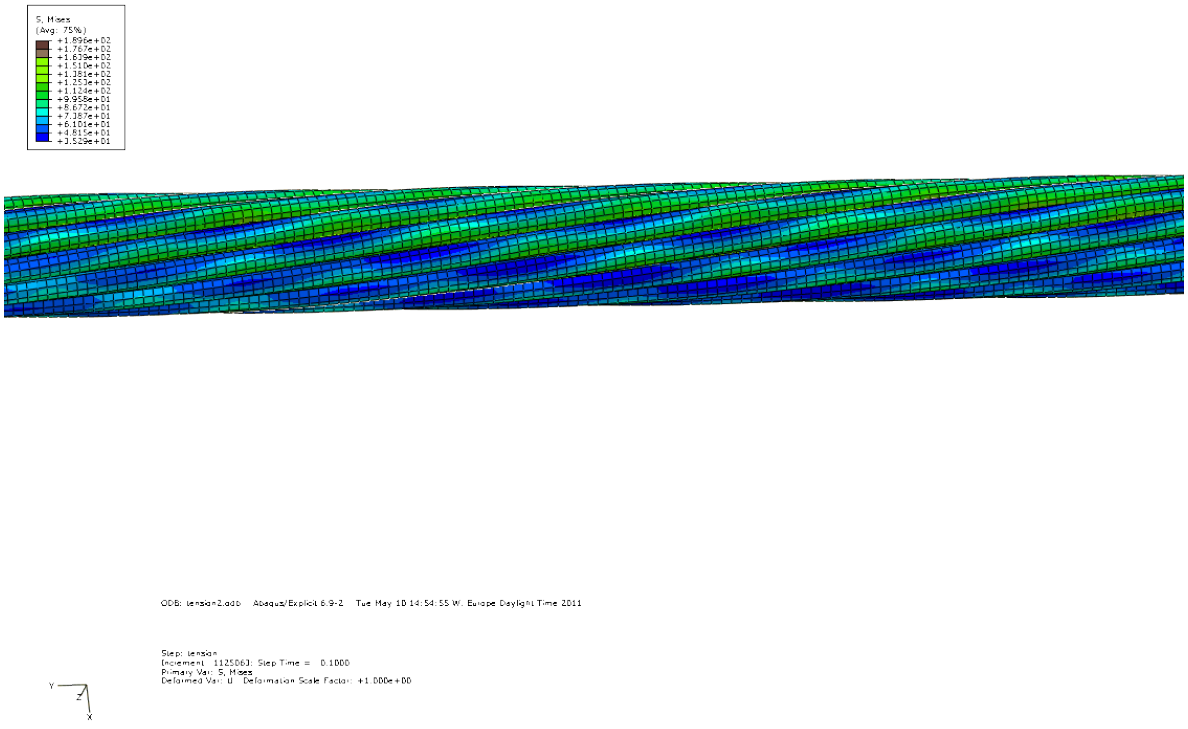

Figure C.3: Axial stress pattern Layer 2

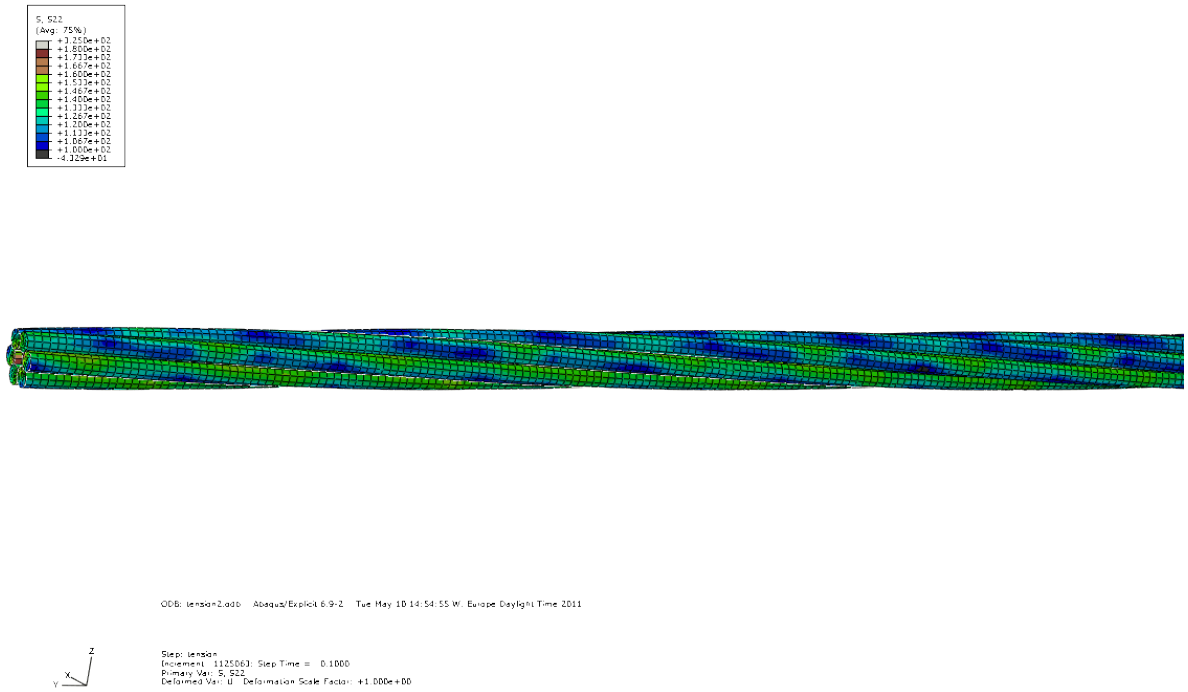

Figure C.4: Axial stress pattern Layer 1

C.2 Case 2

C.2.1 Stress

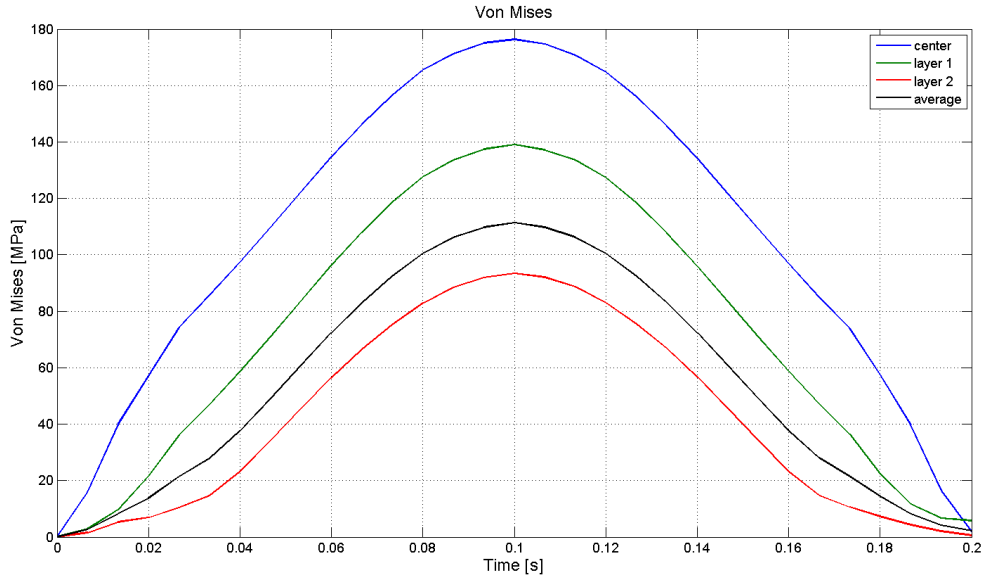

Figure C.5: Von Mises Stress σ_{mises}

C.2.2 Strain

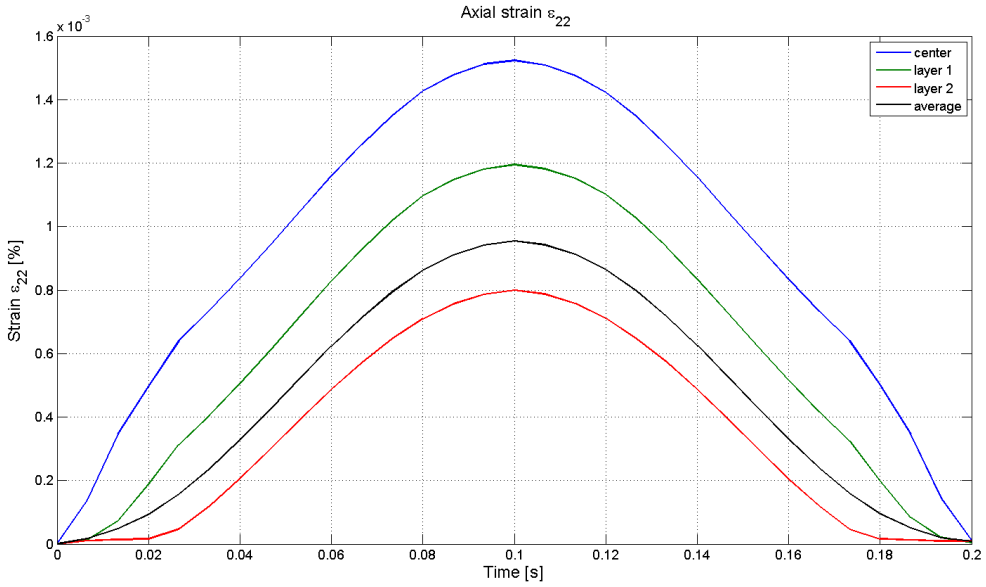

Figure C.6: Logarithmic axial strain ϵ_{22}

C.2.3 Axial stress versus Strain

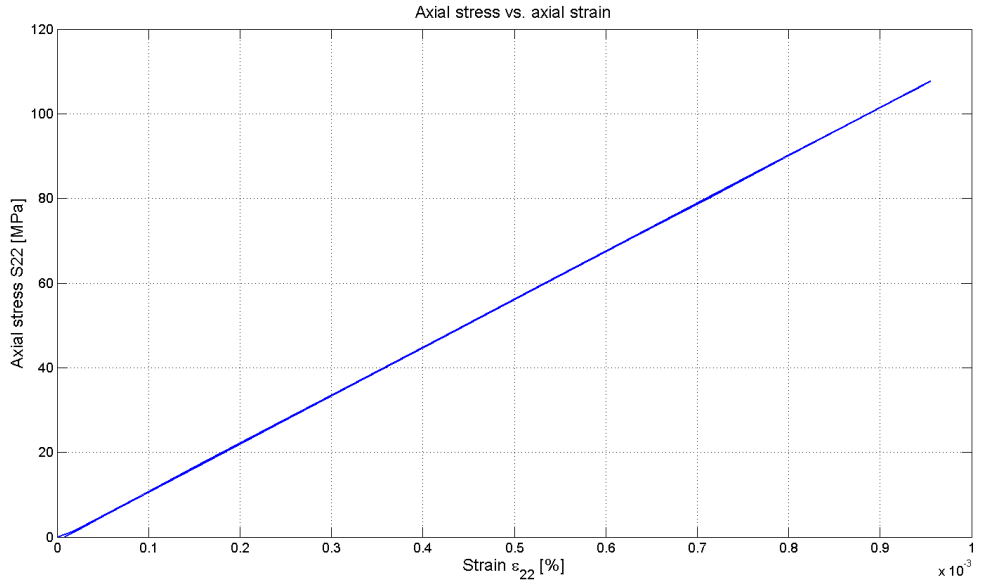

Figure C.7: Axial stress versus strain

C.2.4 Axial stress pattern

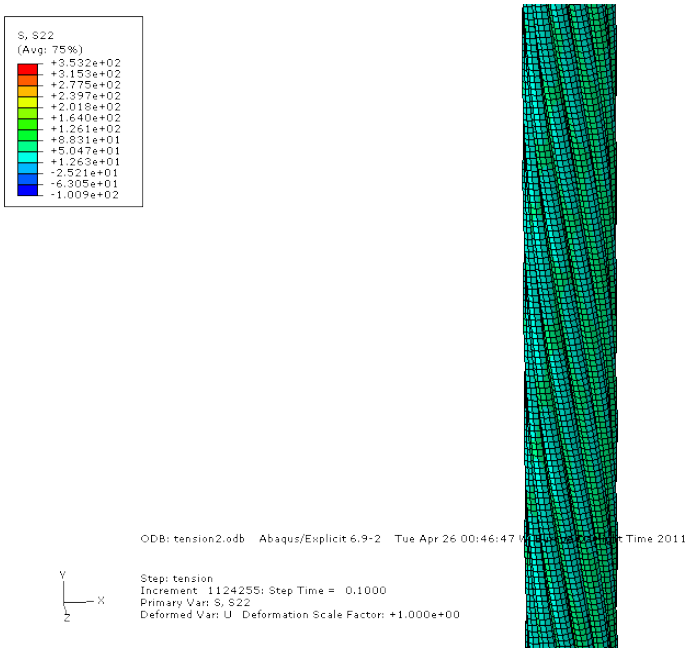

Figure C.8: Axial stress pattern layer 2

C.2.5 Critical Element

The umbilical was examined in ABAQUS, and the location of the hot spot with the highest stress concentration was located. It is shown in figure C.9, and the stress values are shown in figures C.10 and C.11. The hot spot was located in layer 1.

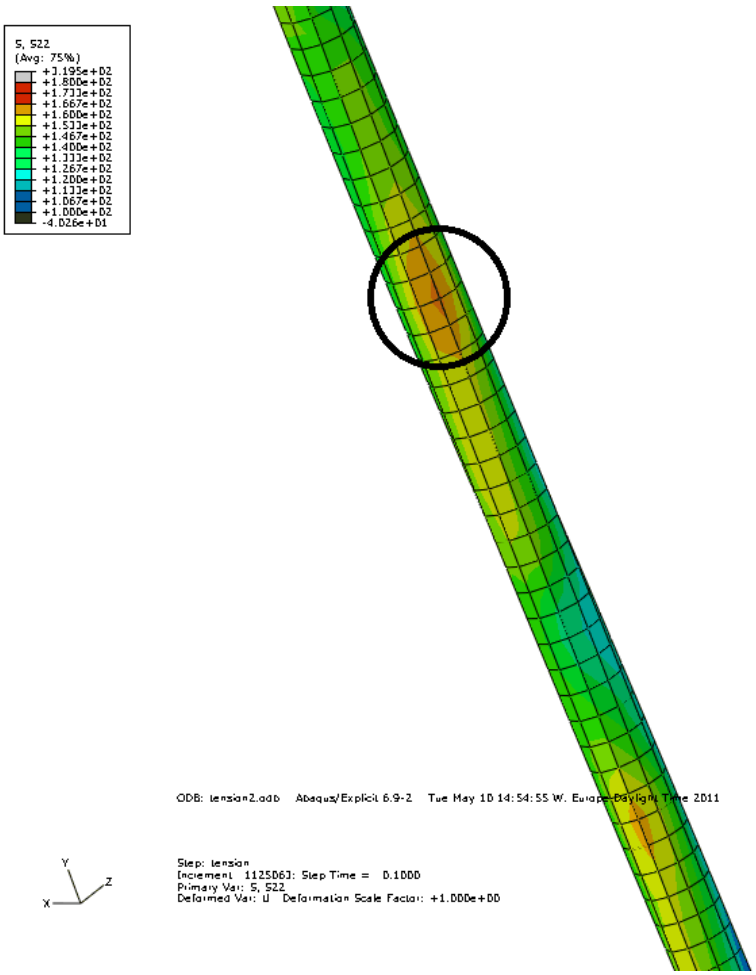

Figure C.9: Critical element layer 1 conductor

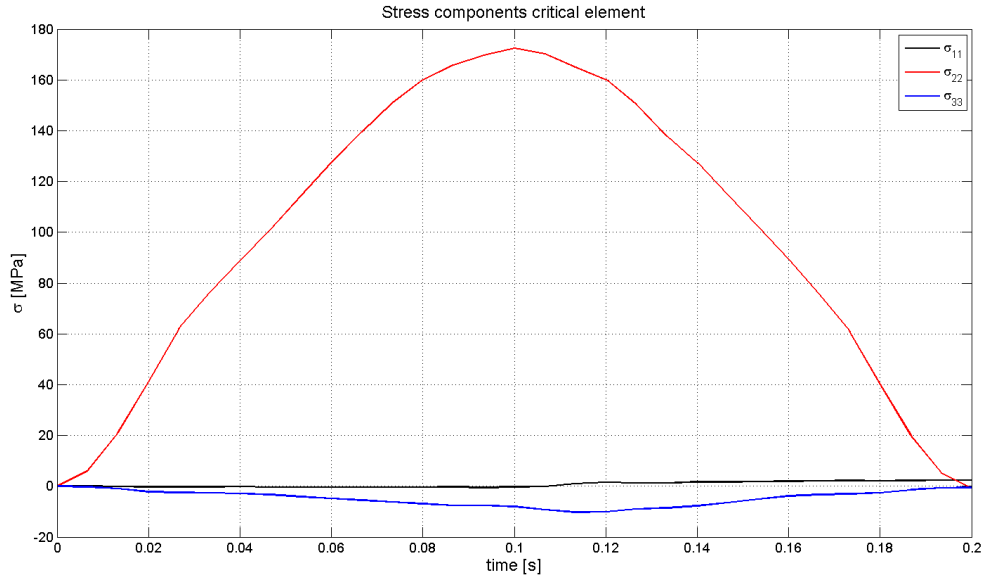

Figure C.10: Stress for critical element

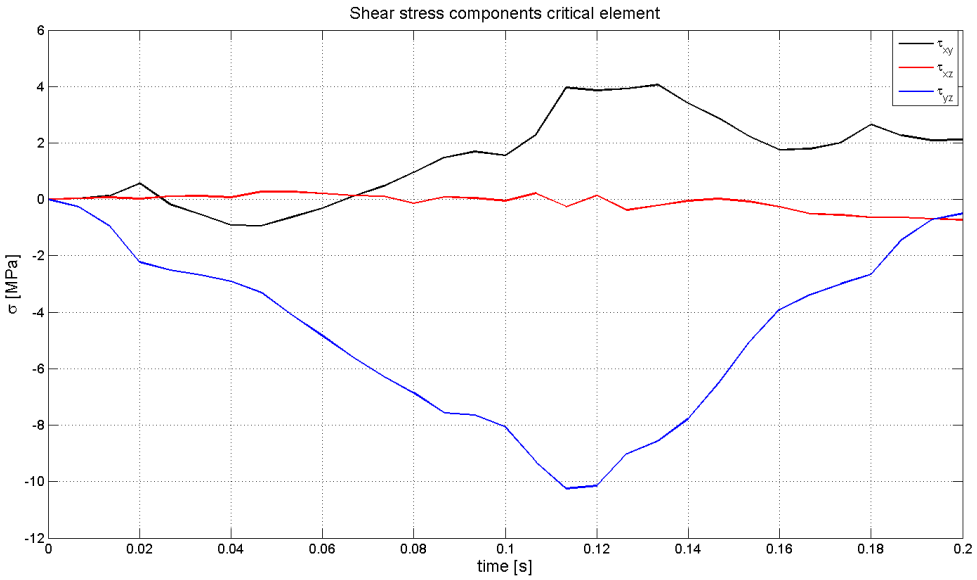

Figure C.11: Shear stress for critical element

C.3 Case 3

C.3.1 Stress

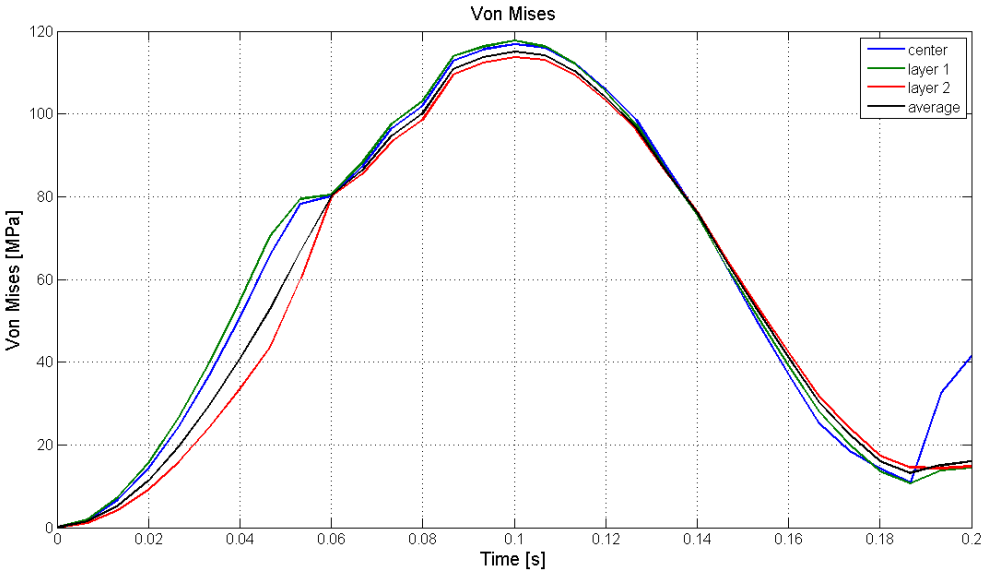

Figure C.12: Von Mises Stress σ_{mises}

C.3.2 Strain

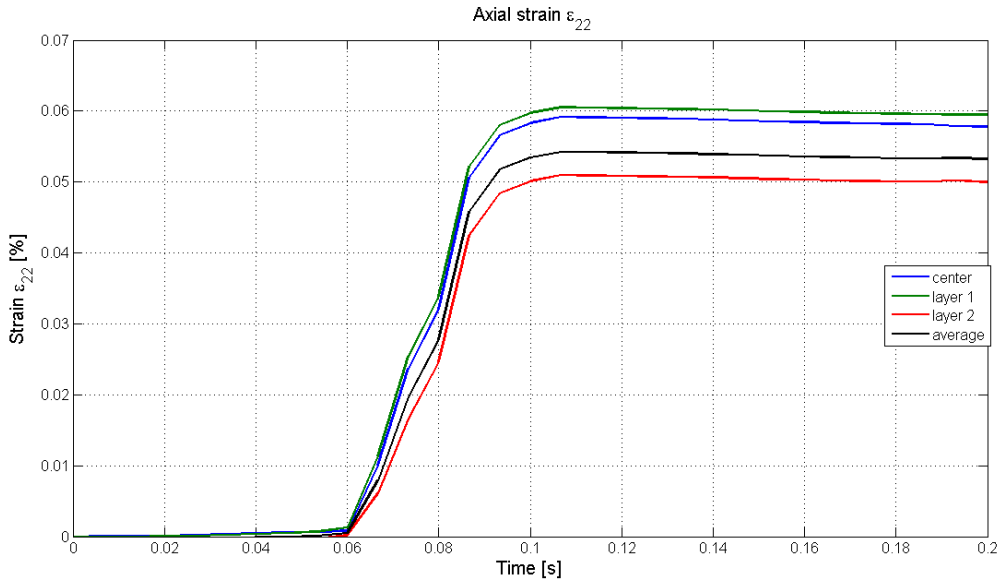

Figure C.13: Logarithmic axial strain ϵ_{22}

C.3.3 Axial stress pattern

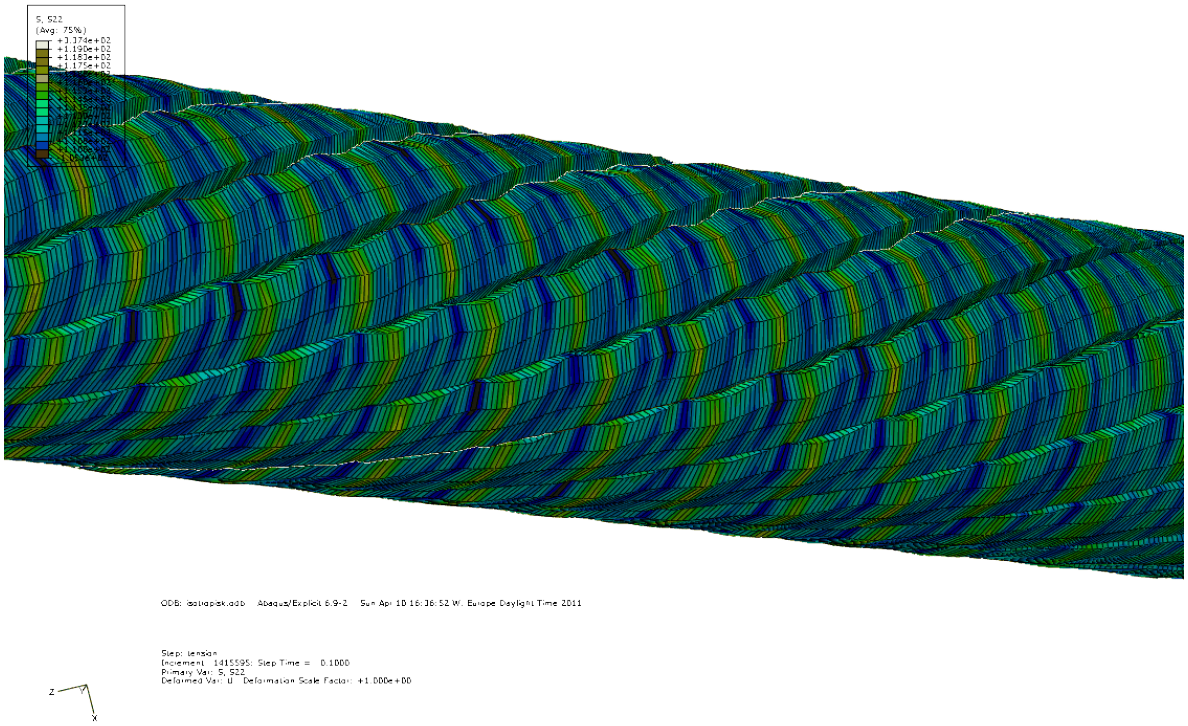

Figure C.14: Axial stress pattern layer 2

C.3.4 Deformed shape

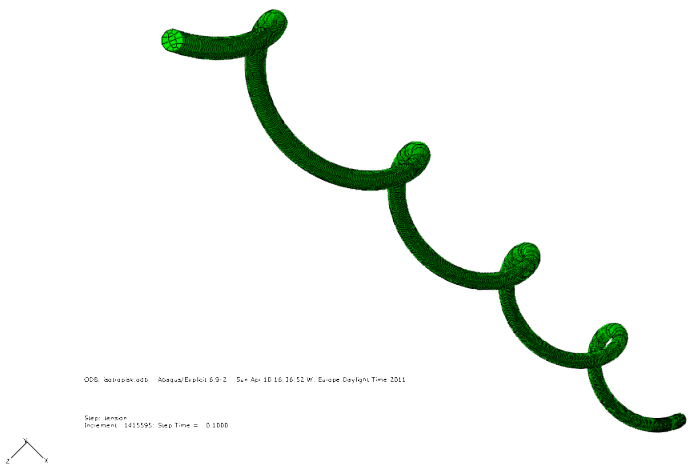

Figure C.15: Layer 2 conductor undeformed case 3

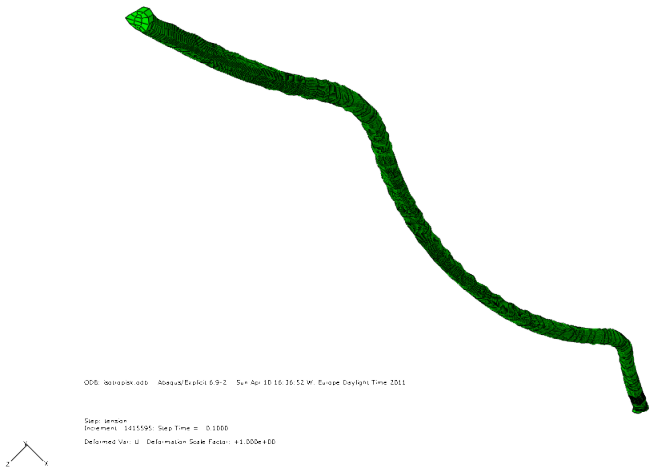

Figure C.16: Layer 2 condcutor deformed case 3

C.3.5 Springback

Figure C.17 shows the deformed state at zero load, in the end of the load step. The springback is clearly visible.

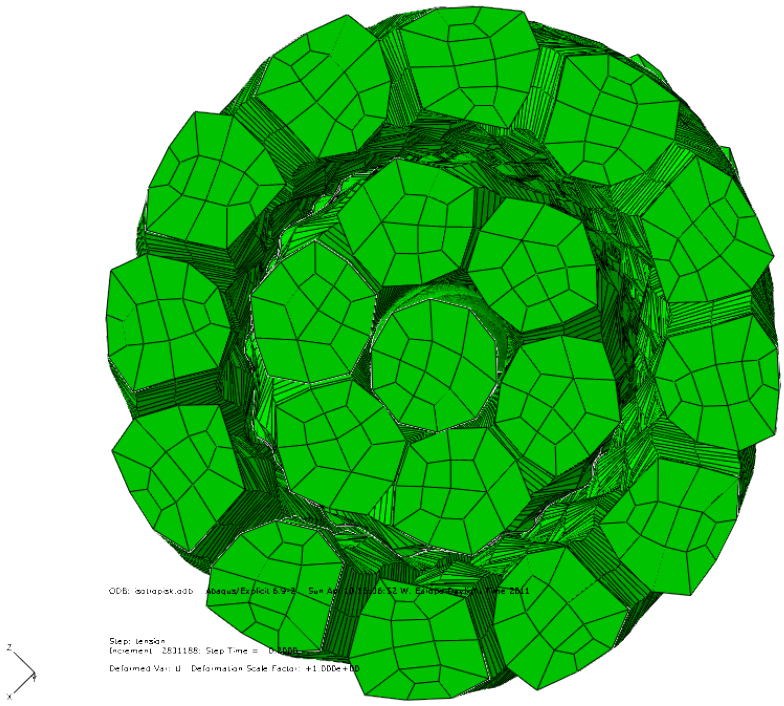

Figure C.17: Springback

C.4 Case 4

C.4.1 Stress

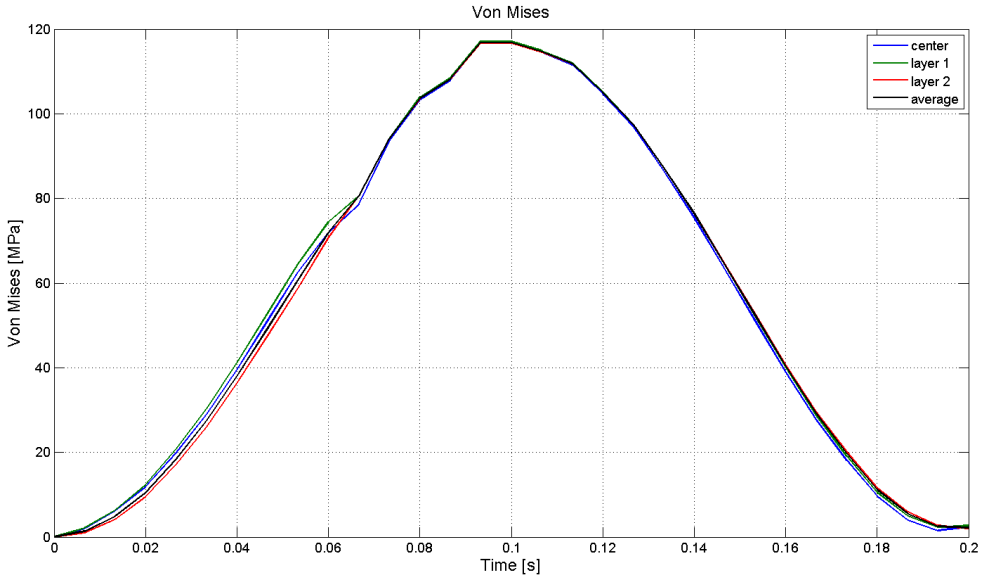

Figure C.18: Von Mises Stress σ_{mises}

C.4.2 Strain

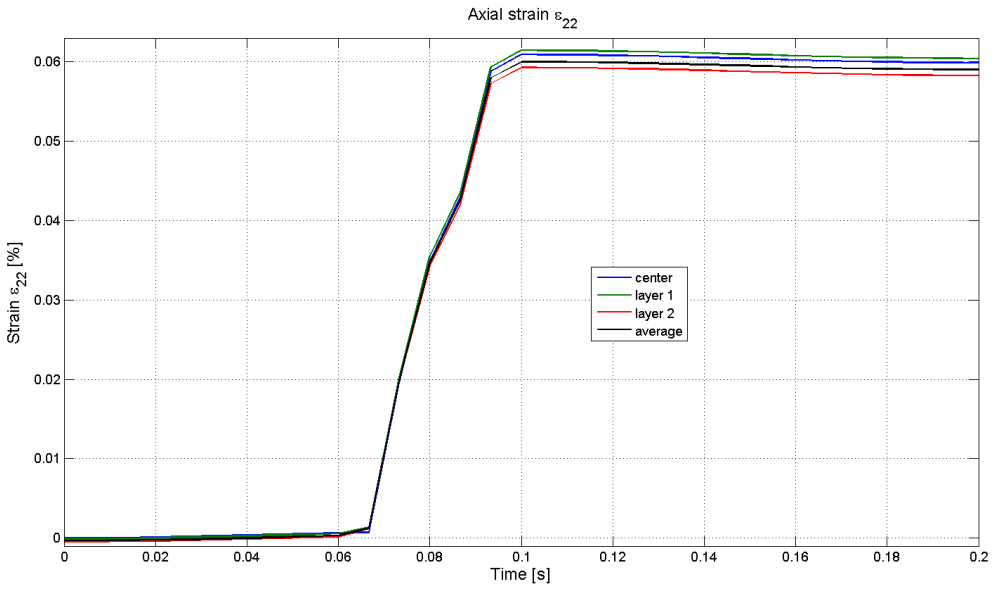

Figure C.19: Logarithmic axial strain ϵ_{22}

C.4.3 Axial stress pattern

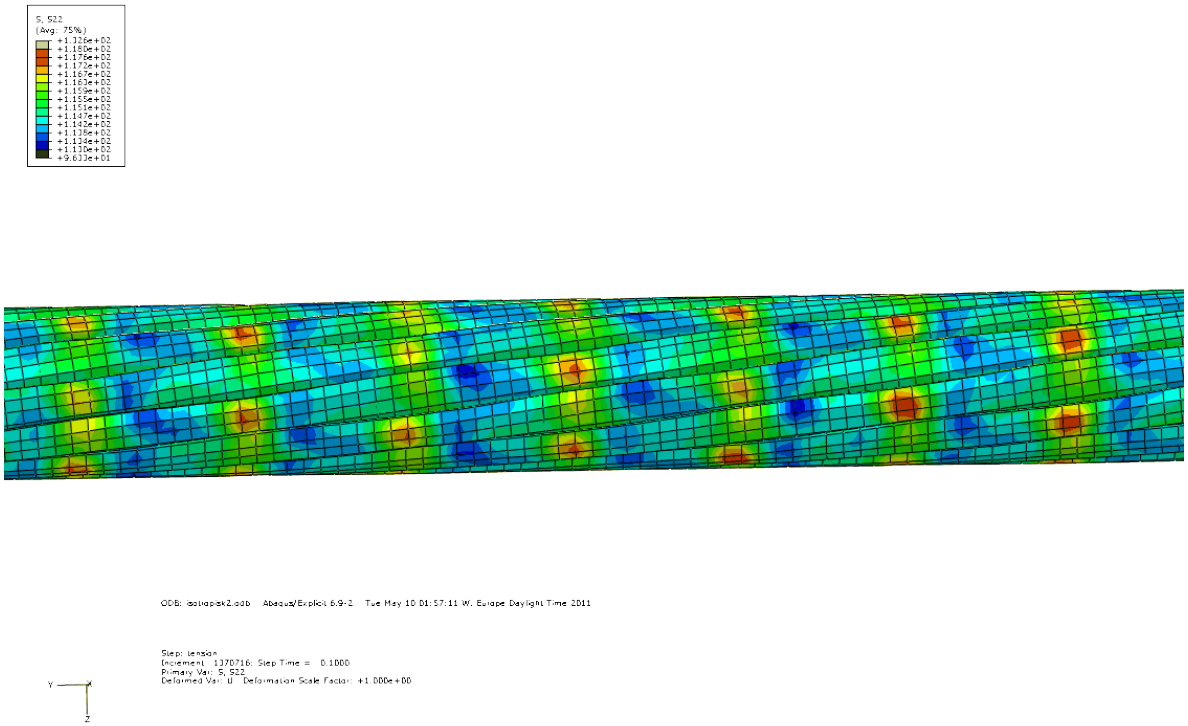

Figure C.20: Axial stress pattern

C.4.4 Force versus axial strain

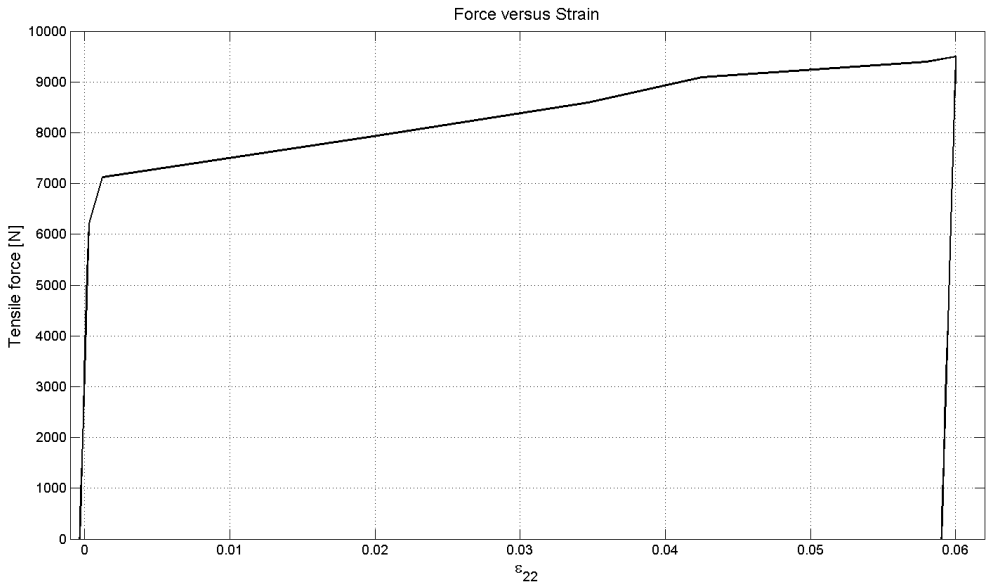

Figure C.21: Force versus axial strain

C.4.5 Critical element

Figure C.22 shows the location of the hot spot for case 4. Notice that for the elastic-plastic case, it is located on layer 2. Stress history for the critical element is given in figures C.23 and C.24.

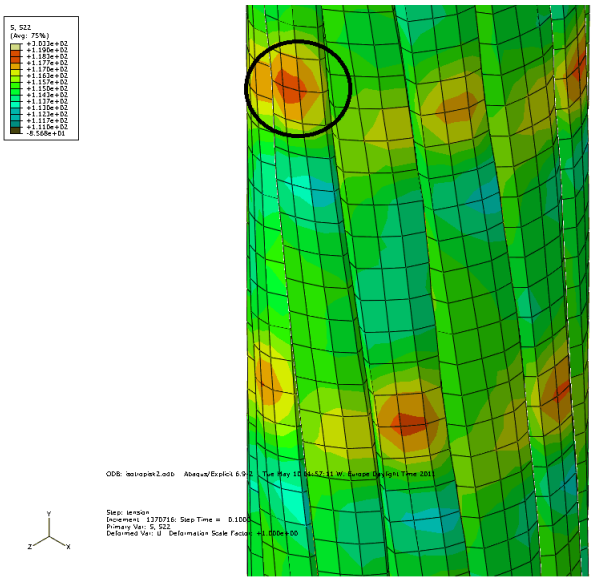

Figure C.22: Critical element layer 2 conductor

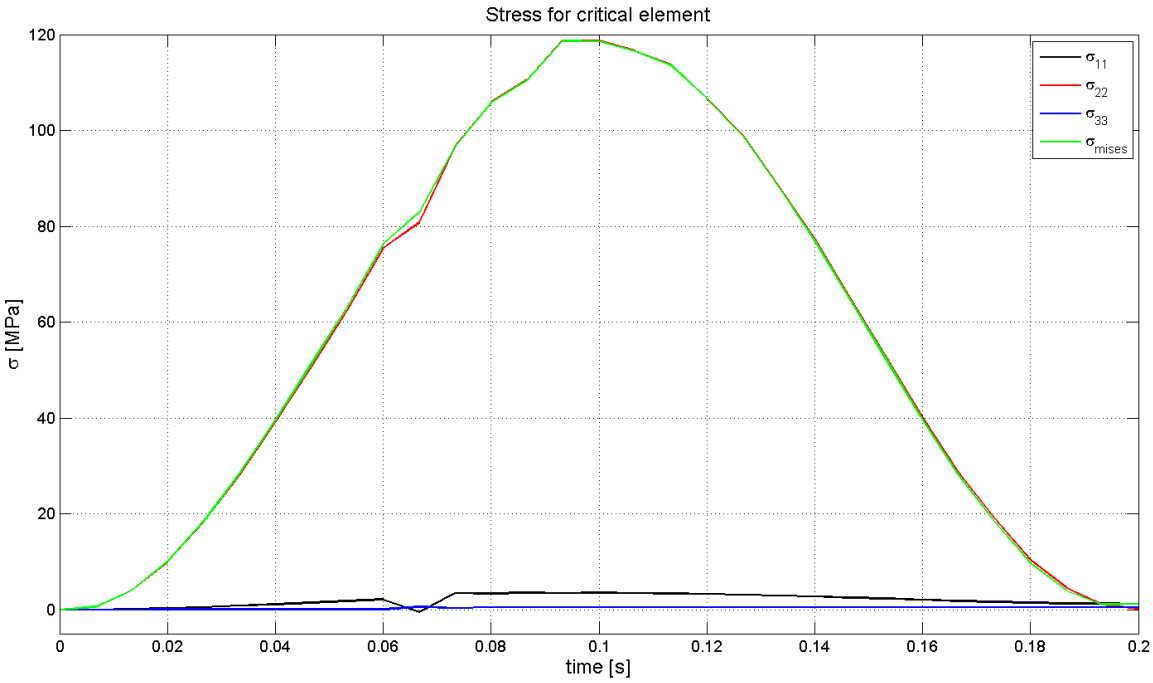

Figure C.23: Stress for critical element

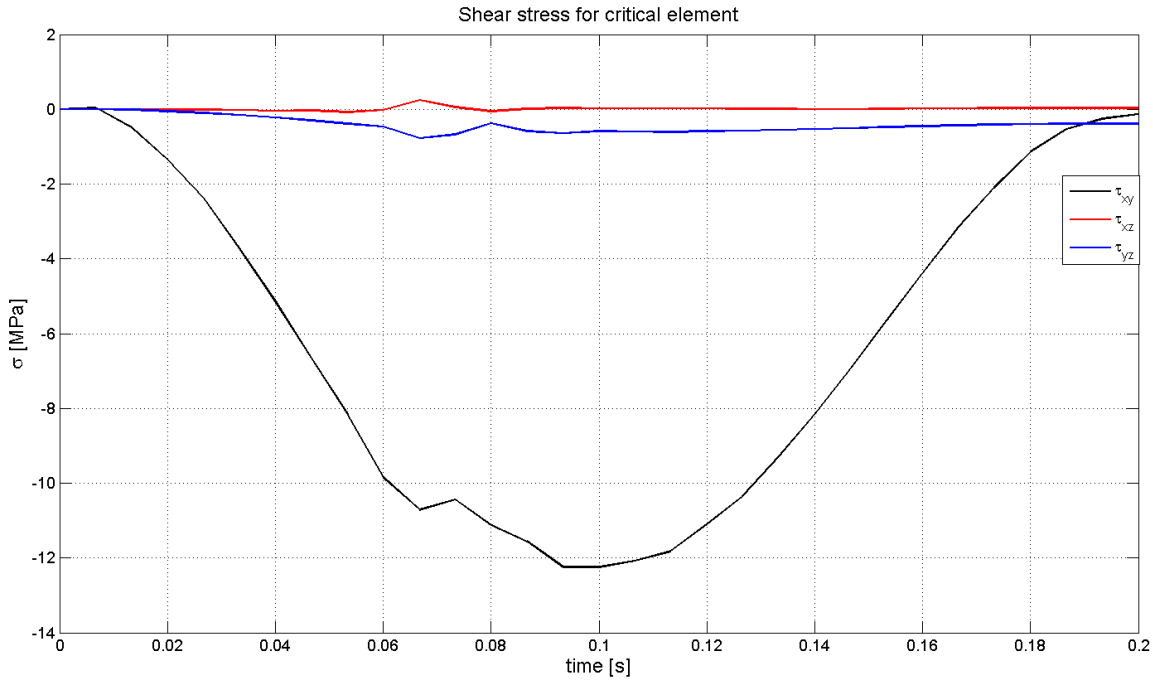

Figure C.24: Shear stress for critical element

C.4.6 Springback

Figure C.25 shows the springback for case 4. The effect of more constraints in the boundary conditions, compared to case 3 is apparent.

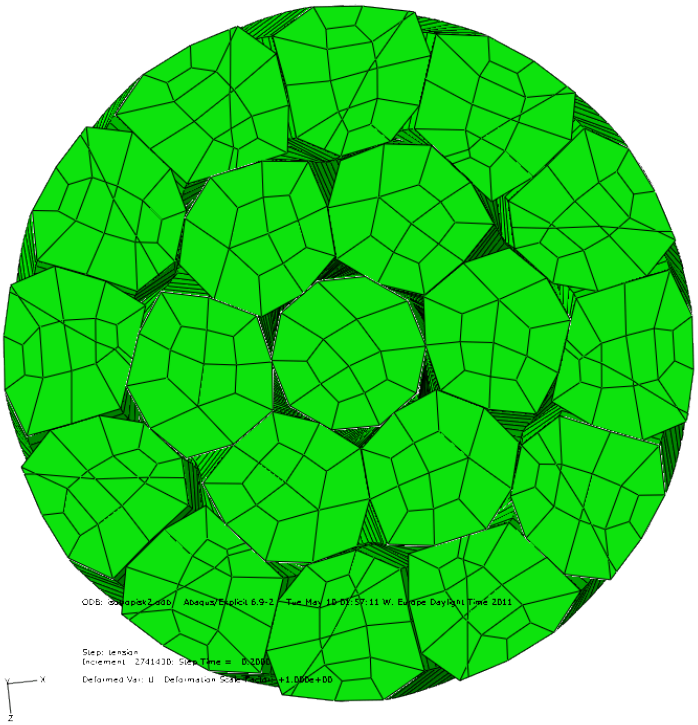

Figure C.25: Springback

Appendix D

Dynamic tension -Range 1

D.1 Analysis data

Table D.1: Analysis statistics, Dynamic tension

	Case 1	Case 2	Case 3	Case 4
Integration scheme	Explicit	Explicit	Explicit	Explicit
Precision	Double	Double	Double	Double
Steps	2	2	4	4
Increment size	8.82×10^{-8}	9.07×10^{-8}	6.60×10^{-8}	6.92×10^{-8}
Total increments	4.53×10^{6}	4.4×10^{6}	12.59×10^{6}	12.43×10^{6}
Processors	160	160	128	128
CPU-time	10:12:12	09:50:10	141:07:34	140:51:30

D.2 Case 1

D.2.1 Fatigue

Table D.2: Fatigue results case 1

Fatigue life Case 1			
	Center	Layer 1	Layer 2
R [-]	0.1		
σ_{UTS} [-]	170		
$\Delta\sigma^c$ [MPa]	178.23	196.08	166.25
σ_m^c [MPa]	147.74	139.07	78.12
$\Delta\sigma_0^c$ [MPa]	728.18	592.82	210.74
$\Delta\sigma^t$ [MPa]	230.08	220.47	149.71
N [-]	-170676	-84204.87	552632

D.2.2 Critical element

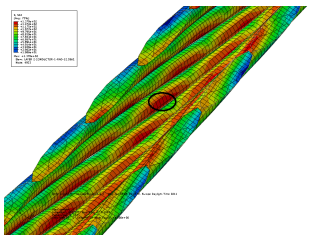

Figure D.1: Critical element layer 2

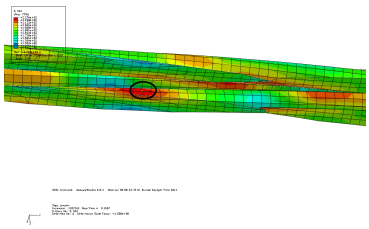

Figure D.2: Critical element layer 1

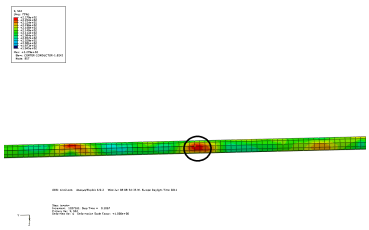

Figure D.3: Critical element center

D.2.3 Stress

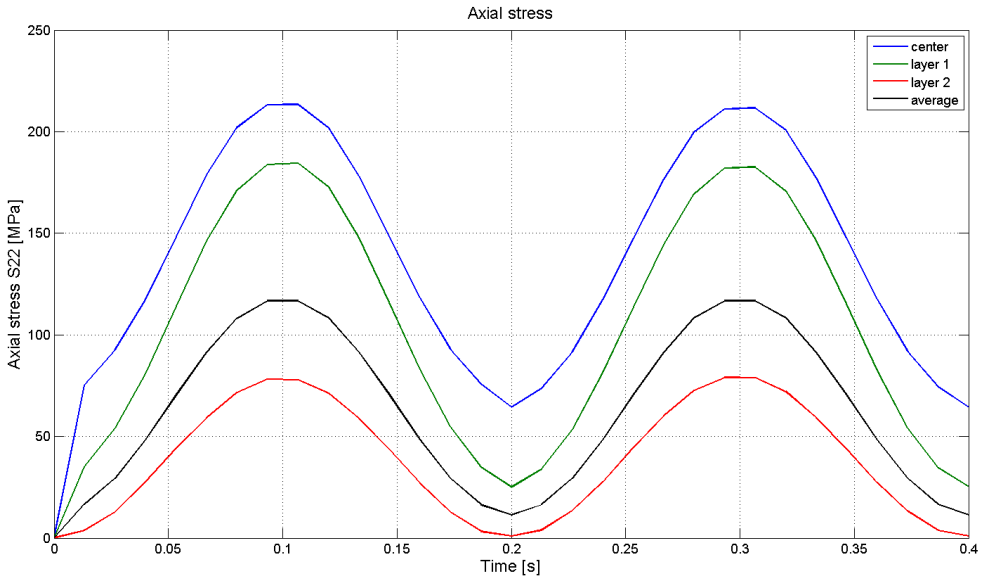

Figure D.4: Axial stress

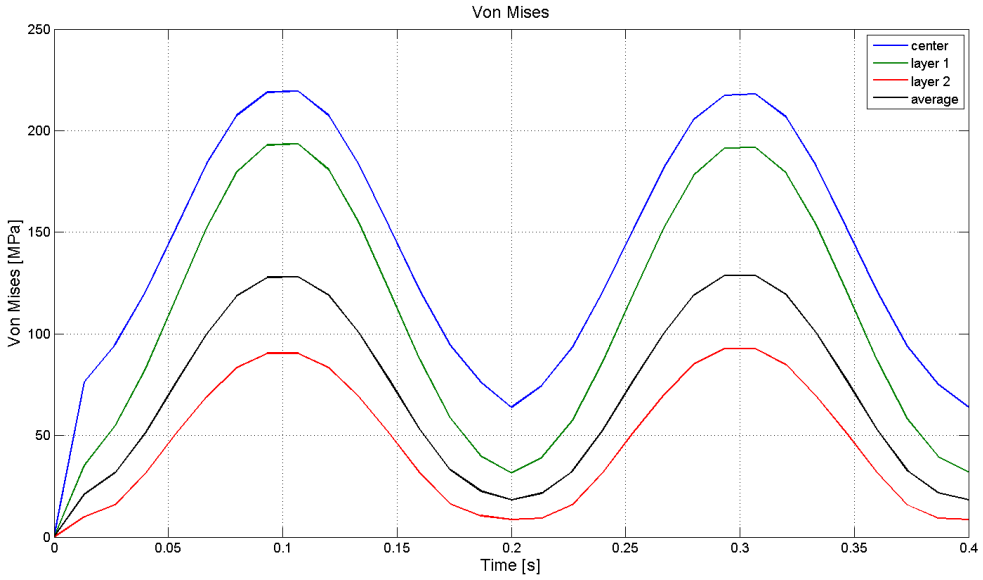

Figure D.5: Von Mises stress

D.2.4 Strain

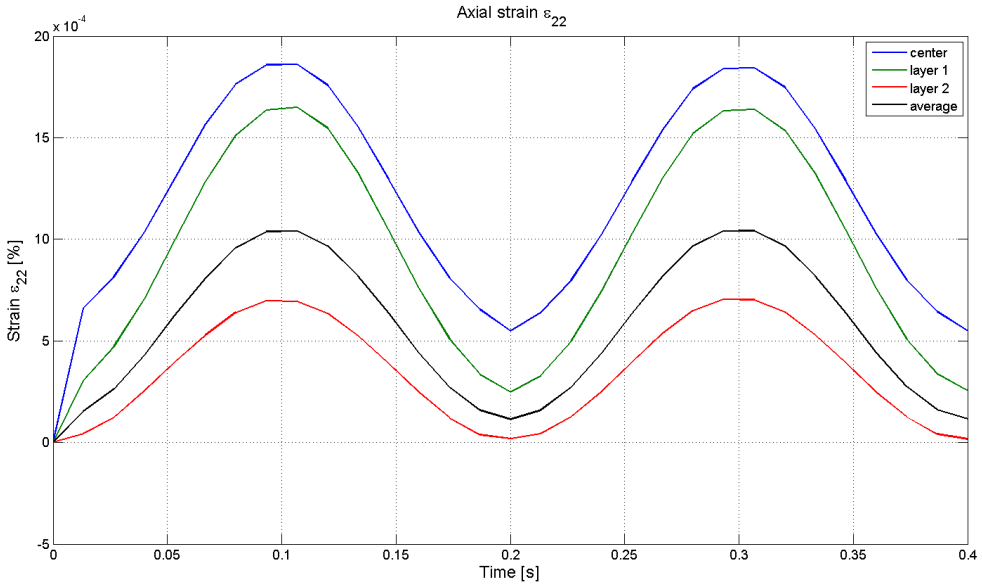

Figure D.6: Axial strain

D.2.5 Axial stress versus strain

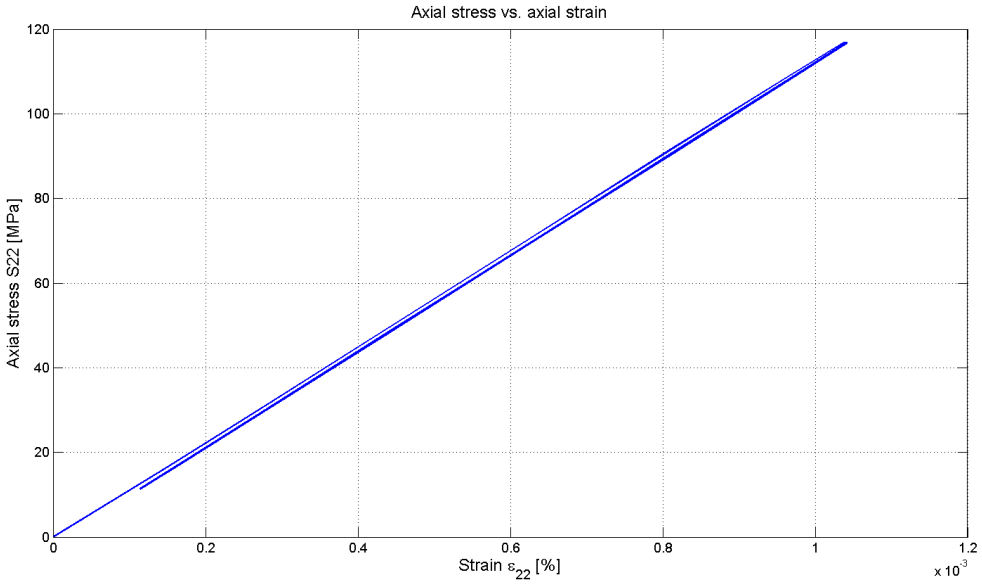

Figure D.7: Axial stress versus strain

D.3 Case 2

D.3.1 Fatigue

Table D.3: Fatigue results case 2

Fatigue life Case 2			
	Center	Layer 1	Layer 2
R [-]	0.1		
σ_{UTS} [-]	170		
$\Delta\sigma^c$ [MPa]	146.90	149.61	145.87
σ_m^c [MPa]	137.59	121.33	79.70
$\Delta\sigma_0^c$ [MPa]	425.88	304.98	186.97
$\Delta\sigma^t$ [MPa]	201.79	178.88	139.77
N [-]	83899	290110	642085

D.3.2 Critical element

The critical elements used for the fatigue calculations are shown in figures D.8, D.9 and D.10. ABAQUS was used to locate the element with the highest axial stress, not including the zones affected by boundary conditions. The elements are encircled.

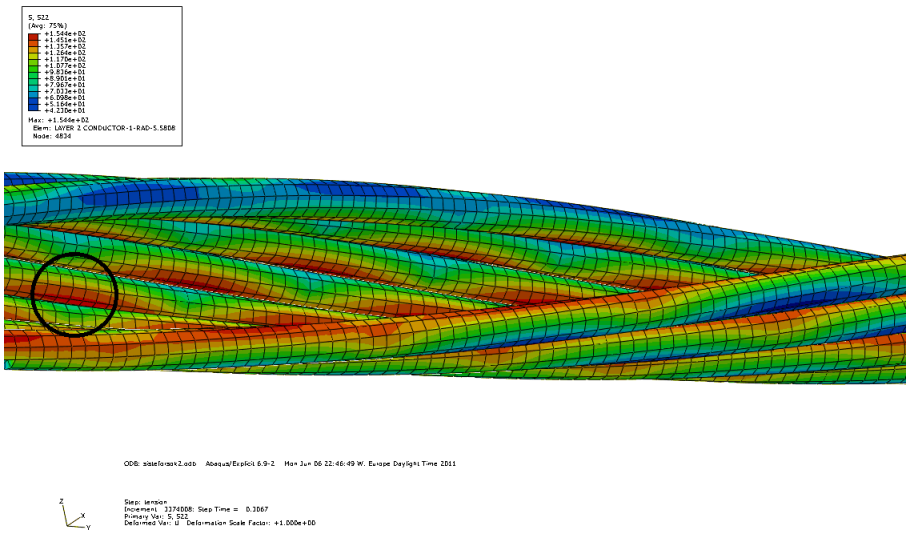

Figure D.8: Critical element layer 2

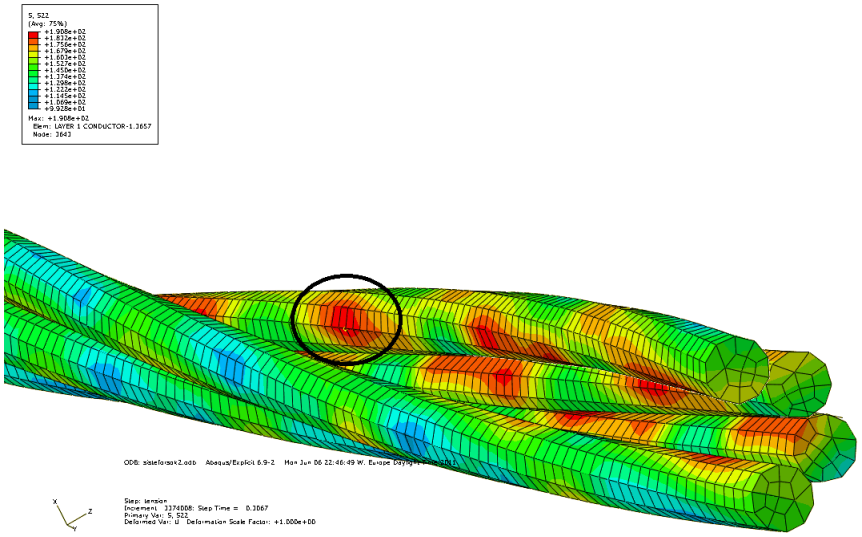

Figure D.9: Critical element layer 1

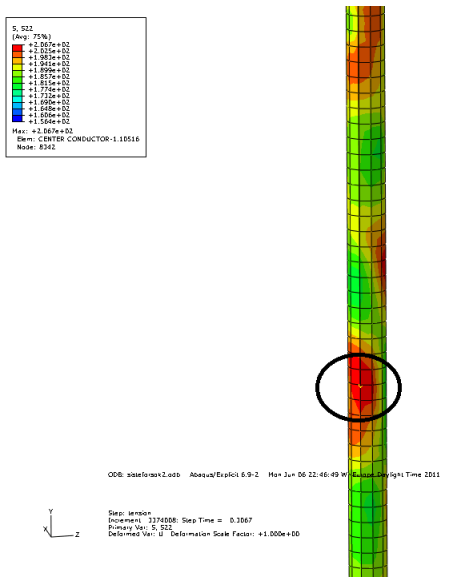

Figure D.10: Critical element center

D.3.3 Stress

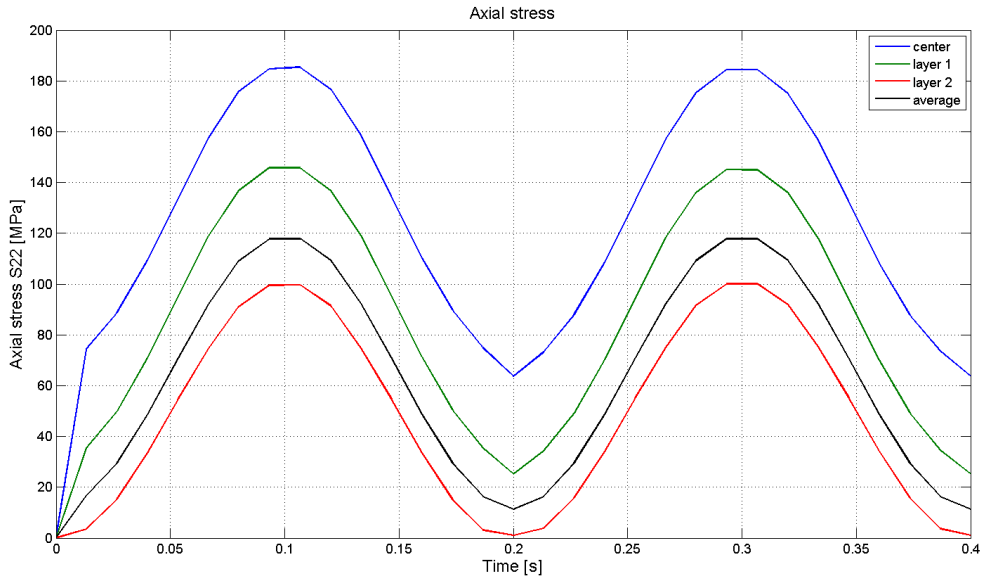

Figure D.11: Axial stress

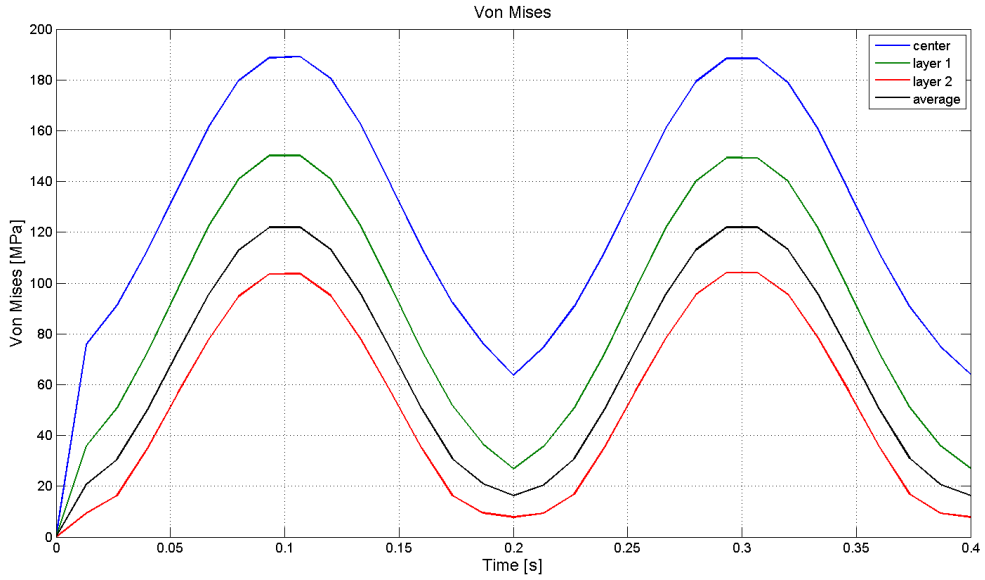

Figure D.12: Von Mises stress

D.3.4 Strain

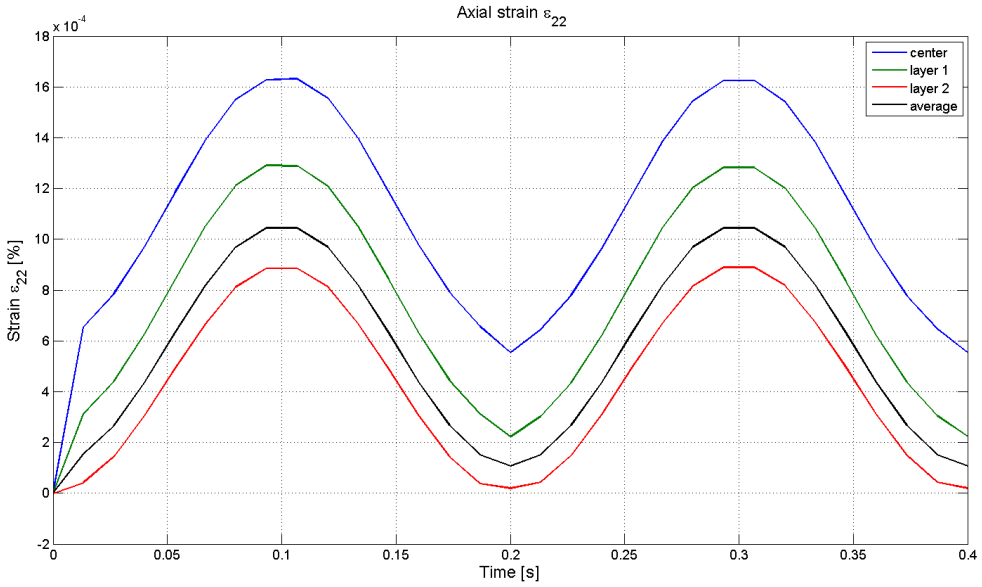

Figure D.13: Axial strain

D.3.5 Axial stress versus strain

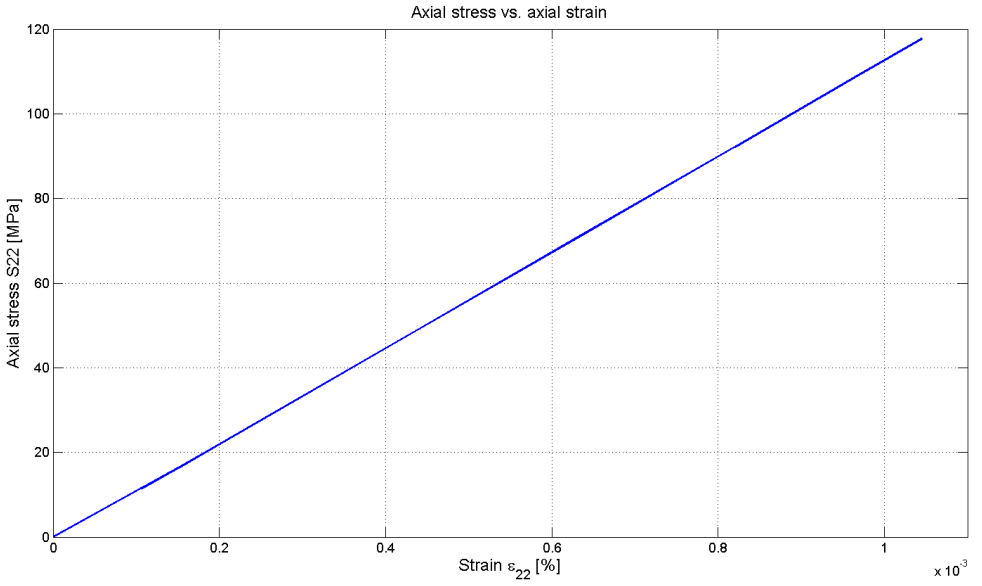

Figure D.14: Axial stress versus strain

D.4 Case 3

D.4.1 Stress

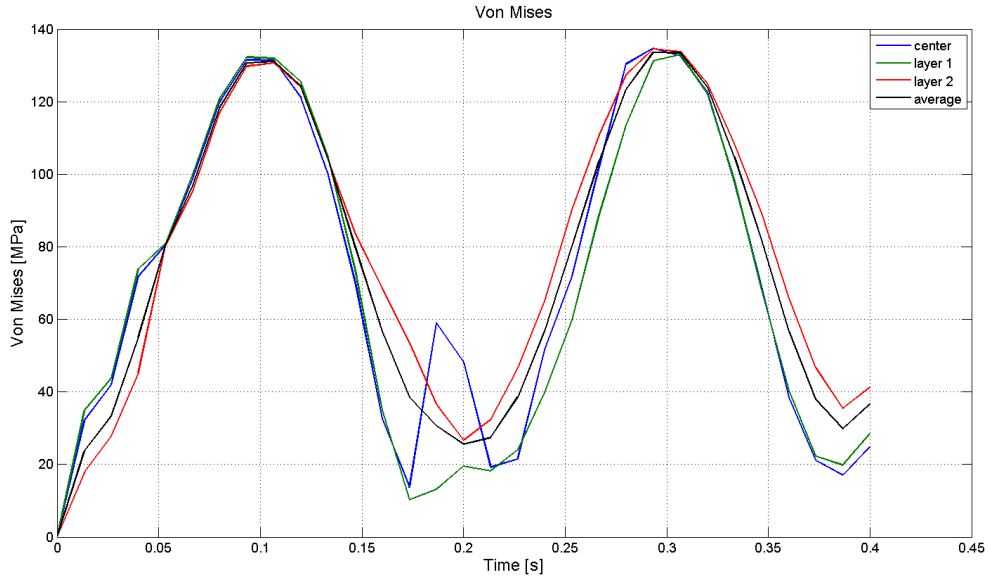

Figure D.15: Von Mises stress

D.4.2 Axial strain

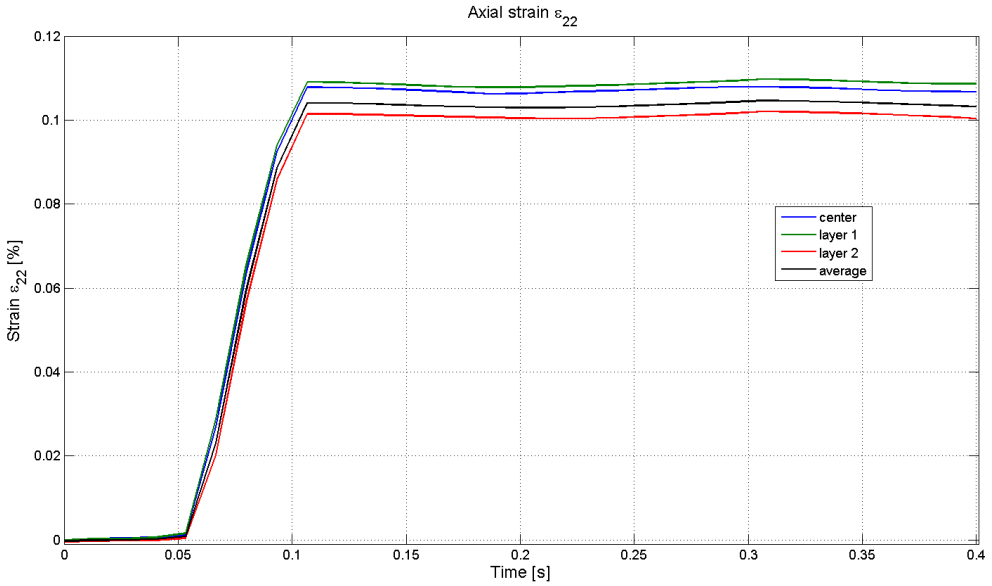

Figure D.16: Axial strain

D.4.3 Stress versus strain

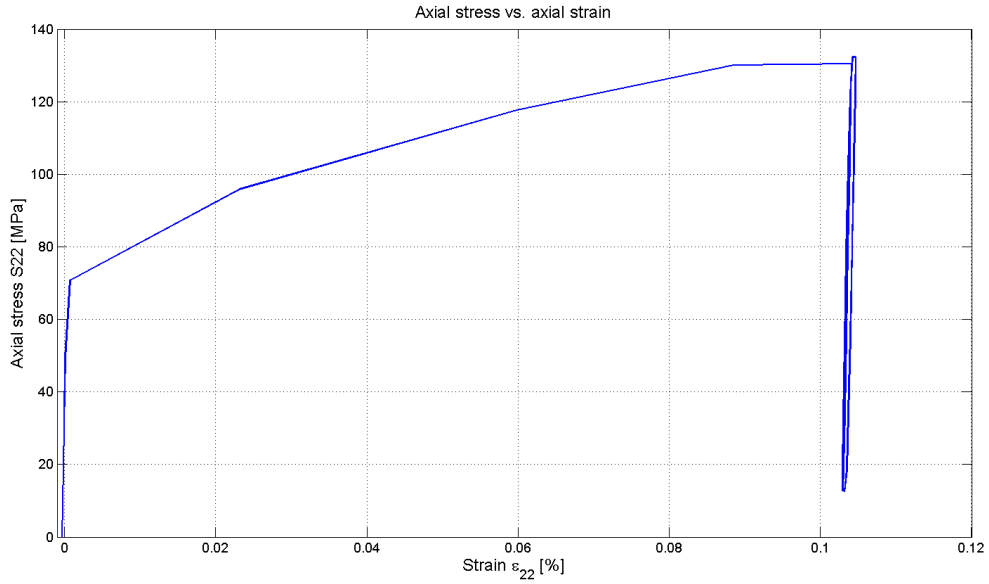

Figure D.17: Axial stress versus strain

D.4.4 Fatigue —critical element

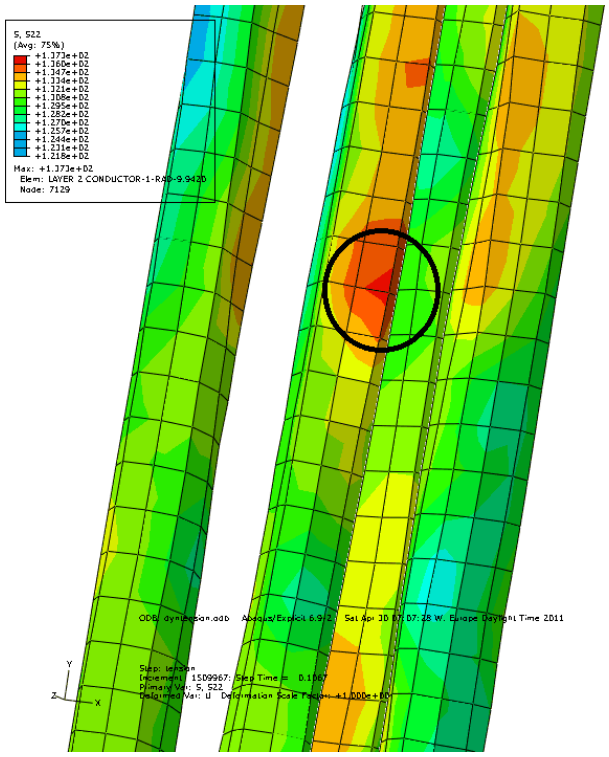

Figure D.18: Critical element Layer 2

D.4.5 Deformed shape

In figure D.19, The deformation of a conductor from layer 2 is shown. It illustrates that it has been unwound, as a result of the boundary conditions do not prevent rotation.

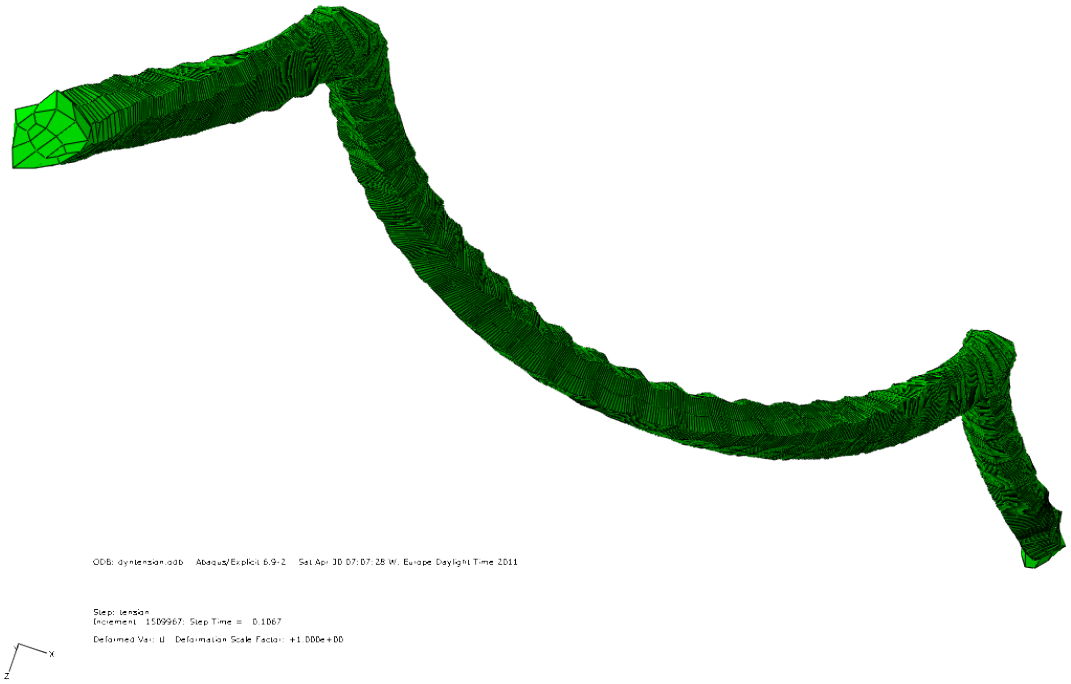

Figure D.19: Layer 2 conductor

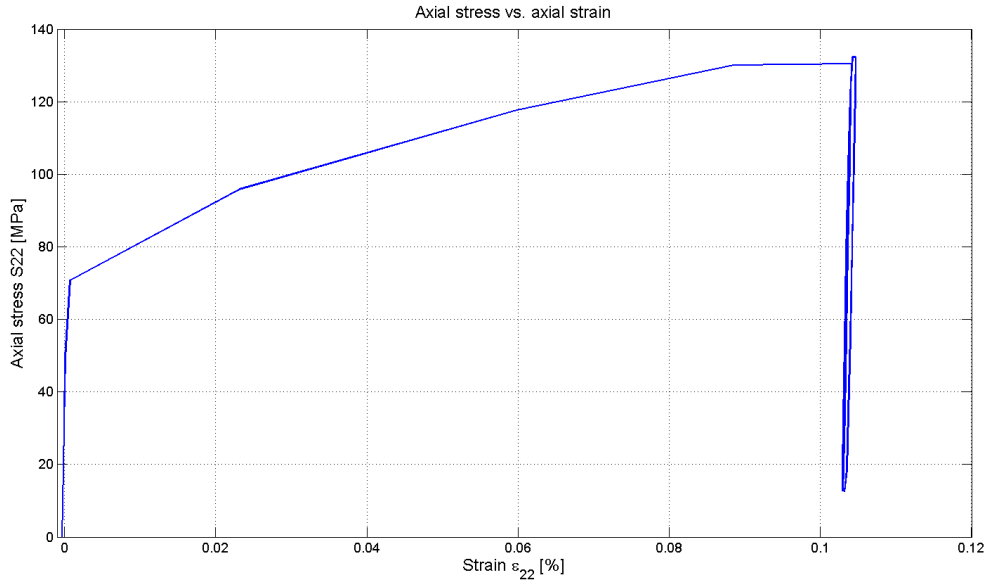

Figure D.20: Axial stress versus strain

D.5 Case 4

D.5.1 Stress

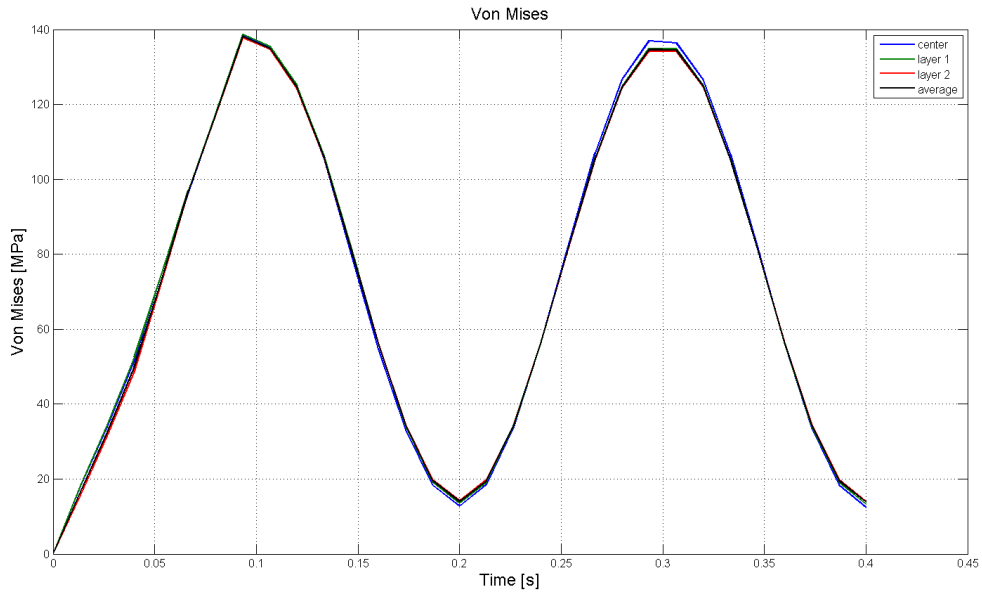

Figure D.21: Von Mises stress

D.5.2 Axial strain

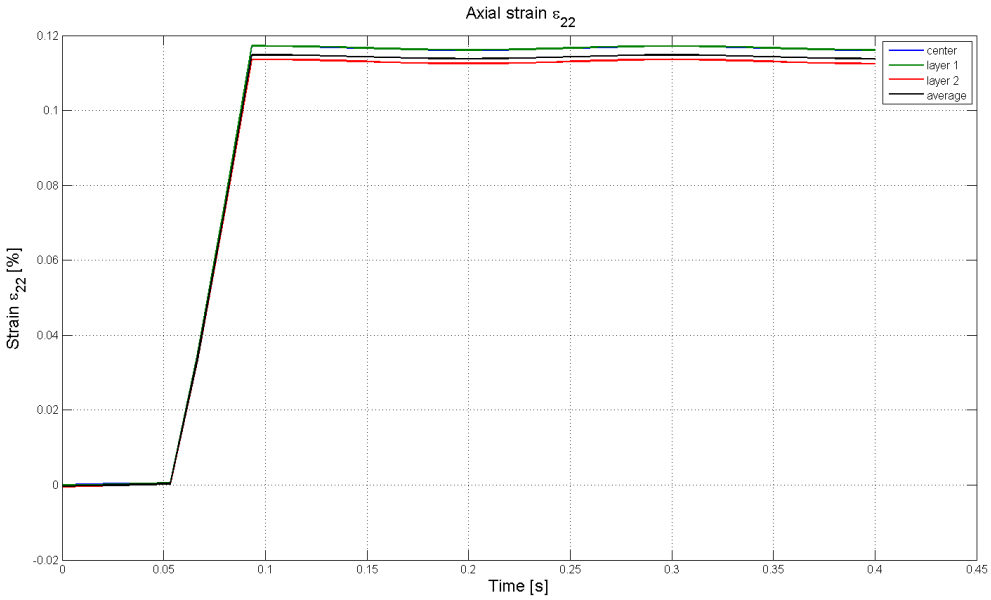

Figure D.22: Axial strain

D.5.3 Axial stress versus strain

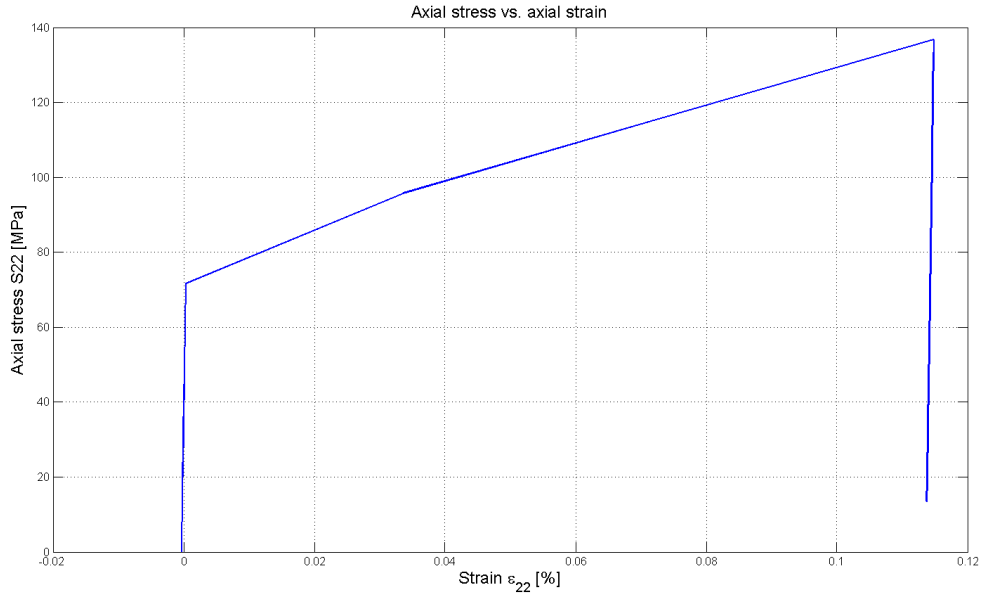

Figure D.23: Axial stress versus strain

D.5.4 Fatigue —Critical element

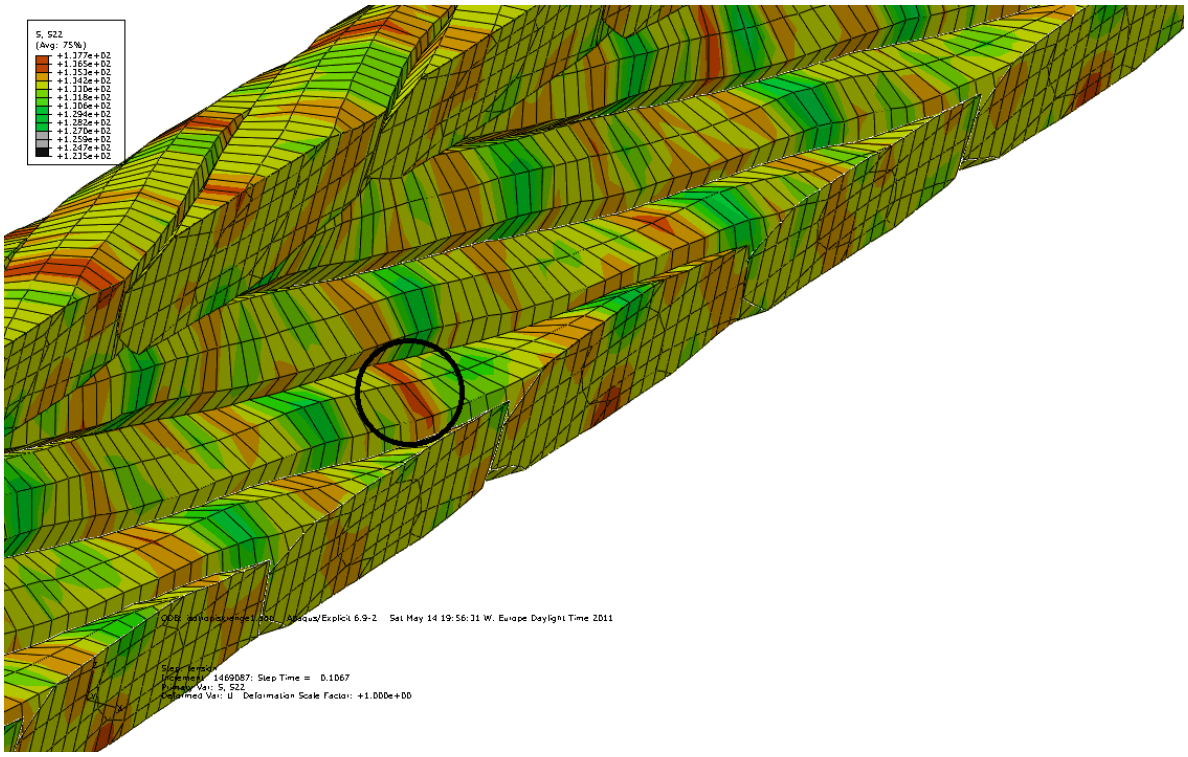

Figure D.24: Critical element Layer 2

D.5.5 Deformed shape

A conductor taken from layer 2 is shown in figure D.25. Unlike Case 3, the conductor has not unwound from its undeformed shape. This is because the boundary conditions prevents rotation.

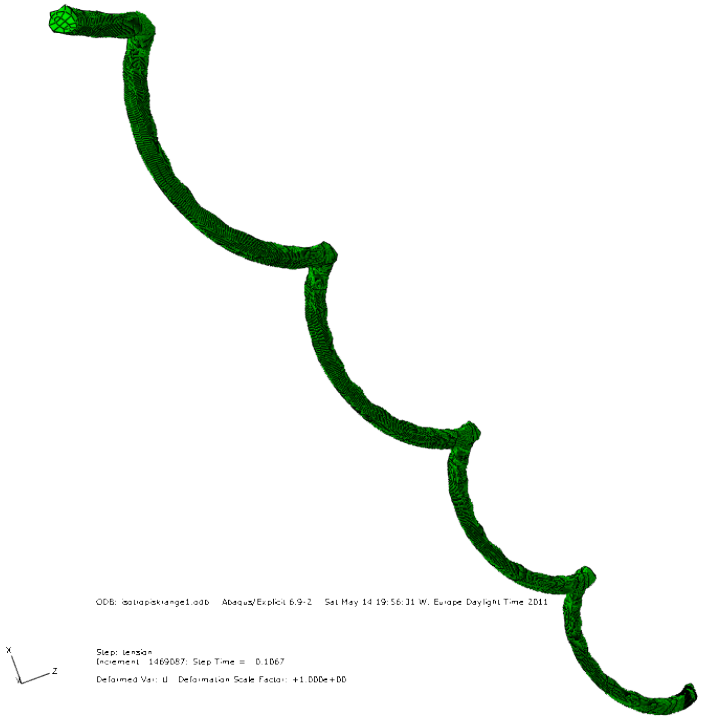

Figure D.25: Layer 2 conductor

D.6 ABAQUS files and MatLab scripts

The size of the ABAQUS files make them unsuited for the appendix. The MatLab files also takes up a lot of space. Therefore they will be included in a hard drive.